Experiments and Simulations of Large-Angle Flexible Beam Control Using an Adaptive Truss

by

Thomas Joseph Warrington

Thesis submitted to the Faculty of the

Virginia Polytechnic Institute and State University

in partial fulfillment of the requirements for the degree of

Master of Science

in

Mechanical Engineering

APPROVED:

H. H. Robertshaw, Chairman

H. H. Cudney

R. G. Leonard

July, 1991

Blacksburg, Virginia

Experiments and Simulations of Large-Angle Flexible Beam Control Using an Adaptive Truss

by

Thomas J. Warrington

Committee Chairman: Harry H. Robertshaw

Mechanical Engineering

Abstract

The objective of this thesis is to study the vibration suppression capabilities of a double-octahedral adaptive truss with an appended flexible beam. Three cases are studied. The first case is an experimental and analytical investigation of flexible beam control using an adaptive truss positioned in an equilibrium configuration such that the beam is parallel to the gravity field. A linear model of the system is derived, and a linear LQR control law is designed. Control experiments are conducted and show that the adaptive truss performs good vibration control of the flexible beam with the effective modal damping increased from 0.012 for the uncontrolled vibrations to 0.19 for the controlled vibrations. Good agreement between the open-loop and closed-loop simulations and experiments is achieved such that a correlation coefficient of 0.92 is observed between the experiment and simulation open-loop data and a correlation coefficient of 0.85 is observed for the experiment and simulation closed-loop data. The second case is the analysis and vibration control of the flexible beam while the adaptive truss is positioned at some large-angle configuration such that the flexible beam is severely affected by gravity. In this case a nonlinear beam model is developed and a linear LQR control law is implemented.

Simulations show vibration control of the flexible beam for large-angle configurations of the truss, and that the vibration control performance is highly dependent on the linearization point of the control law. The third case is the analysis and control of large-angle slewing of a flexible beam using the adaptive truss. In this case the nonlinear beam model is implemented with both linear LQR and nonlinear gain-scheduled control laws. Simulations indicate that the adaptive truss achieves vibration control of the beam during slewing manuevers for all control laws tested with the nonlinear control law achieving superior vibration control performance in comparison to all control laws tested.

Acknowledgements

Many people besides myself are responsible for this hellish endeavor the university calls a thesis. Quite honestly, I don't know whether to thank them for their generous help or scold them for not boding of the enduring torture. But, now that the thesis is finished and feelings of accomplishment abound, countless thank-you's are due many unselfish people.

First, my friend and advisor Harry Robertshaw deserves some kind of medal for his forbearance, understanding, advice, and support. Very few people could tolerate the antics of one T.J. Warrington (just ask any of my ex-girlfriends). Many thanks also go to my fellow graduate students who took time and effort away from their own projects to help me. Among them are Buddy Clark, David Lacy, Babu Pabmanabhan, Will Saunders, Robert Wynn, and Steve Rubenstein.

With out friends to keep things in perspective (like not continuing for a Ph.D.), the craziness of the world would become too overwhelming. I thank Larry, Rob, David, and Mike for their continuing friendship and companionship.

Finally, I would like to thank my Grandmother for her support, guidance, and encouragement. Without her this would all still be a dream.

Contents

List of Figures

Nomenclature

Symbol	Definition
$\hat{b}_{1,2,3}$	unit vectors in beam reference frame
$\vec{B}_{1,2,3}$	actuated plane nodal vectors
$B_{1,2,3}$	actuated plane nodal points
$\vec{B}_{7,8,9}$	top plane vectors
$[\mathbf{C_b}]$	damping matrix
d	gimbal axes offset
E	Young's Modulus
g	gravity constant
g_l	gain of leadscrew
g_r	gear reduction
$I_{x,y}$	area moments of inertia
J_a	motor armature inertia
J_{cost}	LQR performance index
$[\mathbf{J_a}]$	truss acceleration transformation
$[\mathbf{J_p}]$	truss position transformation
$[\mathbf{J_v}]$	truss velocity transformation
k_a	amplifier gain
$k_{\gamma,\beta}$	trunnion stiffness parameters
k_m	lumped motor constant
k_t	torque constant of motor
$[\mathbf{K}]$	feedback matrix
$[\mathbf{K_b}]$	stiffness matrix
$l_{1,2,3}$	active batten lengths
l_b	length of base strut
$l_{i,j}$	strut links between nodes i and j
l_{RS}	equivalent strut length
L	Lagrangian

Symbol	Definition
$\vec{L}$	vector of active batten lengths
L_b	length of beam
$\vec{L}_1$	vector of strut lengths
$\hat{m}_{1,2,3}$	unit vectors of moving frame
$[\mathbf{M_b}]$	mass matrix
$M_{\gamma,\beta}]$	plate bending moments
$N_{1...9}$	truss nodes
$\hat{n}_{1,2,3}$	unit vectors of Newtonian frame
$\vec{N}_{1...9}$	truss nodes vectors
$\vec{O}_{1,2,3}$	revolute vectors
$\hat{p}_{ij}$	unit vector along strut link ij
$\vec{P}_b$	description of beam reference frame
$\vec{P}_m$	reduced description of moving frame
$\vec{P}m_{org}$	origin of moving frame
$\vec{P}_{top}$	description of top plane
$q_{x,y}$	modal coordinates
$\vec{Q}$	vector of modal coordinates
$[\tilde{\mathbf{Q}}]$	LQR state penalty matrix
$R_{x,y,z}$	Newtonian translations of beam frame
$\vec{R}$	differential position vector
$[\tilde{\mathbf{R}}]$	LQR input penalty matrix
r	distance between bottom and actuated planes
$\vec{R}_{1,2,3}$	reference vectors
$[\mathbf{R}_{\gamma,\beta,\alpha}]$	euler angle rotation matrix
$[\mathbf{R}_{\theta_i,\hat{U}_i}]$	revolute rotation matrix
s	length parameter along the beam
T	kinetic energy
T_s	sampling time
$[\mathbf{T_{b/m}}]$	$\hat{m}$ to $\hat{b}$ transformation
$[\mathbf{T_{q/\epsilon}}]$	strain to mode transformation
$[\mathbf{T_Q}]$	mode to bending moment transformation
$\vec{U}$	input vector
$\hat{U}_{n0}$	unit vector normal to bottom plane
$\hat{U}_{n1}$	unit vector normal to actuated plane

Symbol	Definition
$\hat{U}_{n2}$	unit vector normal to top plane plane
$\hat{U}_{1,2,3}$	unit vectors parallel to revolutes
V_ϵ	strain energy
V_g	potential work
$Vin_{1,2,3}$	input voltages
$w_{x,y}$	transverse deflections of beam
X, Y, Z	Newtonian coordinates of moving frame

Greek Letters

$\alpha\ \beta\ \gamma$	Euler rotation angles of moving frame
$\alpha_b\ \beta_b\ \gamma_b$	Euler rotation angles of beam frame
$\epsilon_{x,y}$	beam strains
$\theta_{1,2,3}$	revolute angles
κ	beam curvature
ξ	mass per unit length
$\phi_{x,y}$	Euler shape functions
$\vec{\Upsilon}$	vector of beam strains
$\vec{\Phi}$	vector of Euler angle accelerations
$\vec{\Psi}$	state vector
$\vec{\Omega}$	vector of Euler angle velocities

Chapter 1

Introduction

Recently, much attention has been given to adaptive trusses for their ability to perform as highly evolved actuators. These actuators have a multitude of potential applications as smart mechanisms in which kinematic and dynamic objectives are integrated via feedback control strategies. The primary emphasis for developing adaptive trusses lies in space-related applications including vibration suppression, slewing, articulation, payload isolation, tracking and pointing, docking mechanisms, and deployable trusses. These applications have been investigated by Rockwell International [1982], Miura et al. [1985], Miura and Furuya [1985], and Rhodes and Mikulas [1985]. Obviously, the use of mechanisms (such as adaptive trusses) will be an important aspect of the assembly and maneuvering of future spacecraft. For example, the concept for assembly and service on Space Station Freedom includes a space crane which requires active joints that must be designed to transmit loads and move to a position when commanded. An adaptive truss would be well suited for this task. Or as another example, in platform-type spacecraft a payload will be required to point and track a target independent of the interaction from other disturbances on the spacecraft. Adaptive trusses present at least one possible method of achieving both disturbance rejection and target tracking.

A brief introduction to the adaptive truss concept is discussed here to introduce some of the terminology and to present some of the advantages of adaptive trusses. Adaptive trusses are often referred to as Variable Geometry Trusses or VGT's. A VGT is a statically determinate truss that has been modified to contain some number of variable length members. The number of extensible members is equal to the number of degrees of freedom of the truss. Adaptive trusses are made up of some combination of fundamental units, called unit cells. These include the tetrahedron, the octahedron, the decahedron, and the dodecahedron all of which have triangular faces as described by Arun et al [1990]. The simplest repeating actuation unit within an adaptive truss is referred to as a bay. A bay may be a single cell, or it may be formed from various combinations of the unit cells. These bays are named according to their construction. For example, a single-octahedral adaptive truss is a bay formed by one octahedral unit cell or a triple-tetrahedral adaptive truss is a bay made up of three tetrahedral unit cells.

The principle reasons for the proposed applications of adaptive trusses lie in their inherently high strength-to-weight ratio and the possible ease of stowing and assembling. These attributes occur from the way loads are carried by the members of the truss, that is, in tension and compression. This accounts for the high strength of adaptive truss structures and their potential uses as space booms, supports for space antennae, and as berthing devices. A comparative study by Sincarsin and Hughes [1987] showed that the octahedral type truss held the most promise for these applications. Coincidentally, the adaptive truss utilized in this thesis is a double-octahedral adaptive truss.

This thesis is concerned with investigating the capabilities of the double-octahedral adaptive truss for vibration suppression, large-angle slewing, vibration suppression at large slewed angles, and the simultaneous objective of slewing and vibration suppression. These objectives are directly associated with several of the potential applications discussed above as they demonstrate the dynamic and kinematic capabilities of the adaptive truss which are required to achieve several of these potential applications. As a result, three experiments are performed in this thesis to demonstrate the vibration control capabilities of the adaptive truss. They are

1. Perform computer and hardware experiments that use the double-octahedral adaptive truss to control the flexible motions of an attached continuum about an equilibrium (zero-angle) configuration of the truss.

2. Perform computer experiments that use the adaptive truss to control the vibrations of the attached continuum about various large-angle operating configurations of the truss.

3. Perform computer experiments of the adaptive truss controlling the vibrations of the attached continuum in the process of a slewing maneuver of the adaptive truss.

Experiment 1 investigates what is, perhaps, the simplest problem of flexible beam control with an adaptive truss. This is the case when the adaptive truss operates with small motions about the configuration in which the flexible beam is upright and parallel to the gravity field as shown in Fig. 1.1. This operating position is designated the zero-angle or equilibrium configuration, since the top plane of the truss is horizontal. Gravity effects and kinematic nonlinearities are minimal in this

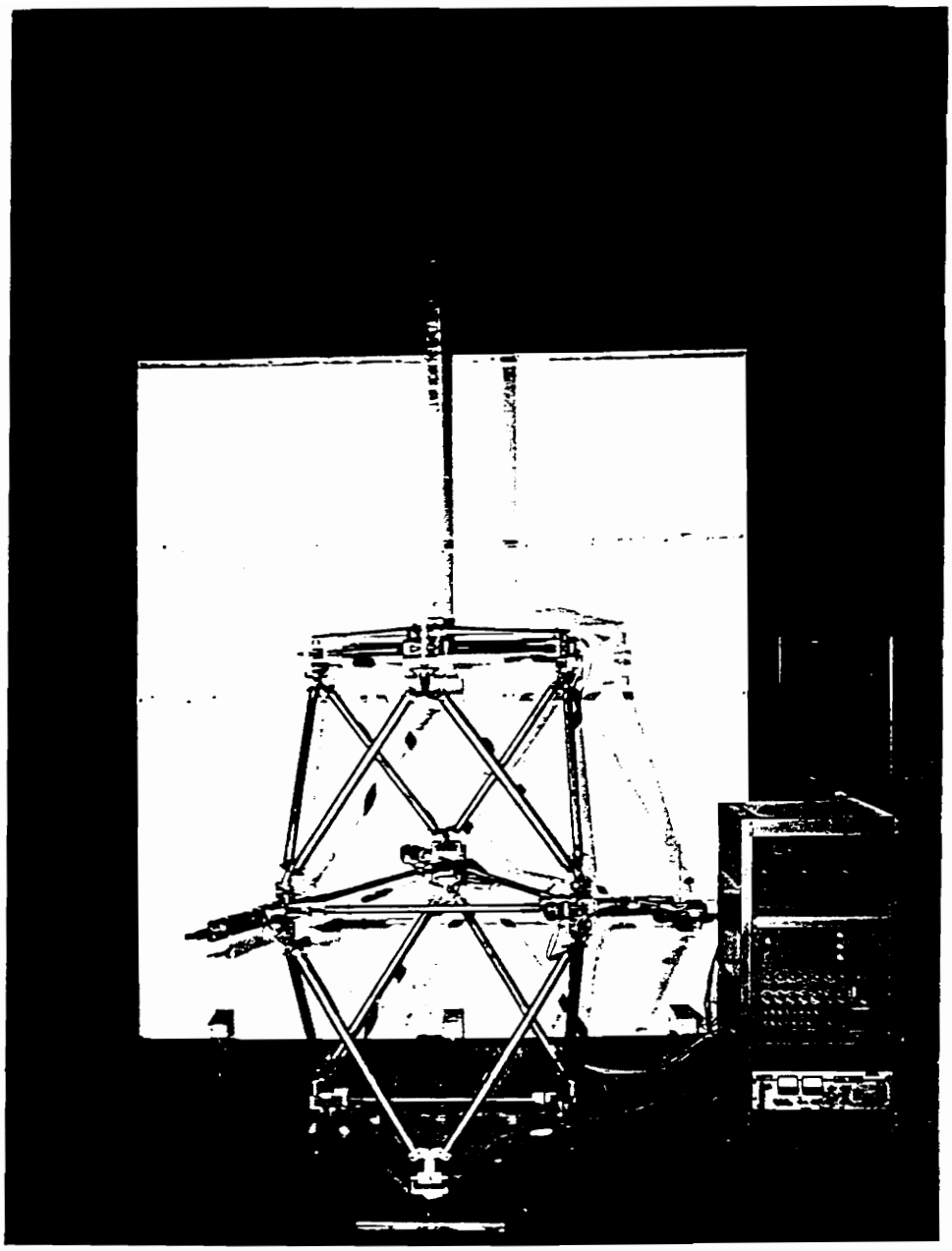

Figure 1.1: Adaptive Truss Positioned in Equilibrium Configuration

position and allow for the formulation of a linear model and linear control law.

Experiment 2 examines the problem of vibration control of the flexible beam in which the adaptive truss operates with small motions about various large-angle configurations. In this situation the flexible beam is not parallel to the gravity field and subject to gravitational nonlinearities as shown in Fig. 1.2, and thus, a nonlinear beam model is developed. The adaptive truss operates with small motions about the large-angle configuration, and the kinematic nonlinearities are again minimal, thus, facilitating the use of a linear control law.

Finally, experiment 3 investigates the ability of the adaptive truss to perform vibration control of the flexible beam while simultaneously slewing the beam through large angles. In this scenario, both gravitational nonlinearities and kinematic nonlinearities due to the large angle slewing are encountered. Accordingly, a nonlinear model and a nonlinear control law are incorporated in the large angle slewing and vibration control simulations.

1.1 Literature Review

The ability of adaptive trusses to perform vibration control of flexible beams has been demonstrated previously. Robertshaw [1989] showed good vibration control of a flexible slender rod appended to the bottom of a quadruple-octahedral adaptive truss. Wynn [1990] later demonstrated vibration control of a thin, flexible beam umbrellaed in the gravity field. Both of these test scenarios positioned the beam hanging downward in the gravity field. In comparison, the three studies in this

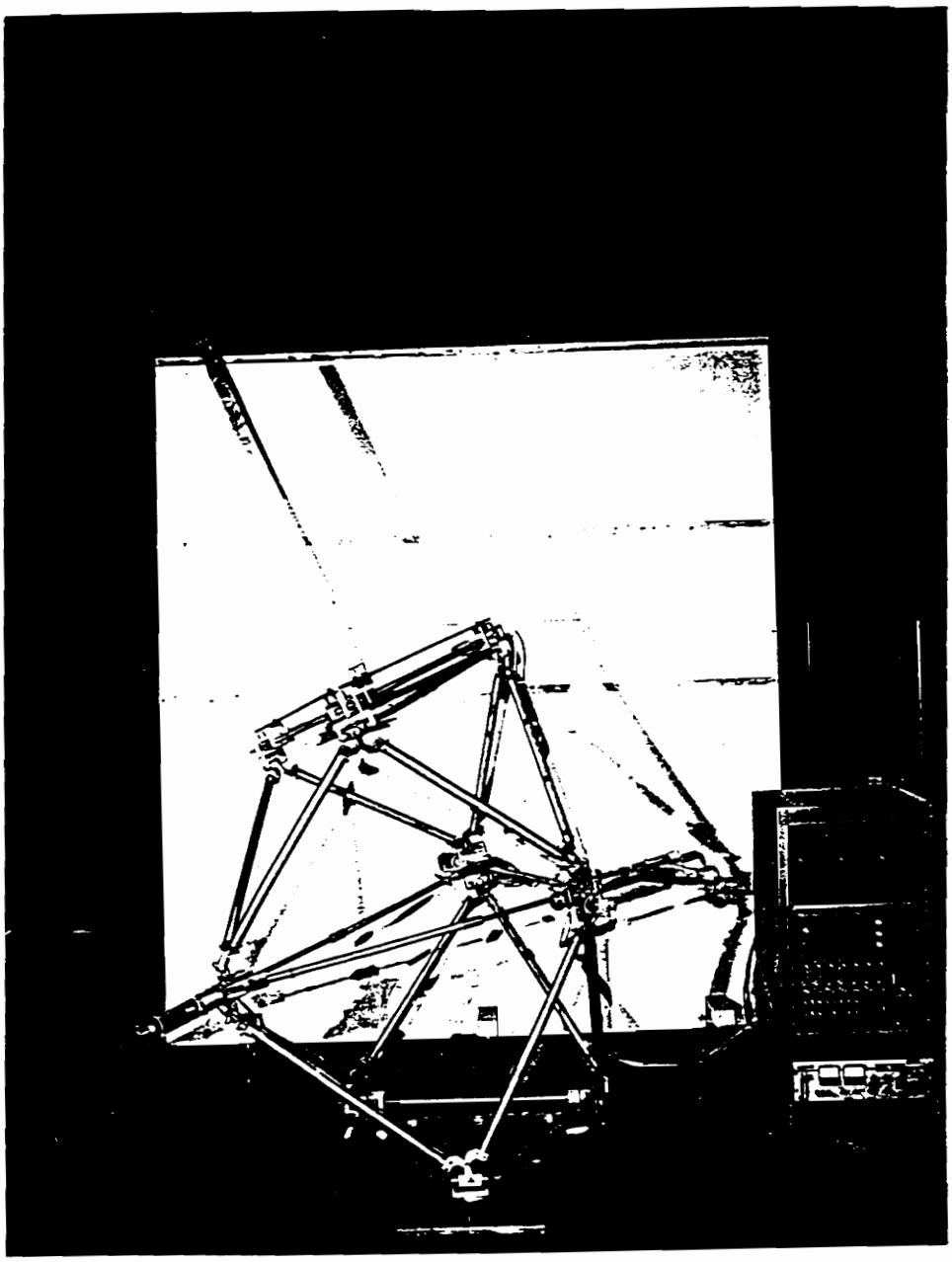

Figure 1.2: Adaptive Truss Positioned at a Large-Angle Configuration

thesis, the flexible beam is positioned upright or at some angle less than 90 degrees from vertical. Another key difference is the actuator drive system incorporated. Robertshaw and Wynn use a voltage-controlled amplifier and DC motor, while a current-controlled amplifier and DC motor are utilized in this thesis. The difference results in less inherent system damping for the current-controlled system.

Vibration suppression or active damping has been achieved with other types of adaptive trusses. Fanson [1989] used piezoelectric active-members to control the flexible motion of spatial truss structure. Natori [1987] utilized voice coil type actuators in a spatial truss structure and provided active damping. Clark [1990] uses a free-free floating planar truss to actively suppress the flexible vibrations of two appended beams. In the cases of Fanson and Natori the active vibration was accomplished with small motions and the spatial kinematic nonlinearities were neglected. In the case studied by Clark, the planar kinematic nonlinearities are also neglected.

The principle reason for neglecting the nonlinear kinematics, as Fanson, Natori, and Clark did in their studies, is the void of closed-form kinematic solutions to many of the proposed adaptive truss geometries. However, with the recent developments by Padmanabhan [1990] in adaptive truss kinematics, closed-form inverse solutions now exist for the double-octahedral and quadruple-octahedral adaptive trusses. Consequently, this thesis exploits the kinematic solution to the double-octahedral adaptive truss such that the kinematic nonlinearities are retained.

Slewing control of a flexible beam has been demonstrated with single-axis root actuation by Robertshaw [1985], Juang [1986], and Alberts [1990]. However, literature

on large-angle control and slewing control of flexible beams with adaptive trusses remains infrequent. Again, the most likely reason is the void of closed-form kinematic solutions to a variety of the adaptive truss geometries. However, the recent development of the closed-form inverse solution to the double-octahedral adaptive truss by Padmanabhan has provided the necessary kinematics to perform, as this thesis does, large-angle positioning and slewing maneuvers with the double-octahedral adaptive truss.

1.2 Outline

This thesis includes three distinct studies and are progressively presented in their order of difficulty. Although only the first study includes measured experimental data, all studies incorporate the physical parameters of the test article. Thus, a short description of the test article is presented in Chapter 2.

Each of the three vibration control studies incorporate different elements of the kinematics of the double-octahedral adaptive truss. So, before the vibration control studies are presented, a comprehensive kinematic analysis of the adaptive truss is included in Chapter 3. Described are the closed-form inverse solution, the iterative forward solution, velocity and acceleration expressions, and linear transformations.

The first study investigates the control of the flexible beam with the double-octahedral adaptive truss while the beam is positioned upright and parallel to the gravity field. Chapter 4 presents the formulation and assembly of the linear systems including a linear 3-mode beam model, motor model, flexible plate model, and linear

truss transformations. Chapter 5 discusses the development of a linear control law and the linear simulation and experimental results of using this control law.

The second study examines the control of the flexible beam with the adaptive truss positioned at some large-angle in which the beam is severely affected by gravity, and the third study investigates the control of the flexible beam as the adaptive truss is maneuvered through a large-angle. Both studies require nonlinear equations of motion to predict the system behavior. Chapter 6 details the development of a single-mode nonlinear beam model and discusses which kinematic equations of Chapter 3 are required for the nonlinear analysis. Chapter 7 presents the linear control law used in the second study and the linear and nonlinear control laws used in the third study. The nonlinear simulation results of implementing these control laws is also presented in Chapter 7.

Finally, Chapter 8 presents concluding remarks and recommendations regarding the three distinct cases investigated in this thesis.

Chapter 2

Description of System

The adaptive truss with a vertical beam on top was shown in Fig. 1.1. The adaptive truss consists of a base plate that is bolted to the floor, six cross longerons that connect the base plate to the three variable length battens, six more cross longerons that connect the variable length battens to the top plate, and the top plate. The three equal but fixed length battens in both the base and top plates are 35.5 in. (90.2 mm) long. Each cross longeron is an aluminum tube 34 in. (86.4 mm) long, 1.5 in. (3.8 mm) in diameter, and has a revolute joint coincident with the longitudinal axis and a revolute joint at each end, perpendicular to the longitudinal axis.

The active battens shown in Fig. 2.1, consist of a 3/4 in. (1.91 mm) diameter threaded steel rod with 10 threads per inch that threads into a bronze nut attached to the end of a 1 in. (2.54 mm) diameter aluminum tube, 35.5 in. (90.2 mm) long. The other end of the threaded rod is mounted in ball bearings and is driven by an 80 watt dc servo motor through a gear train with a 5.1:1 reduction. The motors are powered by pulse-width modulated switching amplifiers. A tachometer measures the motor angular rate and a string or "yo-yo" pot measures the length of the batten which is the distance between the hinge axes at each end. The three active battens

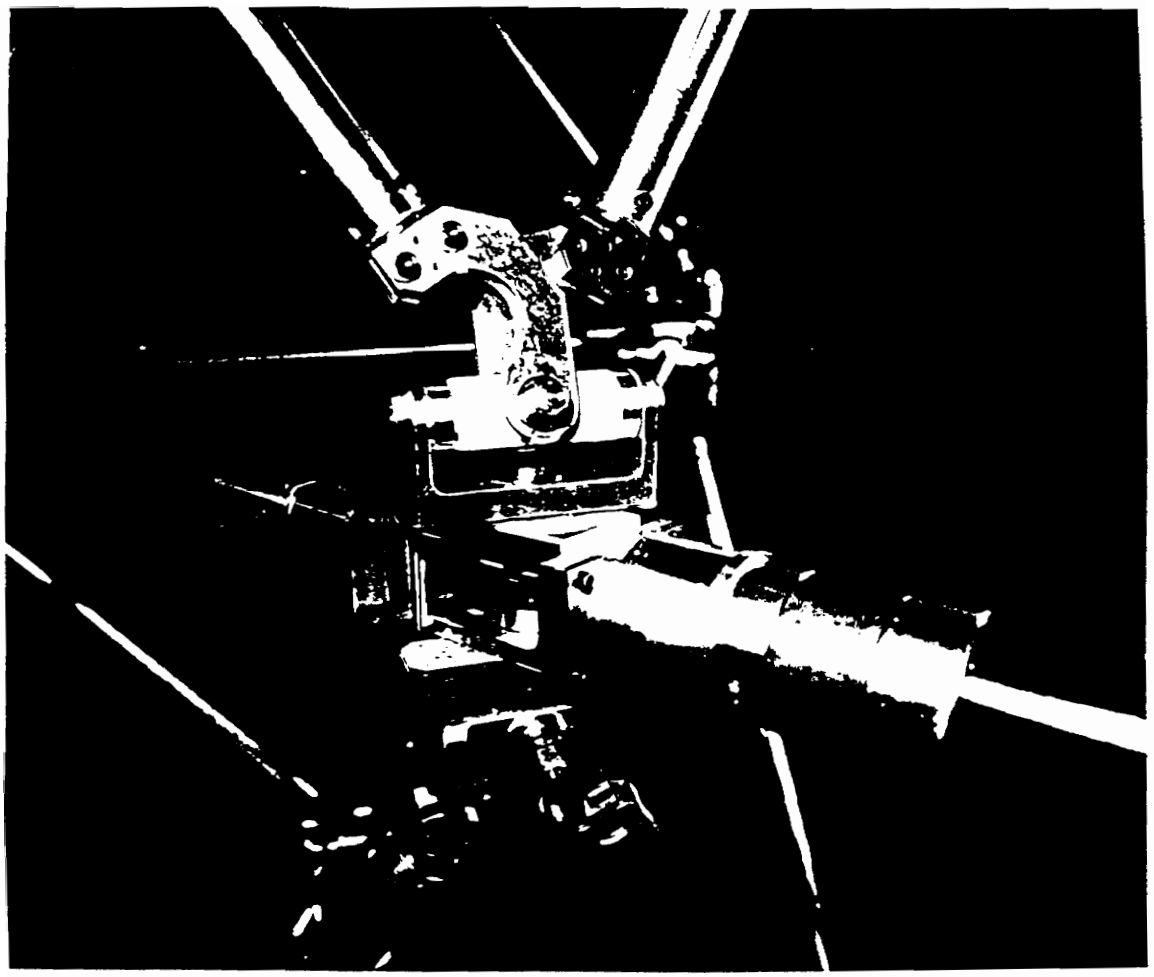

Figure 2.1: Active Batten

are connected by three hinge pins and these pins also adapt the cross longerons through a universal yoke and mechanism.

The top plate is 3/8 in. (0.95 mm) thick aluminum. A longitudinal axis through the center of the aluminum beam atop the truss intersects the top plate at the centroid of the triangle formed by the top three battens and is perpendicular to the top plate. Two steel angles adapt the beam to the plate. The beam is 144 in. (365.8 mm) long with a 1×2 in. (2.54×5.08 mm) solid cross section. Separate strain gages for measuring the bending of the two principle axes are located at the base, 44.4 in. (112.8 mm), and 76.2 in. (193.5 mm) from the base. The locations are also referred to as s_1, s_2, and s_3.

The three tachometer outputs, three string pot outputs, and the six strain outputs are connected to the analog inputs of an A/D board in a PC/XT compatible computer. The three motor command signals come from D/A outputs in the computer. These command signals pass through the amplifiers to independently drive the three dc servo motors which turn the threaded rods and cause the battens to change length.

A block diagram of the PC/XT controlled adaptive truss and beam system is shown in Fig. 2.2. This figure illustrates the system architecture including the sensor signals and motor commands. Sensor signals consist of beam strain, batten length, and motor angular velocity. These signals are multiplied by feedback gains to produce the motor commands.

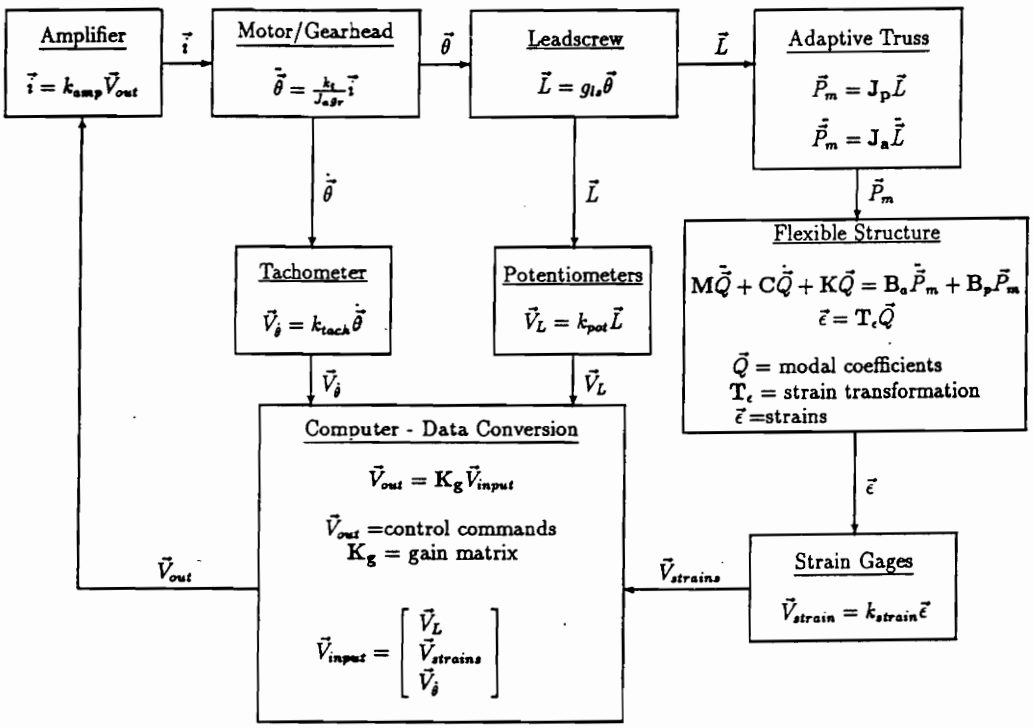

Figure 2.2: System Architecture

Chapter 3

Truss Kinematics

The function of the adaptive truss, in this thesis, is to provide kinematic inputs to the base of the flexible beam. The three degrees of freedom of the adaptive truss arise from the three active batten links and are, in general, related to motions applied to the base of the beam through six coordinates. These motions are the translations, X, Y, and Z, and the rotations, γ, β, and α, which are the Newtonian coordinates describing the spatial position and orientation of a moving reference frame attached to the mid-point of the triangular top plane. This reference frame is described by the $\hat{m}$-coordinate system shown in Fig. 3.1 (note that the Newtonian frame is located at the center of the fixed plane but is shifted for clarity in Fig. 3.1) and of the six coordinates, only three are independent since the adaptive truss has but three active links. The general Newtonian description of the center of the top plane of the truss is $\vec{P}_{top} = [X\ Y\ Z\ \gamma\ \beta\ \alpha]^T$.

In general, two distinct kinematic problems, end point positioning and slew positioning, may be formalized with the double-octahedral adaptive truss actuated as described in Chapter 2. The end point positioning problem involves specifying the global location of a point in the top plane of the truss and determining the required

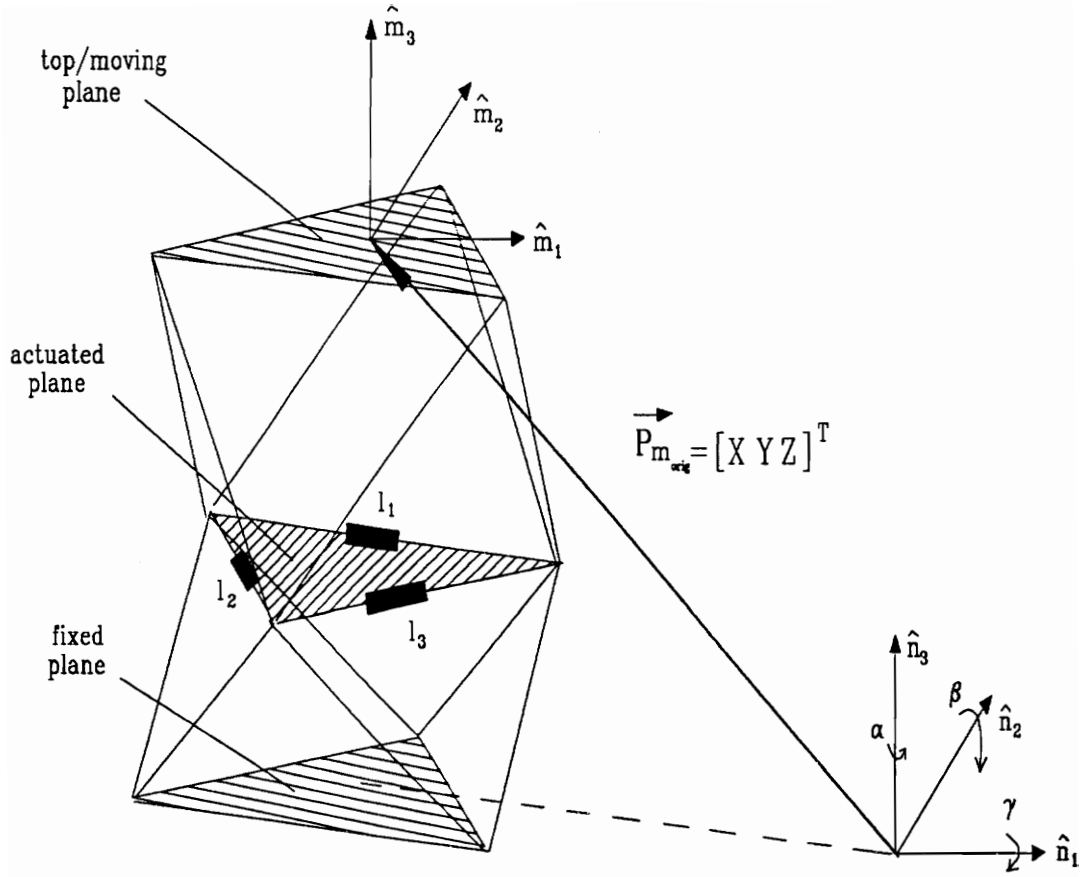

Figure 3.1: Adaptive Truss Schematic and Coordinate System

batten lengths to achieve this position. The slew positioning problem involves specifying the orientation of the top plane and determining the satisfying batten lengths to achieve the desired orientation. This thesis is concerned with the slew positioning problem. Slewing the adaptive truss is equivalent to moving the top plane of the truss from one orientation to another. This orientation could be specified through desired pitch, γ, and roll, β, angles of the moving reference frame. This is often referred to as the gimbal problem. The adaptive truss, however, does not behave as an ideal gimbal since the two axes about which the orientation is specified do not intersect the top plane of the truss at its mid-point, but are instead, offset by a scalar distance, d, as shown in Fig. 3.2. The gimbal axes offset, d, along with the pitch and roll angles complete the necessary set of three independent slew position specifications. The resulting kinematic problem is to determine the lengths of the three actuated battens, $\vec{L} = [l_1 \ l_2 \ l_3]^T$, that will satisfy the slew position specifications. The solution to this problem, also called the inverse problem, is solved in closed form by Padmanabhan [1990].

The opposite of the inverse problem is the forward problem and involves determining the slewed position of the truss satisfying a set of link specifications. The forward problem is solved by iteration of the truss kinematic equations with a root-finding algorithm until a satisfactory solution is obtained. The inverse and forward solutions provide a method of describing the active link positions from the slew position specifications and vice-versa.

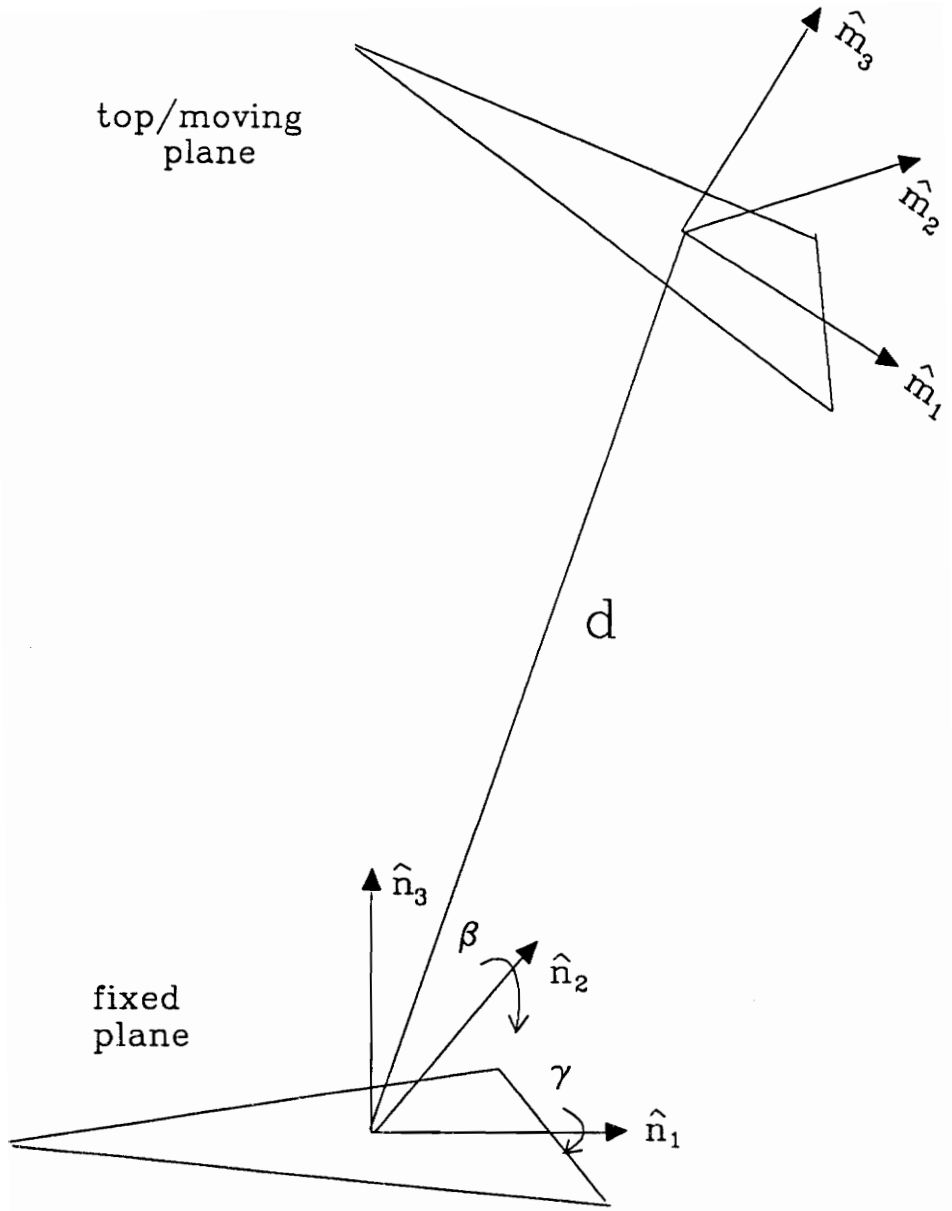

Figure 3.2: Equivalent Gimbal Parameters of Truss

Active Link Positions $\vec{L}$	Forward Solution (Iterative) →	Slew Position Specifications (γ, β, d)
	← Inverse Solution (Closed-Form)	

These position descriptions are necessary for the velocity and acceleration analyses since the velocity and acceleration relationships are position-dependent equations. That is, the truss position (node locations) must be determined before the velocity and acceleration equations can be solved. A general methodology of developing these velocity and acceleration relationships is described by Reinholtz[1990]. These relationships are specifically applied to the double-octahedral adaptive truss such that reversible closed-form solutions between the velocity and acceleration of the moving reference frame, $\dot{\vec{P}}_{top}$ and $\ddot{\vec{P}}_{top}$, and the velocity and acceleration of the active batten links, $\dot{\vec{L}}$ and $\ddot{\vec{L}}$, are determined.

From the inverse position solution and from the velocity and acceleration relationships discussed above, linear kinematic transformations are developed. These linear transformations approximate incremental changes in the position, velocity, and accelerations of the coordinates of the moving reference frame to incremental changes in the position, velocity, and acceleration of the active batten links.

Before the above kinematic relationships are developed in detail, a brief explanation is perhaps needed as to why these kinematic analyses are necessary for the problem of vibration control with the adaptive truss. This thesis conducts three vibration control computer experiments with each one requiring an increasingly detailed analysis of the truss kinematics. The required kinematic relationships for each

experiment is briefly discussed as follows.

In the first case experiments are performed of small motion linear vibration control about the zero-angle ($\gamma = 0$, $\beta = 0$) configuration of the adaptive truss. For this problem linear transformations are required to approximate the position, velocity, and acceleration relationships between the active batten links and the coordinates, $\vec{P}_{top}$, describing the center of the top plane. The reason this is necessary is that linear state-feedback control is developed such that the states of the adaptive truss and flexible beam system are the batten lengths, the beam modal coordinates, and their rates. The bridge between the batten lengths and the modal coordinates is spanned by these linear kinematic transformations.

In the second case experiments are performed of linear vibration control about a large-angle operating configuration of the adaptive truss. Linear transformations are again needed for the linear control law (now described at some large-angle configuration), but the inverse position solution is also necessary such that the batten link positions are known for a specified orientation of the truss. These are the reference batten link positions used for position control and are needed when maneuvering the adaptive truss into a large-angle configuration.

In the third case experiments are performed of linear and nonlinear vibration control during the process of a slewing maneuver. In the nonlinear case, a gain-scheduled vibration control law is implemented such that linear control laws are updated from one discrete truss position to the next, requiring that the linear kinematic transformations are updated for each of these positions. The inverse position solution

is again necessary to determine the reference batten link positions for the position control required to slew the truss from one orientation to another.

In each of the above computer experiments, state-space linear control is performed on the highly non-linear adaptive truss and flexible beam system. If the linear state-space equations were used to simulate the behavior of this system, erroneous predictions of the system behavior would undoubtedly result since the state-space representation does not accommodate the non-linear kinematic behavior of the truss. To predict these non-linearities, the forward solution and velocity and acceleration relationships are required. These relationships are evaluated at each time step in the computer experiments to accurately simulate the adaptive truss and flexible beam system.

3.1 Inverse Solution for Slewed Truss

The solution of orienting the truss for a desired slew position starts with specifying three input parameters, two angles, γ and β, specifying the desired pitch and roll orientation of the top plane, and a scalar distance, d, between the origins of the Newtonian reference frame and the moving reference frame. Also needed for the solution are the fixed geometrical parameters of the double-octahedral adaptive truss, including the length of the cross longerons and the lengths of the fixed battens at the top and bottom planes of the truss. These dimensions are specified in Chapter 2. From these given parameters, the lengths of the active batten links, $\vec{L}$'s, are determined as follows.

3.1.1 End Point specification

First, the end points, X, Y, and Z, of the vector to the origin of the moving reference frame are determined from the slew position specifications, γ, β, and d. Let $\hat{U}_{n2}$, $\hat{U}_{n1}$, and $\hat{U}_{n0}$ be unit vectors normal to the top, actuated, and bottom planes, respectively, as shown in Fig. 3.3. The unit vector, $\hat{U}_{n2}$, gives the orientation of the moving reference frame with respect to the Newtonian reference frame in terms of the γ and β angles previously specified and is given by

$$\hat{U}_{n2} = \begin{bmatrix} \sin\beta \\ -\sin\gamma\cos\beta \\ \cos\beta\cos\gamma \end{bmatrix} \tag{3.1}$$

The unit vector $\hat{U}_{n0}$ is fixed to the Newtonian reference frame such that

$$\hat{U}_{n0} = \begin{bmatrix} 0 \\ 0 \\ 1 \end{bmatrix} \tag{3.2}$$

From Fig. 3.3, it is observed that r is the length of a vector that is drawn from the origin of the Newtonian frame and normal to the fixed-plane to meet the actuated plane. Due to symmetry, the length of a vector drawn from the moving frame origin of the top plane and normal to the top plane to meet the actuated plane is the same. Imposing this symmetry condition, the following loop closure equation can be written

$$r\hat{U}_{n0} + r\hat{U}_{n2} - d\hat{U}_{n1} = 0 \tag{3.3}$$

$\hat{U}_{n1}$ is unknown, but because it is a unit vector, it follows that

$$\hat{U}_{n1} \bullet \hat{U}_{n1} = 1$$

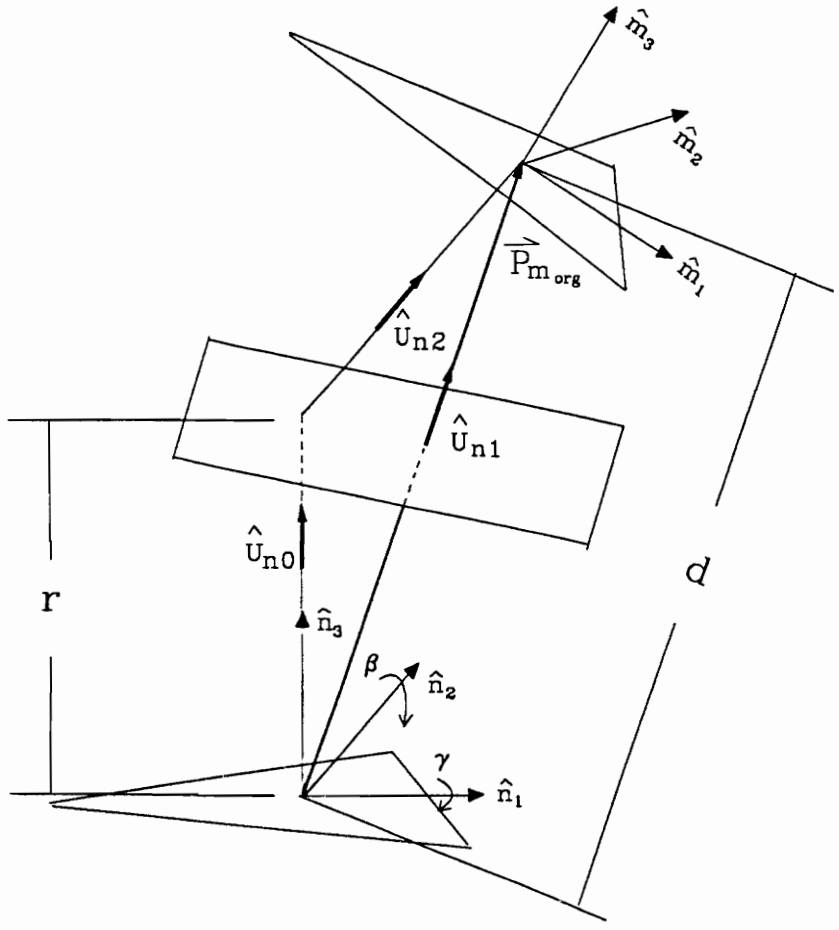

Figure 3.3: Vector Notation for Inverse Solution of Adaptive Truss

Taking into account the above identity and rearranging equation 3.3, r is obtained as

$$r = \frac{d}{\sqrt{2(1 + \hat{U}_{n0} \bullet \hat{U}_{n2})}} \tag{3.4}$$

By performing vector addition in accordance with Fig 3.3, the origin of the moving frame, $\vec{P}m_{org} = [X\ Y\ Z]^T$, is calculated as

$$\vec{P}m_{org} = r(\hat{U}_{n0} + \hat{U}_{n2}) \tag{3.5}$$

Upon substitution of equations 3.1, 3.2, and 3.4, the end point locations are explicitly expressed in terms of the input specifications, γ, β, and d as

$$\begin{aligned} X &= -\frac{d \sin\beta}{\sqrt{2(1 + \cos\beta\cos\gamma)}} \\ Y &= \frac{-d \sin\gamma\cos\beta}{\sqrt{2(1 + \cos\beta\cos\gamma)}} \\ Z &= \frac{d\,(1 + \cos\beta\cos\gamma)}{\sqrt{2(1 + \cos\beta\cos\gamma)}} \end{aligned} \tag{3.6}$$

The resulting end point specifications define the spatial position of the origin of the moving reference frame for the desired orientation of the top plane of the adaptive truss.

3.1.2 Equivalent Kinematic Model

Next, a simplifying equivalent kinematic model is constructed by replacing the octahedral unit cell with the three RS (revolute-spherical) mechanism model devised by Reinholtz and Gokhale [1987] shown in Fig. 3.4. The equivalent kinematic model

assumes the actuated nodal points, B_1, B_2, and B_3, pivot about a revolute joint through an equivalent strut length, l_{RS}. The angles about which the revolute joints rotate are θ_1, θ_2, and θ_3. Using the equivalent kinematic model and the fixed geometrical parameters of the truss, the following time-invariant vector quantities are defined in the Newtonian reference frame as illustrated in Fig. 3.4:

Unit vectors parallel to revolutes	$\hat{U}_1, \hat{U}_2, \hat{U}_3$
Reference vectors of length l_{RS}	$\vec{R}_1, \vec{R}_2, \vec{R}_3$
Vectors locating origins of revolutes	$\vec{O}_1, \vec{O}_2, \vec{O}_3$

3.1.3 Actuated Link Lengths

The spatial positions of the actuated nodal points, B_1, B_2, and B_3, can be expressed as a function of the fixed vector quantities and the revolute angles identified in Section 3.1.2. The three vectors, for $i = 1, 2, 3$, locating the three vertices of the actuated plane triangle are given by

$$\vec{B}_i = \vec{O}_i + [\mathbf{R}_{\theta_i,\hat{U}_i}]\vec{R}_i \tag{3.7}$$

where $[\mathbf{R}_{\theta_i,\hat{U}_i}]$ is the rotation matrix rotating the reference vector, $\vec{R}_i$, about the unit axis, $\hat{U}_i$, by an amount θ_i. Expanding the above equation results in

$$\vec{B}_i = \begin{bmatrix} (U_{xi}^2 v\theta_i + c\theta_i)R_{xi} + (U_{xi}U_{yi}v\theta_i - U_{zi}s\theta_i)R_{yi} + (U_{xi}U_{zi}v\theta_i + U_{yi}s\theta_i)R_{zi} + O_{xi} \\ (U_{xi}U_{yi}v\theta_i + U_{zi}s\theta_i)R_{xi} + (U_{yi}^2 v\theta_i + c\theta_i)R_{yi} + (U_{yi}U_{zi}v\theta_i - U_{xi}s\theta_i)R_{zi} + O_{yi} \\ (U_{xi}U_{zi}v\theta_i - U_{yi}s\theta_i)R_{xi} + (U_{yi}U_{zi}v\theta_i + U_{xi}s\theta_i)R_{yi} + (U_{zi}^2 v\theta_i + c\theta_i)R_{zi} + O_{zi} \end{bmatrix} \tag{3.8}$$

where

$$v\theta_i = 1 - \cos\theta_i$$

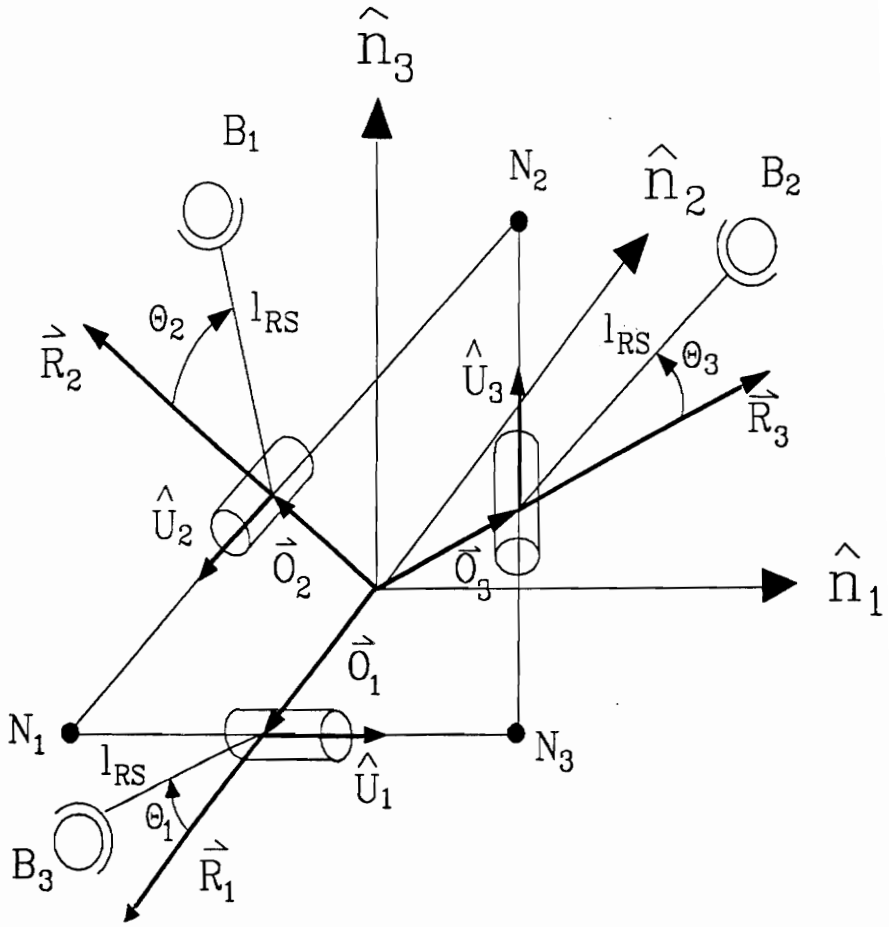

Figure 3.4: Equivalent Kinematic Model of Truss

$$s\theta_i = \sin\theta_i$$

$$c\theta_i = \cos\theta_i$$

Referring to Fig. 3.3, the unit vector normal to the actuated plane, $\vec{U}_{n1}$, and the vector specifying the origin of the moving reference frame, $\vec{P}m_{org}$, are co linear. Consequently, this unit vector is now defined as

$$\hat{U}_{n1} = \frac{\vec{P}m_{org}}{|\ \vec{P}m_{org}\ |} \tag{3.9}$$

Noting that the vertices, or the nodal points, of the actuated plane, B_1, B_2, and B_3, are constrained to this plane, a set of constraint equations are obtained by observing that $(\vec{B}_i - \vec{P}m_{org}/2)$ is a vector lying in the actuated plane. This vector must be normal to the unit normal vector, $\hat{U}_{n1}$, such that

$$\left[\vec{B}_i - \frac{\vec{P}m_{org}}{2}\right] \bullet \hat{U}_{n1} = 0 \tag{3.10}$$

Substituting the expression for $\vec{B}_i$ from equation 3.8 into the above equation, the Newtonian coordinates of the vertices of the actuated plane are found, for $i = 1, 2, 3$, as follows

$$\begin{aligned} B_{xi} &= k_{1i} + k_{4i}C\theta_i + k_{7i}S\theta_i \\ B_{yi} &= k_{2i} + k_{5i}C\theta_i + k_{8i}S\theta_i \\ B_{zi} &= k_{3i} + k_{6i}C\theta_i + k_{9i}S\theta_i \end{aligned} \tag{3.11}$$

where the intermediate variables are defined as

$$\begin{aligned}
k_{1i} &= R_{xi}U_{xi}^2 + R_{yi}U_{yi}U_{xi} + R_{zi}U_{zi}U_{xi} + O_{xi} \\
k_{2i} &= R_{yi}U_{yi}^2 + R_{xi}U_{xi}U_{yi} + R_{zi}U_{zi}U_{yi} + O_{yi} \\
k_{3i} &= R_{zi}U_{zi}^2 + R_{xi}U_{xi}U_{zi} + R_{yi}U_{yi}U_{zi} + O_{zi} \\
k_{4i} &= R_{xi}(1 - U_{xi}^2) - R_{yi}U_{yi}U_{xi} - R_{zi}U_{zi}U_{xi} \\
k_{5i} &= R_{yi}(1 - U_{yi}^2) - R_{xi}U_{xi}U_{yi} - R_{zi}U_{zi}U_{yi} \\
k_{6i} &= R_{zi}(1 - U_{zi}^2) - R_{xi}U_{xi}U_{zi} - R_{yi}U_{yi}U_{zi} \\
k_{7i} &= R_{zi}U_{yi} - R_{yi}U_{zi} \\
k_{8i} &= R_{xi}U_{zi} - R_{zi}U_{xi} \\
k_{9i} &= R_{yi}U_{xi} - R_{xi}U_{yi}
\end{aligned} \tag{3.12}$$

and

$$\begin{aligned}
C\theta_i &= \frac{a_{3i}^2 - a_{3i}a_{1i} - a_{2i}^2 + a_{2i}\sqrt{a_{2i}^2 - a_{3i}^2 + a_{1i}^2}}{a_{1i}^2 - a_{3i}a_{1i} + a_{2i}^2 - a_{2i}\sqrt{a_{2i}^2 - a_{3i}^2 + a_{1i}^2}} \\
S\theta_i &= \frac{-a_{2i} + \sqrt{a_{2i}^2 - a_{3i}^2 + a_{1i}^2}(a_{3i} - a_{1i})}{a_{1i}^2 - a_{3i}a_{1i} + a_{2i}^2 - a_{2i}\sqrt{a_{2i}^2 - a_{3i}^2 + a_{1i}^2}}
\end{aligned} \tag{3.13}$$

for

$$\begin{aligned}
a_{1i} &= k_{4i}X + k_{5i}Y + k_{6i}Z \\
a_{2i} &= k_{7i}X + k_{8i}Y + k_{9i}Z \\
a_{3i} &= k_{1i}X + k_{2i}Y + k_{3i}Z - \frac{X^2}{2} - \frac{Y^2}{2} - \frac{Z^2}{2}
\end{aligned} \tag{3.14}$$

Back-solving the above set of equations (3.14, 3.13, 3.12) and 3.11, the active batten lengths are found by calculating the spatial distance between the actuated plane vertices and are determined as

$$\begin{aligned}
l_1 &= \sqrt{(B_{x3} - B_{x2})^2 + (B_{y3} - B_{y2})^2 + (B_{z3} - B_{z2})^2} \\
l_2 &= \sqrt{(B_{x1} - B_{x3})^2 + (B_{y1} - B_{y3})^2 + (B_{z1} - B_{z3})^2} \\
l_3 &= \sqrt{(B_{x2} - B_{x1})^2 + (B_{y2} - B_{y1})^2 + (B_{z2} - B_{z1})^2}
\end{aligned} \tag{3.15}$$

These are the active link positions that mathematically satisfy the three slew inputs, γ, β, and d. It is, however, possible to choose a set of slew inputs that do not physically satisfy the above equations for the truss dimensions specified in Chapter 2. This condition is checked by observing the sign of $a_{2i}^2 - a_{3i}^2 + a_{1i}^2$ inside the square-

root expression of equation 3.13. If the sign is negative there is no real solution of equations 3.13, and consequently there is no physically realizable assembly of the double-octahedral adaptive truss for the specified slew inputs.

3.2 Forward Solution

If the positions of the active batten links, $\vec{L}$, are known and the slewed position (γ, β, and d) of the truss is desired, the forward solution must be solved. The forward solution is an iterative procedure requiring numerical techniques, but by taking advantage of the equivalent kinematic model discussed in Section 3.1.2, the solution is made easier. By using the kinematic angles, θ_1, θ_2, and θ_3, instead of the slew parameters, γ, β, and d, to describe the position of the adaptive truss, iterations on the equations of Section 3.1.3 can be performed to find the equivalent kinematic angles satisfying the known link positions. Once the iteration is complete and the kinematic angles are known, the slew parameters can be determined from these angles. The details to the above approach are as follows.

3.2.1 Solution Method for Finding the Equivalent Kinematic Angles

In general, the active link lengths are explicit functions of the three equivalent kinematic angles and are generically expressed as

$$\begin{aligned} l_1 &= f_1(\theta_1, \theta_2, \theta_3) \\ l_2 &= f_2(\theta_1, \theta_2, \theta_3) \\ l_3 &= f_3(\theta_1, \theta_2, \theta_3) \end{aligned} \tag{3.16}$$

where the three functions, f_1, f_2, and f_3, are found by combining equation 3.8 and

equation 3.15. Given the lengths of the active battens, the set of angles or roots that satisfy the above equation can be found by employing the Newton-Raphson iteration technique. For a single scalar problem, an improved estimate is generated from an initial estimate using the following recursive equation,

$$x_{n+1} = x_n - \frac{g(x_n)}{g'(x_n)}$$

Rearranging the above equation, we obtain

$$g'(x_n)(x_{n+1} - x_n) = -g(x_n)$$

For the three-variable system given by equation 3.16, the equivalent vector expression is

$$\begin{bmatrix} \frac{\partial G_1}{\partial \theta_1} & \frac{\partial G_1}{\partial \theta_2} & \frac{\partial G_1}{\partial \theta_3} \\ \frac{\partial G_2}{\partial \theta_1} & \frac{\partial G_2}{\partial \theta_2} & \frac{\partial G_2}{\partial \theta_3} \\ \frac{\partial G_3}{\partial \theta_1} & \frac{\partial G_3}{\partial \theta_2} & \frac{\partial G_3}{\partial \theta_3} \end{bmatrix} \left(\begin{bmatrix} \theta_1 \\ \theta_2 \\ \theta_3 \end{bmatrix}_{n+1} - \begin{bmatrix} \theta_1 \\ \theta_2 \\ \theta_3 \end{bmatrix}_n \right) = \begin{bmatrix} -G_1 \\ -G_2 \\ -G_3 \end{bmatrix} \tag{3.17}$$

where

$$G_1 = f_1(\theta_1, \theta_2, \theta_3)_n - l_1$$

$$G_2 = f_2(\theta_1, \theta_2, \theta_3)_n - l_2$$

$$G_3 = f_3(\theta_1, \theta_2, \theta_3)_n - l_3$$

The partial derivatives of the functions, G_1, G_2, and G_3, with respect to the equivalent kinematic angles, are found by using a finite-difference approximation. Once

these partials are created the new estimate of the kinematic angles are evaluated as

$$\begin{bmatrix} \theta_1 \\ \theta_2 \\ \theta_3 \end{bmatrix}_{n+1} = \begin{bmatrix} \theta_1 \\ \theta_2 \\ \theta_3 \end{bmatrix}_n + \begin{bmatrix} \frac{\partial G_1}{\partial \theta_1} & \frac{\partial G_1}{\partial \theta_2} & \frac{\partial G_1}{\partial \theta_3} \\ \frac{\partial G_2}{\partial \theta_1} & \frac{\partial G_2}{\partial \theta_2} & \frac{\partial G_2}{\partial \theta_3} \\ \frac{\partial G_3}{\partial \theta_1} & \frac{\partial G_3}{\partial \theta_2} & \frac{\partial G_3}{\partial \theta_3} \end{bmatrix}^{-1} \begin{bmatrix} -G_1 \\ -G_2 \\ -G_3 \end{bmatrix} \tag{3.18}$$

The above equation is recursively applied until convergence is achieved such that $G_1 = G_2 = G_3 = 0$, within a prespecified tolerance. Consequently, the values for θ_1, θ_2, and θ_3 are approximately true with greater accuracy achieved by specifying a stricter tolerance.

3.2.2 Slew Position Parameters

The orientation of the top plane is given by the unit vector, $\hat{U}_{n2}$, normal to the top plane. To find $\hat{U}_{n2}$ the unit vectors $\hat{U}_{n1}$ and $\hat{U}_{n0}$ must be determined and geometric insight employed.

Knowing the equivalent kinematic angles, the vectors locating the actuated nodes, $\vec{B}_1$, $\vec{B}_2$, and $\vec{B}_3$, are easily evaluated from equation 3.8. The unit vector, $\hat{U}_{n1}$, normal to the actuated plane is determined from these vectors by forming relative position vectors between the actuated nodes and performing the cross product. This unit vector is given by

$$\hat{U}_{n1} = \frac{(\vec{B}_1 - \vec{B}_2) \times (\vec{B}_1 - \vec{B}_3)}{|\,(\vec{B}_1 - \vec{B}_2) \times (\vec{B}_1 - \vec{B}_3)\,|} \tag{3.19}$$

The unit vector, $\hat{U}_{n0}$, normal to the fixed plane is fixed to the Newtonian reference frame and is given by equation 3.2.

The scalar distance r shown in Fig. 3.3 is found by projecting one of the actuated node vectors, $\vec{B}_1$ for this case, onto the unit normal vector, $\hat{U}_{n1}$, and then applying Pythagorean's Theorem. The distance r is found by

$$r = \frac{\vec{B}_1 \bullet \hat{U}_{n1}}{\hat{U}_{n0} \bullet \hat{U}_{n1}} \tag{3.20}$$

The gimbal axes offset distance d, also shown in Fig. 3.3, is also found from Pythagorean's Theorem and is given as

$$d = 2r(\hat{U}_{n1} \bullet \hat{U}_{n0}) \tag{3.21}$$

The unit normal vector, $\hat{U}_{n2}$, to the top plane can now be determined from the loop closure equation 3.3. The orientation of the top plane of the adaptive truss is determined by projecting x, y, and z components of $\hat{U}_{n2}$ on the fixed Newtonian frame. The resulting pitch, γ, and roll, β, angles are determined as

$$\begin{aligned} \gamma &= \arctan\left(\frac{-U_{n2y}}{U_{n2z}}\right) \\ \beta &= \arctan\left(\frac{U_{n2x}}{\sqrt{U_{n2y}^2+U_{n2z}^2}}\right) \end{aligned} \tag{3.22}$$

3.3 Velocity and Acceleration Analysis

General closed-form techniques are applied to find the velocities and accelerations of the double-octahedral adaptive truss. The method of analysis is based on strut-length constraint equations. These equations each express the constraint of a known

strut-length between two truss nodes and are of the form

$$(l_{ij})^2 = (\vec{N}_i - \vec{N}_j) \bullet (\vec{N}_i - \vec{N}_j) \tag{3.23}$$

for all 21 combinations of i and j that correspond to the 21 fixed and variable strut-links of the double-octahedral adaptive truss as labeled in Fig. 3.5. The velocity and acceleration equations are found by taking the time derivative of equation 3.23 once and twice, respectively. They are given as

$$2l_{ij}\dot{l}_{ij} = 2(\vec{N}_i - \vec{N}_j) \bullet (\dot{\vec{N}}_i - \dot{\vec{N}}_j) \tag{3.24}$$

$$\dot{l}_{ij}\dot{l}_{ij} + l_{ij}\ddot{l}_{ij} = (\dot{\vec{N}}_i - \dot{\vec{N}}_j) \bullet (\dot{\vec{N}}_i - \dot{\vec{N}}_j) + (\vec{N}_i - \vec{N}_j) \bullet (\ddot{\vec{N}}_i - \ddot{\vec{N}}_j) \tag{3.25}$$

The above equations are useful only if the nodal positions of the truss are known. This position-dependency of the velocity and acceleration equations requires that the nodal positions be analyzed each time the velocity and acceleration equations are evaluated.

3.3.1 Nodal Position Analysis

The analysis begins with describing the spatial locations of the nine vertices or nodes of the double-octahedral adaptive truss. The numbering scheme of these truss nodes are shown in Fig. 3.5. The spatial positions of the actuated nodes, N_4, N_5, and N_6, have already been found as described in Section 3.1.3 ($N_4 = B_1$, $N_5 = B_2$, $N_6 = B_3$). The fixed nodes of the truss locating the vertices of the fixed plane triangle, N_1, N_2, and N_3, can easily be found by observing the geometry of the fixed

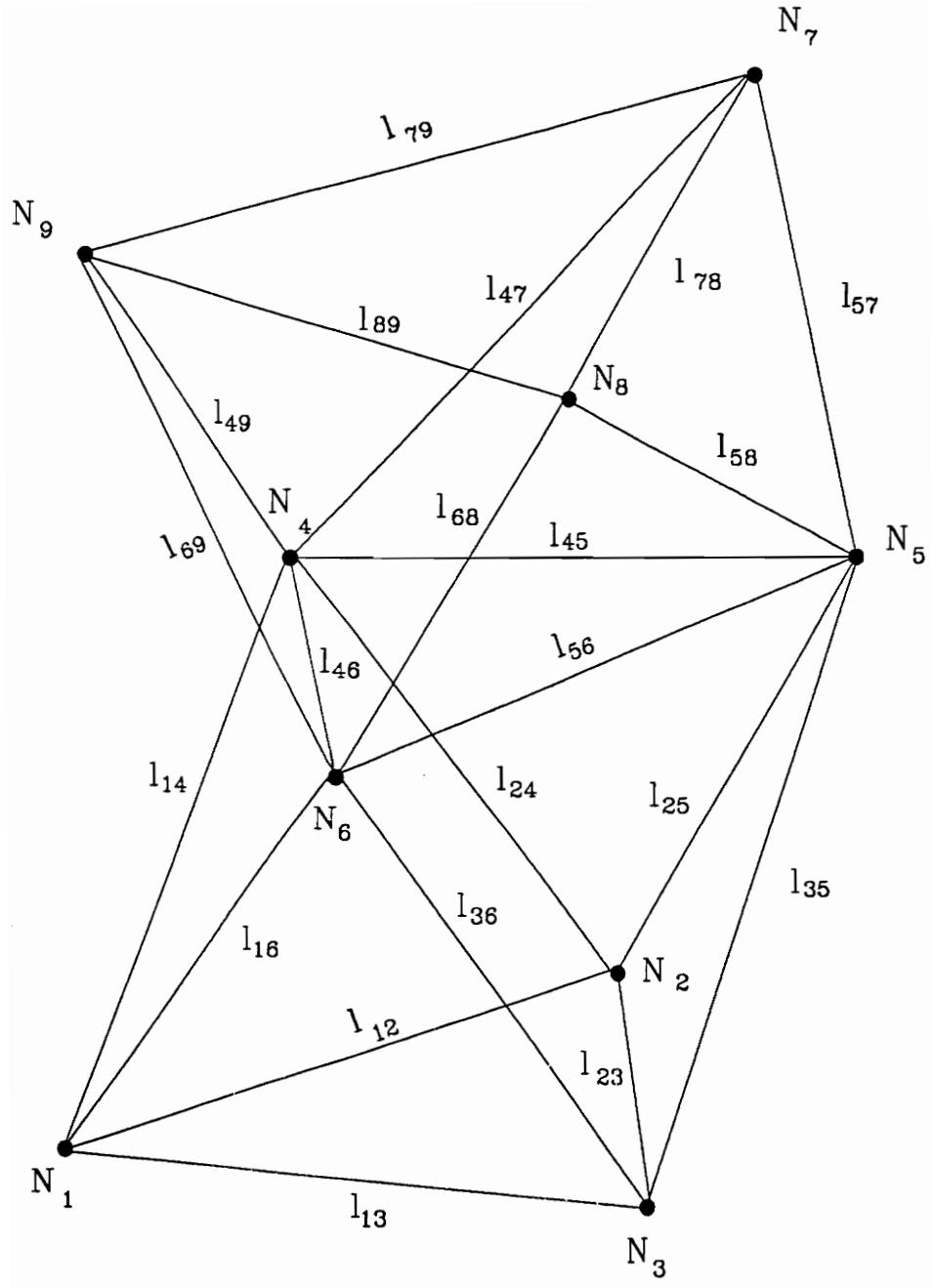

Figure 3.5: Truss Node and Strut-Link Nomenclature

plane triangle shown in Fig. 3.6. Vector addition with respect to the Newtonian reference frame yields

$$\begin{aligned} \vec{N}_1 &= \vec{O}_1 - \hat{U}_1 \tfrac{l_b}{2} \\ \vec{N}_2 &= \vec{O}_2 - \hat{U}_2 \tfrac{l_b}{2} \\ \vec{N}_3 &= \vec{O}_3 - \hat{U}_3 \tfrac{l_b}{2} \end{aligned} \tag{3.26}$$

where l_b is the scalar length of the base strut as specified in Chapter 2, and $\vec{O}_i$ and $\hat{U}_i$, for $i = 1, 2, 3$, are fixed vectors specified in Section 3.1.2.

Next, the nodal positions, N_7, N_8, and N_9, of the top plane are determined. The spatial location of the geometrical center of the top triangular plane, and equivalently the origin of the moving reference frame, has been previously specified as $\vec{P}m_{org}$ by equation 3.5. Three fixed vectors, $\vec{B}_7$, $\vec{B}_8$, and $\vec{B}_9$, relative to the moving reference frame are drawn from the origin of the moving frame to each of the top plane nodes as shown in Fig. 3.7. Vector addition may be performed to obtain the spatial locations of the top plane nodes. But first, the vectors, $\vec{B}_7$, $\vec{B}_8$, and $\vec{B}_9$, must be oriented with respect to the Newtonian reference frame by premultiplying by a rotation transformation.

The rotation transformation is a roll, pitch, and yaw rotation description about the fixed Newtonian axes. The roll angle (γ), rotation about the $\hat{n}_1$-axis, and pitch angle (β), rotation about the $\hat{n}_2$-axis, are previously specified as inputs to the slew position analysis in Section 3.1. The yaw angle (α), is the rotation about the $\hat{n}_3$-axis, or "twist" that the adaptive truss possesses as a result of specifying the orientation

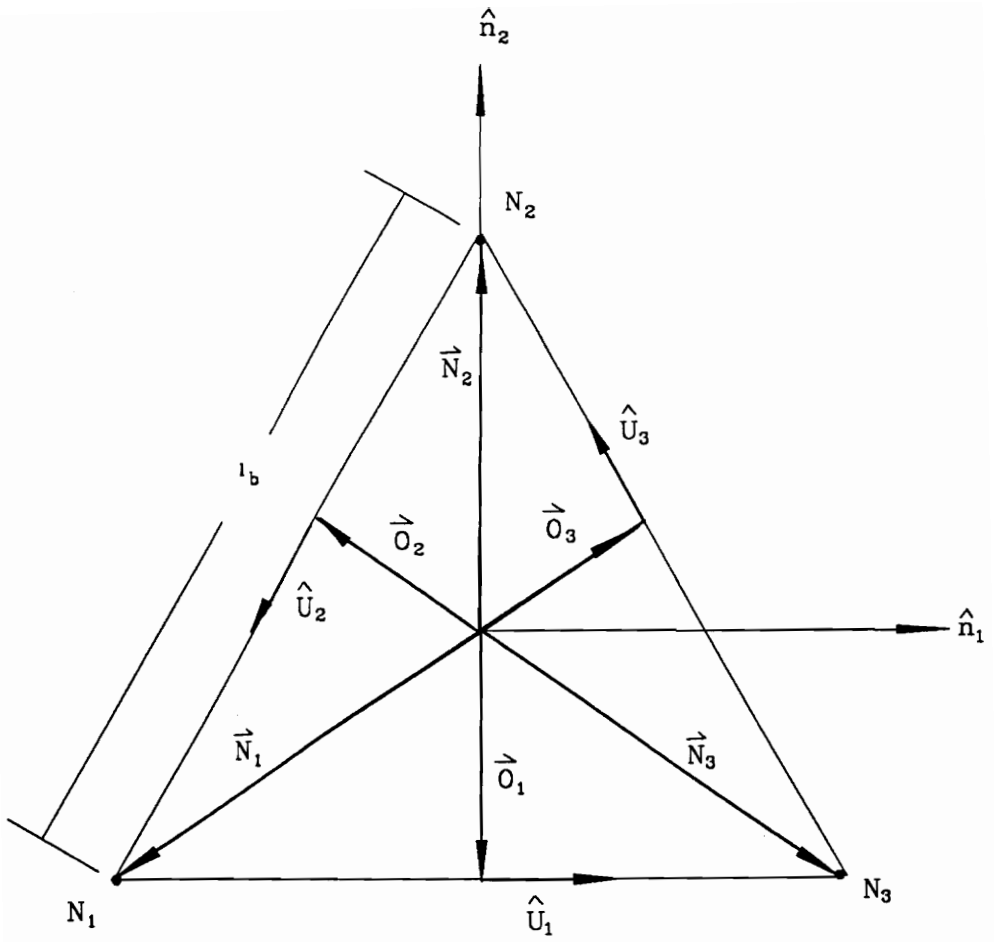

Figure 3.6: Fixed Plane Vectors

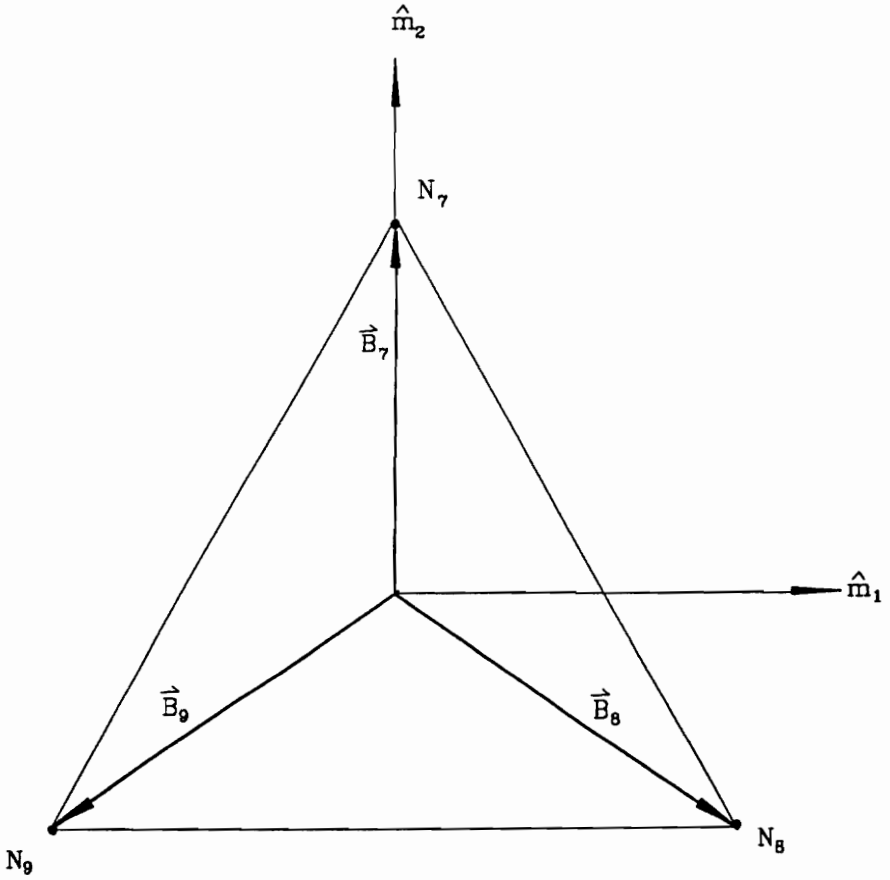

Figure 3.7: Top Plane Vectors

of the top plane. It is dependent on the pitch and roll angles and is given by

$$\alpha = \arctan \frac{\sin\gamma \sin\beta}{\cos\gamma + \cos\beta} \tag{3.27}$$

The rotation matrix is the product of the yaw rotation matrix, pitch rotation matrix, and roll rotation matrix and is

$$[\mathbf{R}_{\gamma,\beta,\alpha}] = \begin{bmatrix} 1 & 0 & 0 \\ 0 & c\gamma & s\gamma \\ 0 & -s\gamma & c\gamma \end{bmatrix} \begin{bmatrix} c\beta & 0 & -s\beta \\ 0 & 1 & 0 \\ s\beta & 0 & c\beta \end{bmatrix} \begin{bmatrix} c\alpha & s\alpha & 0 \\ -s\alpha & c\alpha & 0 \\ 0 & 0 & 1 \end{bmatrix} \tag{3.28}$$

where again $c\gamma$ is shorthand for $\cos\gamma$ and $s\gamma$ for $\sin\gamma$, etc. Performing the matrix multiplication, the rotation matrix becomes

$$[\mathbf{R}_{\gamma,\beta,\alpha}] = \begin{bmatrix} c\alpha c\beta + s\alpha s\beta s\gamma & s\alpha c\gamma & c\alpha s\beta - s\alpha s\gamma c\beta \\ -s\alpha c\beta + c\alpha + s\beta s\gamma & c\alpha c\gamma & -s\alpha s\beta - c\alpha s\gamma c\beta \\ -s\beta c\gamma & s\gamma & c\beta c\gamma \end{bmatrix} \tag{3.29}$$

Now, the vectors, $\vec{B}_7$, $\vec{B}_8$, and $\vec{B}_9$, can be properly rotated with respect to the Newtonian reference frame. Vector addition results with the spatial position of the top plane nodes determined as

$$\begin{aligned} \vec{N}_7 &= \vec{P}m_{org} + [\mathbf{R}_{\gamma,\beta,\alpha}]\vec{B}_7 \\ \vec{N}_8 &= \vec{P}m_{org} + [\mathbf{R}_{\gamma,\beta,\alpha}]\vec{B}_8 \\ \vec{N}_9 &= \vec{P}m_{org} + [\mathbf{R}_{\gamma,\beta,\alpha}]\vec{B}_9 \end{aligned} \tag{3.30}$$

The spatial positions of all nine nodes of the adaptive truss, $\vec{N}_i$, for $i = 1, \ldots, 9$, are now represented in the Newtonian reference frame. The nodal position analysis is complete.

3.3.2 Velocity Analysis

The velocity analysis begins with the velocity expression given by equation 3.24 as

$$2l_{ij}\dot{l}_{ij} = 2(\vec{N}_i - \vec{N}_j) \bullet (\dot{\vec{N}}_i - \dot{\vec{N}}_j)$$

The position-dependent terms are combined to form a 1×3 position unit vector along the length of the strut and are given by

$$\hat{p}_{ij} = \frac{(\vec{N}_i - \vec{N}_j)^T}{l_{ij}} \tag{3.31}$$

Substituting the position unit vector into equation 3.24, results in

$$\dot{l}_{ij} = \hat{p}_{ij} \bullet (\dot{\vec{N}}_i - \dot{\vec{N}}_j)^T \tag{3.32}$$

The quantity $\dot{l}_{ij}$ is the scalar link velocity and is the difference between the velocities of the nodes in the direction of the strut link. These equations are written and assembled for each of the two octahedral bays of the double-octahedral adaptive truss. Knowing all the positions, all the $\vec{N}_i$'s and l_{ij}'s, the system of velocity equations for the first bay is expressed as

$$\begin{bmatrix} \dot{l}_{14} \\ \dot{l}_{24} \\ \dot{l}_{45} \\ \dot{l}_{25} \\ \dot{l}_{46} \\ \dot{l}_{35} \\ \dot{l}_{56} \\ \dot{l}_{36} \\ \dot{l}_{16} \end{bmatrix} = \begin{bmatrix} \hat{p}_{14} & 0 & 0 \\ 0 & \hat{p}_{24} & 0 \\ 0 & 0 & 0 \\ 0 & \hat{p}_{25} & 0 \\ 0 & 0 & 0 \\ 0 & 0 & \hat{p}_{35} \\ 0 & 0 & 0 \\ 0 & 0 & \hat{p}_{36} \\ \hat{p}_{16} & 0 & 0 \end{bmatrix} \begin{bmatrix} \dot{\vec{N}}_1 \\ \dot{\vec{N}}_2 \\ \dot{\vec{N}}_3 \end{bmatrix} + \begin{bmatrix} -\hat{p}_{14} & 0 & 0 \\ -\hat{p}_{24} & 0 & 0 \\ \hat{p}_{45} & -\hat{p}_{45} & 0 \\ 0 & -\hat{p}_{25} & 0 \\ \hat{p}_{46} & 0 & -\hat{p}_{46} \\ 0 & -\hat{p}_{35} & 0 \\ 0 & \hat{p}_{56} & -\hat{p}_{56} \\ 0 & 0 & -\hat{p}_{36} \\ 0 & 0 & -\hat{p}_{16} \end{bmatrix} \begin{bmatrix} \dot{\vec{N}}_4 \\ \dot{\vec{N}}_5 \\ \dot{\vec{N}}_6 \end{bmatrix} \tag{3.33}$$

where the zeros in the above matrices are 1×3 zero vectors such that the matrices are 9×9 square, and the vectors, $\vec{N}_i$'s, are 3×1. Equivalently the above equation is expressed as

$$\dot{\vec{L}}_1 = [\mathbf{R_1}] \begin{bmatrix} \dot{\vec{N}}_1 \\ \dot{\vec{N}}_2 \\ \dot{\vec{N}}_3 \end{bmatrix} + [\mathbf{P_1}] \begin{bmatrix} \dot{\vec{N}}_4 \\ \dot{\vec{N}}_5 \\ \dot{\vec{N}}_6 \end{bmatrix} \tag{3.34}$$

Only three struts, the three active batten links ($l_{45} = l_1$, $l_{46} = l_2$, $l_{56} = l_3$), of the first octahedral bay are variable length members. Hence, they are the only links capable of changing length. The vector of scalar link velocities of the first octahedral bay, $\dot{\vec{L}}_1$, reduces to

$$\dot{\vec{L}}_1 = \begin{bmatrix} 0 \\ 0 \\ \dot{l}_1 \\ 0 \\ \dot{l}_2 \\ 0 \\ \dot{l}_3 \\ 0 \\ 0 \end{bmatrix} \tag{3.35}$$

Nodes, N_1, N_2, and N_3, are fixed to ground, and consequently their rates are zero. Equation 3.34 reduces to

$$\dot{\vec{L}}_1 = [\mathbf{P_1}] \begin{bmatrix} \dot{\vec{N}}_4 \\ \dot{\vec{N}}_5 \\ \dot{\vec{N}}_6 \end{bmatrix} \tag{3.36}$$

At this point, it is important to note that since the octahedral unit cell of the adaptive truss is a statically determinate truss, the unit position vectors, $\hat{p}_{ij}$ of $[\mathbf{P_1}]$ are unique, such that $[\mathbf{P_1}]$ has no linearly dependent rows and is full rank. Consequently, $[\mathbf{P_1}]$ is invertible, and the nodal velocities, $\dot{\vec{N}}_4$, $\dot{\vec{N}}_5$, and $\dot{\vec{N}}_6$, are

readily solved by rearranging the above equation to give

$$\begin{bmatrix} \dot{\vec{N}}_4 \\ \dot{\vec{N}}_5 \\ \dot{\vec{N}}_6 \end{bmatrix} = [\mathbf{P_1}]^{-1} \dot{\vec{L}}_1 \tag{3.37}$$

A system of velocity equations are similarly written for the second octahedral bay, and are expressed as

$$\begin{bmatrix} \dot{l}_{47} \\ \dot{l}_{57} \\ \dot{l}_{78} \\ \dot{l}_{58} \\ \dot{l}_{79} \\ \dot{l}_{68} \\ \dot{l}_{89} \\ \dot{l}_{69} \\ \dot{l}_{49} \end{bmatrix} = \begin{bmatrix} \hat{p}_{47} & 0 & 0 \\ 0 & \hat{p}_{57} & 0 \\ 0 & 0 & 0 \\ 0 & \hat{p}_{58} & 0 \\ 0 & 0 & 0 \\ 0 & 0 & \hat{p}_{68} \\ 0 & 0 & 0 \\ 0 & 0 & \hat{p}_{69} \\ \hat{p}_{49} & 0 & 0 \end{bmatrix} \begin{bmatrix} \dot{\vec{N}}_4 \\ \dot{\vec{N}}_5 \\ \dot{\vec{N}}_6 \end{bmatrix} + \begin{bmatrix} -\hat{p}_{47} & 0 & 0 \\ -\hat{p}_{57} & 0 & 0 \\ \hat{p}_{78} & -\hat{p}_{78} & 0 \\ 0 & -\hat{p}_{58} & 0 \\ \hat{p}_{79} & 0 & -\hat{p}_{79} \\ 0 & -\hat{p}_{68} & 0 \\ 0 & \hat{p}_{89} & -\hat{p}_{89} \\ 0 & 0 & -\hat{p}_{69} \\ 0 & 0 & -\hat{p}_{49} \end{bmatrix} \begin{bmatrix} \dot{\vec{N}}_7 \\ \dot{\vec{N}}_8 \\ \dot{\vec{N}}_9 \end{bmatrix} \tag{3.38}$$

or

$$\dot{\vec{L}}_2 = [\mathbf{R_2}] \begin{bmatrix} \dot{\vec{N}}_4 \\ \dot{\vec{N}}_5 \\ \dot{\vec{N}}_6 \end{bmatrix} + [\mathbf{P_2}] \begin{bmatrix} \dot{\vec{N}}_7 \\ \dot{\vec{N}}_8 \\ \dot{\vec{N}}_9 \end{bmatrix} \tag{3.39}$$

None of the strut lengths of the second octahedral bay are variable length members and thus, $\dot{\vec{L}}_2 = 0$. Rearranging equation 3.39 and again noting that $[\mathbf{P_2}]$ is invertible since the second octahedral bay is a statically determinate truss, the nodal velocities of the top plane are solved as

$$\begin{bmatrix} \dot{\vec{N}}_7 \\ \dot{\vec{N}}_8 \\ \dot{\vec{N}}_9 \end{bmatrix} = -[\mathbf{P_2}]^{-1}[\mathbf{R_2}] \begin{bmatrix} \dot{\vec{N}}_4 \\ \dot{\vec{N}}_5 \\ \dot{\vec{N}}_6 \end{bmatrix} \tag{3.40}$$

Substituting equation 3.37 into the above equation gives the nodal velocities of the top plane as a function of the actuated batten links. This relationship is given by

$$\begin{bmatrix} \dot{\vec{N}}_7 \\ \dot{\vec{N}}_8 \\ \dot{\vec{N}}_9 \end{bmatrix} = -[\mathbf{P_2}]^{-1}[\mathbf{R_2}][\mathbf{P_1}]^{-1}\dot{\vec{L}}_1 \tag{3.41}$$

The velocities of the nodes of the adaptive truss, $\dot{\vec{N}}_i$, for $i = 1, \ldots, 9$, are now determined and represented in the Newtonian reference frame.

3.3.3 Velocity of Mid-Point of Top Plane

The velocities of the mid-point of the top plane, or the origin of the moving reference frame, are found by exploiting the special geometry of the top plane. Since the top plane is an equilateral triangle, the Newtonian position, $\vec{P}m_{org} = [X\ Y\ Z]^T$, of the center of this triangle is described by

$$\vec{P}m_{org} = \frac{\vec{N}_7 + \vec{N}_8 + \vec{N}_9}{3} \tag{3.42}$$

Differentiating with respect to time leads to the velocity of the origin of the moving reference frame, and results in

$$\dot{\vec{P}}m_{org} = \frac{\dot{\vec{N}}_7 + \dot{\vec{N}}_8 + \dot{\vec{N}}_9}{3} \tag{3.43}$$

3.3.4 Angular Velocities

Since the top plane of the adaptive truss is a rigid body, relative velocity equations can be written between any two of the three nodes of the top plane. Relative velocity equations between nodes 7 and 8 and 7 and 9 are given as

$$\begin{aligned} \dot{\vec{N}}_7 &= \dot{\vec{N}}_8 + \vec{\Omega} \times \vec{R}_{7/8} \\ \dot{\vec{N}}_7 &= \dot{\vec{N}}_9 + \vec{\Omega} \times \vec{R}_{7/9} \end{aligned} \tag{3.44}$$

where

$$\vec{\Omega} = \begin{bmatrix} \dot{\gamma} \\ \dot{\beta} \\ \dot{\alpha} \end{bmatrix}$$

$\vec{R}_{7/8}$ and $\vec{R}_{7/9}$ are relative position vectors of node 7 to node 8 and node 7 to node 9, respectively. They are given by

$$\begin{aligned} \vec{R}_{7/8} &= \vec{N}_7 - \vec{N}_8 \\ \vec{R}_{7/9} &= \vec{N}_7 - \vec{N}_9 \end{aligned} \tag{3.45}$$

Equation 3.44 represents two vector equations, or equivalently a system of six scalar equations, with only three unknowns, $\dot{\gamma}$, $\dot{\beta}$, and $\dot{\alpha}$. The redundancy of these six equations are readily apparent when equation 3.44 is expanded as

$$\begin{bmatrix} \dot{N}_{7x} - \dot{N}_{8x} \\ \dot{N}_{7y} - \dot{N}_{8y} \\ \dot{N}_{7z} - \dot{N}_{8z} \end{bmatrix} = \begin{bmatrix} 0 & R_{78z} & -R_{78y} \\ -R_{78y} & R_{78x} & 0 \\ -R_{78z} & 0 & R_{78x} \end{bmatrix} \begin{bmatrix} \dot{\gamma} \\ \dot{\beta} \\ \dot{\alpha} \end{bmatrix}$$

$$\begin{bmatrix} \dot{N}_{7x} - \dot{N}_{9x} \\ \dot{N}_{7y} - \dot{N}_{9y} \\ \dot{N}_{7z} - \dot{N}_{9z} \end{bmatrix} = \begin{bmatrix} 0 & R_{79z} & -R_{79y} \\ -R_{79y} & R_{79x} & 0 \\ -R_{79z} & 0 & R_{79x} \end{bmatrix} \begin{bmatrix} \dot{\gamma} \\ \dot{\beta} \\ \dot{\alpha} \end{bmatrix} \tag{3.46}$$

The diagonals of both of the above 3×3 matrices are zeros, hence they are singular. But, by forming a set of three independent scalar equations from the available six,

the angular velocities can be determined from the following

$$\begin{bmatrix} \dot{\gamma} \\ \dot{\beta} \\ \dot{\alpha} \end{bmatrix} = \begin{bmatrix} 0 & R_{78z} & -R_{78y} \\ R_{79z} & 0 & -R_{79x} \\ -R_{78z} & 0 & R_{78x} \end{bmatrix}^{-1} \begin{bmatrix} \dot{N}_{7x} - \dot{N}_{8x} \\ \dot{N}_{7y} - \dot{N}_{8y} \\ \dot{N}_{7y} - \dot{N}_{9y} \end{bmatrix} \tag{3.47}$$

3.3.5 Acceleration Analysis

The acceleration analysis begins with the acceleration relationship of equation 3.25 given as

$$\dot{l}_{ij}\dot{l}_{ij} + l_{ij}\ddot{l}_{ij} = (\dot{\vec{N}}_i - \dot{\vec{N}}_j) \bullet (\dot{\vec{N}}_i - \dot{\vec{N}}_j) + (\vec{N}_i - \vec{N}_j) \bullet (\ddot{\vec{N}}_i - \ddot{\vec{N}}_j)$$

Solving for the second time derivative of a general strut link results in

$$\ddot{l}_{ij} = \frac{(\dot{\vec{N}}_i - \dot{\vec{N}}_j) \bullet (\dot{\vec{N}}_i - \dot{\vec{N}}_j) - (\dot{l}_{ij})^2 + (\vec{N}_i - \vec{N}_j) \bullet (\ddot{\vec{N}}_i - \ddot{\vec{N}}_j)}{l_{ij}} \tag{3.48}$$

letting

$$q_{ij} = \frac{(\dot{\vec{N}}_i - \dot{\vec{N}}_j) \bullet (\dot{\vec{N}}_i - \dot{\vec{N}}_j) - (\dot{l}_{ij})^2}{l_{ij}} \tag{3.49}$$

and using $\hat{p}_{ij}$ as defined in equation 3.31, equation 3.48 becomes

$$\ddot{l}_{ij} = q_{ij} + \hat{p}_{ij} \bullet (\ddot{\vec{N}}_i - \ddot{\vec{N}}_j) \tag{3.50}$$

With the nodal positions and velocities previously specified, the nodal accelerations can be determined by writing equation 3.50 for each strut of the adaptive truss. The system of acceleration equations for the first octahedral bay of the truss is

$$\begin{bmatrix} \ddot{l}_{14} \\ \ddot{l}_{24} \\ \ddot{l}_{45} \\ \ddot{l}_{25} \\ \ddot{l}_{46} \\ \ddot{l}_{35} \\ \ddot{l}_{56} \\ \ddot{l}_{36} \\ \ddot{l}_{16} \end{bmatrix} = \begin{bmatrix} q_{14} \\ q_{24} \\ q_{45} \\ q_{25} \\ q_{46} \\ q_{35} \\ q_{56} \\ q_{36} \\ q_{16} \end{bmatrix} + \begin{bmatrix} \hat{p}_{14} & 0 & 0 \\ 0 & \hat{p}_{24} & 0 \\ 0 & 0 & 0 \\ 0 & \hat{p}_{25} & 0 \\ 0 & 0 & 0 \\ 0 & 0 & \hat{p}_{35} \\ 0 & 0 & 0 \\ 0 & 0 & \hat{p}_{36} \\ \hat{p}_{16} & 0 & 0 \end{bmatrix} \begin{bmatrix} \ddot{\vec{N}}_1 \\ \ddot{\vec{N}}_2 \\ \ddot{\vec{N}}_3 \end{bmatrix} + \begin{bmatrix} -\hat{p}_{14} & 0 & 0 \\ -\hat{p}_{24} & 0 & 0 \\ \hat{p}_{45} & -\hat{p}_{45} & 0 \\ 0 & -\hat{p}_{25} & 0 \\ \hat{p}_{46} & 0 & -\hat{p}_{46} \\ 0 & -\hat{p}_{35} & 0 \\ 0 & \hat{p}_{56} & -\hat{p}_{56} \\ 0 & 0 & -\hat{p}_{36} \\ 0 & 0 & -\hat{p}_{16} \end{bmatrix} \begin{bmatrix} \ddot{\vec{N}}_4 \\ \ddot{\vec{N}}_5 \\ \ddot{\vec{N}}_6 \end{bmatrix} \tag{3.51}$$

or equivalently

$$\ddot{\vec{L}}_1 = \vec{Q}_1 + [\mathbf{R_1}] \begin{bmatrix} \ddot{\vec{N}}_1 \\ \ddot{\vec{N}}_2 \\ \ddot{\vec{N}}_3 \end{bmatrix} + [\mathbf{P_1}] \begin{bmatrix} \ddot{\vec{N}}_4 \\ \ddot{\vec{N}}_5 \\ \ddot{\vec{N}}_6 \end{bmatrix} \tag{3.52}$$

Again noting that nodes, N_1, N_2, and N_3, are fixed to ground, and that $\ddot{\vec{L}}_1$ reduces to the time derivative of equation 3.35, the above equation reduces to

$$\ddot{\vec{L}}_1 = \vec{Q}_1 + [\mathbf{P_1}] \begin{bmatrix} \ddot{\vec{N}}_4 \\ \ddot{\vec{N}}_5 \\ \ddot{\vec{N}}_6 \end{bmatrix} \tag{3.53}$$

Rearranging and multiplying by $[\mathbf{P_1}]^{-1}$ the nodal accelerations of the first bay are found as

$$\begin{bmatrix} \ddot{\vec{N}}_4 \\ \ddot{\vec{N}}_5 \\ \ddot{\vec{N}}_6 \end{bmatrix} = [\mathbf{P_1}]^{-1}(\ddot{\vec{L}}_1 - \vec{Q}_1) \tag{3.54}$$

Similarly, a system of acceleration equations can be written for the second octahedral bay of the adaptive truss as

$$\begin{bmatrix} \ddot{l}_{47} \\ \ddot{l}_{57} \\ \ddot{l}_{78} \\ \ddot{l}_{58} \\ \ddot{l}_{79} \\ \ddot{l}_{68} \\ \ddot{l}_{89} \\ \ddot{l}_{69} \\ \ddot{l}_{49} \end{bmatrix} = \begin{bmatrix} q_{47} \\ q_{57} \\ q_{78} \\ q_{58} \\ q_{79} \\ q_{68} \\ q_{89} \\ q_{69} \\ q_{49} \end{bmatrix} + \begin{bmatrix} \hat{p}_{47} & 0 & 0 \\ 0 & \hat{p}_{57} & 0 \\ 0 & 0 & 0 \\ 0 & \hat{p}_{58} & 0 \\ 0 & 0 & 0 \\ 0 & 0 & \hat{p}_{68} \\ 0 & 0 & 0 \\ 0 & 0 & \hat{p}_{69} \\ \hat{p}_{49} & 0 & 0 \end{bmatrix} \begin{bmatrix} \ddot{\vec{N}}_4 \\ \ddot{\vec{N}}_5 \\ \ddot{\vec{N}}_6 \end{bmatrix} + \begin{bmatrix} -\hat{p}_{47} & 0 & 0 \\ -\hat{p}_{57} & 0 & 0 \\ \hat{p}_{78} & -\hat{p}_{78} & 0 \\ 0 & -\hat{p}_{58} & 0 \\ \hat{p}_{79} & 0 & -\hat{p}_{79} \\ 0 & -\hat{p}_{68} & 0 \\ 0 & \hat{p}_{89} & -\hat{p}_{89} \\ 0 & 0 & -\hat{p}_{69} \\ 0 & 0 & -\hat{p}_{49} \end{bmatrix} \begin{bmatrix} \ddot{\vec{N}}_7 \\ \ddot{\vec{N}}_8 \\ \ddot{\vec{N}}_9 \end{bmatrix} \tag{3.55}$$

or

$$\ddot{\vec{L}}_2 = \vec{Q}_2 + [\mathbf{R_2}] \begin{bmatrix} \ddot{\vec{N}}_4 \\ \ddot{\vec{N}}_5 \\ \ddot{\vec{N}}_6 \end{bmatrix} + [\mathbf{P_2}] \begin{bmatrix} \ddot{\vec{N}}_7 \\ \ddot{\vec{N}}_8 \\ \ddot{\vec{N}}_9 \end{bmatrix} \tag{3.56}$$

None of the struts of the second octahedral bay are variable length struts and thus, $\ddot{\vec{L}}_2 = 0$. Substituting for the nodal accelerations of the actuated plane given by equation 3.54 and again noting that $[\mathbf{R_2}]$ is invertible, equation 3.56 is rewritten as

$$\begin{bmatrix} \ddot{\vec{N}}_7 \\ \ddot{\vec{N}}_8 \\ \ddot{\vec{N}}_9 \end{bmatrix} = -[\mathbf{P_2}]^{-1} \left(\vec{Q}_2 + [\mathbf{R_2}][\mathbf{P_1}]^{-1} (\ddot{\vec{L}}_1 - \vec{Q}_1) \right) \tag{3.57}$$

These are the nodal accelerations of the top plane. It is noted that these acceleration equations are nonlinear since they are dependent on quadratic velocity terms (note the structure of equation 3.49). This is important when linear transformations are developed for control law design. A linearization scheme is required as Section 3.4 will show.

3.3.6 Acceleration of Mid-Point of Top Plane

The acceleration of the center of the top plane is developed from the top plane velocity equation 3.43. Differentiating this equation once more with respect to time results in the acceleration of the top plane and is given as

$$\ddot{\vec{P}}m_{org} = \frac{\ddot{\vec{N}}_7 + \ddot{\vec{N}}_8 + \ddot{\vec{N}}_9}{3} \tag{3.58}$$

3.3.7 Angular Accelerations of the Top Plane

Again the top plane of the adaptive truss is a rigid body, and therefore, relative acceleration equations for rigid body motion in space can be written. The relative acceleration equations between nodes 7 and 8, and 7 and 9 are given as

$$\begin{aligned} \ddot{\vec{N}}_7 &= \ddot{\vec{N}}_8 + \vec{\Phi} \times \vec{R}_{7/8} + \vec{\Omega} \times (\vec{\Omega} \times \vec{R}_{7/8}) \\ \ddot{\vec{N}}_7 &= \ddot{\vec{N}}_9 + \vec{\Phi} \times \vec{R}_{7/9} + \vec{\Omega} \times (\vec{\Omega} \times \vec{R}_{7/9}) \end{aligned} \tag{3.59}$$

where $\vec{\Omega}$ is the vector of angular velocities previously determined from equation 3.47, and $\vec{R}_{7/8}$ and $\vec{R}_{7/9}$ are the relative position vectors given by equation 3.45. The vector of angular accelerations is given by

$$\vec{\Phi} = \begin{bmatrix} \ddot{\gamma} \\ \ddot{\beta} \\ \ddot{\alpha} \end{bmatrix}$$

The only unknowns of equation 3.59 are the three angular accelerations, $\ddot{\gamma}$, $\ddot{\beta}$, and $\ddot{\alpha}$. Much like the relative velocity equations of Section 3.3.4, equation 3.59 represents a system of six scalar equations with only three unknowns with the redundancy

evident by performing the cross products and rearranging equation 3.59 as

$$\begin{bmatrix} \ddot{N}_{7x} - \ddot{N}_{8x} \\ \ddot{N}_{7y} - \ddot{N}_{8y} \\ \ddot{N}_{7z} - \ddot{N}_{8z} \end{bmatrix} - \begin{bmatrix} \dot{\alpha}(R_{78y}\dot{\beta} - R_{78x}\dot{\alpha}) - \dot{\gamma}(R_{78x}\dot{\gamma} - R_{78z}\dot{\beta}) \\ \dot{\gamma}(R_{78z}\dot{\alpha} - R_{78y}\dot{\gamma}) - \dot{\beta}(R_{78y}\dot{\beta} - R_{78x}\dot{\alpha}) \\ \dot{\beta}(R_{78x}\dot{\gamma} - R_{78z}\dot{\beta}) - \dot{\alpha}(R_{78x}alpha - R_{78y}\dot{\gamma}) \end{bmatrix} = \begin{bmatrix} 0 & R_{78z} & -R_{78y} \\ -R_{78z} & 0 & R_{78x} \\ R_{78y} & -R_{78x} & 0 \end{bmatrix} \begin{bmatrix} \ddot{\gamma} \\ \ddot{\beta} \\ \ddot{\alpha} \end{bmatrix}$$
$$\begin{bmatrix} \ddot{N}_{7x} - \ddot{N}_{9x} \\ \ddot{N}_{7y} - \ddot{N}_{9y} \\ \ddot{N}_{7z} - \ddot{N}_{9z} \end{bmatrix} - \begin{bmatrix} \dot{\alpha}(R_{79y}\dot{\beta} - R_{79x}\dot{\alpha}) - \dot{\gamma}(R_{79x}\dot{\gamma} - R_{79z}\dot{\beta}) \\ \dot{\gamma}(R_{79z}\dot{\alpha} - R_{79y}\dot{\gamma}) - \dot{\beta}(R_{79y}\dot{\beta} - R_{79x}\dot{\alpha}) \\ \dot{\beta}(R_{79x}\dot{\gamma} - R_{79z}\dot{\beta}) - \dot{\alpha}(R_{79z}alpha - R_{79y}\dot{\gamma}) \end{bmatrix} = \begin{bmatrix} 0 & R_{79z} & -R_{79y} \\ -R_{79z} & 0 & R_{79x} \\ R_{79y} & -R_{79x} & 0 \end{bmatrix} \begin{bmatrix} \ddot{\gamma} \\ \ddot{\beta} \\ \ddot{\alpha} \end{bmatrix} \quad (3.60)$$

The diagonals of both of the above 3×3 matrices are zeros indicating they are singular. However, just as in Section 3.3.4, a set of three independent equations can be assembled from the available six, and the angular accelerations can be determined. They are given as

$$\begin{bmatrix} \ddot{\gamma} \\ \ddot{\beta} \\ \ddot{\alpha} \end{bmatrix} = \begin{bmatrix} 0 & R_{78z} & -R_{78y} \\ -R_{78z} & 0 & R_{78x} \\ -R_{79z} & 0 & R_{79x} \end{bmatrix}^{-1} \left(\begin{bmatrix} \ddot{N}_{7x} - \ddot{N}_{8x} \\ \ddot{N}_{7y} - \ddot{N}_{8y} \\ \ddot{N}_{7y} - \ddot{N}_{9y} \end{bmatrix} - \begin{bmatrix} \dot{\alpha}(R_{78y}\dot{\beta} - R_{78x}\dot{\alpha}) - \dot{\gamma}(R_{78x}\dot{\gamma} - R_{78z}\dot{\beta}) \\ \dot{\gamma}(R_{78x}\dot{\alpha} - R_{78y}\dot{\gamma}) - \dot{\beta}(R_{78y}\dot{\beta} - R_{78x}\dot{\alpha}) \\ \dot{\gamma}(R_{79x}\dot{\alpha} - R_{79y}\dot{\gamma}) - \dot{\beta}(R_{79y}\dot{\beta} - R_{79x}\dot{\alpha}) \end{bmatrix} \right) \quad (3.61)$$

Before preceding on to the next section, perhaps a few words on "where we stand" would be helpful. At this point we have the closed-form inverse solution of Section 3.1 from the slew parameters, γ, β, and d to the batten lengths $\vec{L}$. In Section 3.2 the iterative forward solution from the batten lengths to the slew parameters is given. Finally, based on the slew parameters and batten lengths, we have reversible expressions between the position, velocity, and accelerations of all truss nodes and truss links given in Section 3.3. These expressions are transformed to the point atop the adaptive truss where the flexible beam is attached, resulting in exact position, velocity, and acceleration relationships between this point and the active links.

3.4 Forward Kinematic Transformations

In this section linear kinematic transformations relating the positions, velocities, and accelerations of the coordinates of the moving reference frame and the active batten links are developed. These transformations are linear approximations of the exact position, velocity, and acceleration relationships discussed in Sections 3.1 and 3.3 and are linearized about a specified configuration of the truss. Such an approximation is necessary in order to develop a linear control law, as will be shown in Chapter 5.

The coordinates $\vec{P}_{top} = [X\ Y\ Z\ \gamma\ \beta\ \alpha\ ]$ are the six general degrees of freedom of the moving reference frame. But the adaptive truss used in this study has a small α rotation compared to the other rotations and is approximately zero if the other rotations are small, as indicated by equation 3.27. For this reason, α is neglected in the development of the following linear kinematic transformations, and the vector specifying the remaining coordinates of $\vec{P}_{top}$ is given as $\vec{P}_m = [X\ Y\ Z\ \gamma\ \beta]^T$.

3.4.1 Position Transformation

The position transformation approximates the coordinates of the moving reference frame as linear combinations of the active batten lengths and is referred to as the position Jacobian. The position Jacobian is expressed as a matrix of partial derivatives of each of the moving frame coordinates with respect to the lengths of the active battens.

The position Jacobian is evaluated for specific positions of the adaptive truss since

the partial derivatives are position-dependent relationships and are developed from the inverse solution of Section 3.1. The results of the inverse solution provide the lengths of the actuated battens, l_1, l_2, and l_3, for a specified truss position given in terms of the inputs γ, β, and d. From these results, numerical perturbation methods are used to approximate the following relationship,

$$\begin{bmatrix} \partial l_1 \\ \partial l_2 \\ \partial l_3 \end{bmatrix} = \begin{bmatrix} \frac{\partial l_1}{\partial \gamma} & \frac{\partial l_1}{\partial \beta} & \frac{\partial l_1}{\partial d} \\ \frac{\partial l_2}{\partial \gamma} & \frac{\partial l_2}{\partial \beta} & \frac{\partial l_3}{\partial d} \\ \frac{\partial l_3}{\partial \gamma} & \frac{\partial l_3}{\partial \beta} & \frac{\partial l_3}{\partial d} \end{bmatrix} \begin{bmatrix} \partial \gamma \\ \partial \beta \\ \partial d \end{bmatrix} \tag{3.62}$$

To justify taking the inverse of the above 3×3 matrix, it is noted that the three degrees-of-freedom of the adaptive truss correspond to each of the three active batten links. Physically, these link lengths are independent of each other such that any link can be lengthened or shortened without changing one or both of the other links. Consequently, none of the link lengths are linearly dependent on the others, and the above 3×3 matrix has full row rank and is invertible. Performing the inversion results in

$$\begin{bmatrix} \partial \gamma \\ \partial \beta \\ \partial d \end{bmatrix} = \begin{bmatrix} \frac{\partial \gamma}{\partial l_1} & \frac{\partial \gamma}{\partial l_2} & \frac{\partial \gamma}{\partial l_3} \\ \frac{\partial \beta}{\partial l_1} & \frac{\partial \beta}{\partial l_2} & \frac{\partial \beta}{\partial l_3} \\ \frac{\partial d}{\partial l_1} & \frac{\partial d}{\partial l_2} & \frac{\partial d}{\partial l_3} \end{bmatrix} \begin{bmatrix} \partial l_1 \\ \partial l_2 \\ \partial l_3 \end{bmatrix} \tag{3.63}$$

The above expression relates changes in the three independent slew parameters as linear combinations of changes in the active batten lengths. Two of the slew parameters, γ and β, are coordinates of $\vec{P}m$ such that the partial derivatives of these coordinates with respect to the active batten lengths are given by the first two rows of the above 3×3 matrix.

The partial derivatives with respect to the active batten lengths of the remaining coordinates of $\vec{P}m$ are determined by first considering that X, Y, and Z are explicit

functions of γ, β, and d, given by equations 3.6 as

$$\begin{aligned} X &= -\frac{d\sin\gamma}{\sqrt{2(1+\cos\beta\cos\gamma)}} \\ Y &= \frac{d\,[1+\cos\beta\cos\gamma]}{\sqrt{2(1+\cos\beta\cos\gamma)}} \\ Z &= \frac{d\sin\beta\cos\gamma}{\sqrt{2(1+\cos\beta\cos\gamma)}} \end{aligned}$$

The partial derivatives of X, Y, and Z are each evaluated with respect to each of the slew parameters, γ, β, and d and are determined as follows,

$$\begin{aligned}
\frac{\partial X}{\partial \gamma} &= \frac{-d\cos\gamma}{\sqrt{2+2\cos\beta\cos\gamma}} - \frac{d\sin^2\gamma\cos\beta}{(2+2\cos\beta\cos\gamma)^{3/2}} \\
\frac{\partial X}{\partial \beta} &= \frac{-d\sin\gamma\sin\beta\cos\gamma}{(2+2\cos\beta\cos\gamma)^{3/2}} \\
\frac{\partial X}{\partial d} &= \frac{-\sin\gamma}{\sqrt{2+2\cos\beta\cos\gamma}} \\
\frac{\partial Y}{\partial \gamma} &= \frac{-d\cos\beta\sin\gamma}{\sqrt{2+2\cos\beta\cos\gamma}} + \frac{d\,(1+\cos\beta\cos\gamma)\,(\cos\beta\sin\gamma)}{(2+2\cos\beta\cos\gamma)^{3/2}} \\
\frac{\partial Y}{\partial \beta} &= \frac{-d\sin\beta\cos\gamma}{\sqrt{2+2\cos\beta\cos\gamma}} + \frac{d\,(1+\cos\beta\cos\gamma)\,(\sin\beta\cos\gamma)}{(2+2\cos\beta\cos\gamma)^{3/2}} \\
\frac{\partial Y}{\partial d} &= \frac{1+\cos\beta\cos\gamma}{\sqrt{2+2\cos\beta\cos\gamma}} \\
\frac{\partial Z}{\partial \gamma} &= \frac{-d\sin\beta\sin\gamma}{\sqrt{2+2\cos\beta\cos\gamma}} + \frac{d\,(\cos\beta\sin\gamma)\,(\sin\beta\cos\gamma)}{(2+2\cos\beta\cos\gamma)^{3/2}} \\
\frac{\partial Z}{\partial \beta} &= \frac{d\cos\beta\cos\gamma}{\sqrt{2+2\cos\beta\cos\gamma}} + \frac{d\left(\sin^2\beta\cos^2\gamma\right)}{(2+2\cos\beta\cos\gamma)^{3/2}} \\
\frac{\partial Z}{\partial d} &= \frac{\sin\beta\cos\gamma}{\sqrt{2+2\cos\beta\cos\gamma}}
\end{aligned} \tag{3.64}$$

Once the above partials are determined and evaluated for a specific set of slew parameters, the partial differential chain rule is employed to determine the partial

derivatives of X, Y, and Z with respect to the three active batten lengths. By using the partial derivatives from equations 3.64 and the partial derivatives given by the matrix in equation 3.63 the partial derivatives of X, Y, and Z with respect to l_1, l_2, and l_3 are determined as

$$\begin{aligned}
\frac{\partial X}{\partial l_1} &= \frac{\partial X}{\partial \gamma}\frac{\partial \gamma}{\partial l_1} + \frac{\partial X}{\partial \beta}\frac{\partial \beta}{\partial l_1} + \frac{\partial X}{\partial d}\frac{\partial d}{\partial l_1} \\
\frac{\partial X}{\partial l_2} &= \frac{\partial X}{\partial \gamma}\frac{\partial \gamma}{\partial l_2} + \frac{\partial X}{\partial \beta}\frac{\partial \beta}{\partial l_2} + \frac{\partial X}{\partial d}\frac{\partial d}{\partial l_2} \\
\frac{\partial X}{\partial l_3} &= \frac{\partial X}{\partial \gamma}\frac{\partial \gamma}{\partial l_3} + \frac{\partial X}{\partial \beta}\frac{\partial \beta}{\partial l_3} + \frac{\partial X}{\partial d}\frac{\partial d}{\partial l_3} \\
\frac{\partial Y}{\partial l_1} &= \frac{\partial Y}{\partial \gamma}\frac{\partial \gamma}{\partial l_1} + \frac{\partial Y}{\partial \beta}\frac{\partial \beta}{\partial l_1} + \frac{\partial Y}{\partial d}\frac{\partial d}{\partial l_1} \\
\frac{\partial Y}{\partial l_2} &= \frac{\partial Y}{\partial \gamma}\frac{\partial \gamma}{\partial l_2} + \frac{\partial Y}{\partial \beta}\frac{\partial \beta}{\partial l_2} + \frac{\partial Y}{\partial d}\frac{\partial d}{\partial l_2} \\
\frac{\partial Y}{\partial l_3} &= \frac{\partial Y}{\partial \gamma}\frac{\partial \gamma}{\partial l_3} + \frac{\partial Y}{\partial \beta}\frac{\partial \beta}{\partial l_3} + \frac{\partial Y}{\partial d}\frac{\partial d}{\partial l_3} \\
\frac{\partial Z}{\partial l_1} &= \frac{\partial Z}{\partial \gamma}\frac{\partial \gamma}{\partial l_1} + \frac{\partial Z}{\partial \beta}\frac{\partial \beta}{\partial l_1} + \frac{\partial Z}{\partial d}\frac{\partial d}{\partial l_1} \\
\frac{\partial Z}{\partial l_2} &= \frac{\partial Z}{\partial \gamma}\frac{\partial \gamma}{\partial l_2} + \frac{\partial Z}{\partial \beta}\frac{\partial \beta}{\partial l_2} + \frac{\partial Z}{\partial d}\frac{\partial d}{\partial l_2} \\
\frac{\partial Z}{\partial l_3} &= \frac{\partial Z}{\partial \gamma}\frac{\partial \gamma}{\partial l_3} + \frac{\partial Z}{\partial \beta}\frac{\partial \beta}{\partial l_3} + \frac{\partial Z}{\partial d}\frac{\partial d}{\partial l_3}
\end{aligned} \tag{3.65}$$

Collecting the partial derivatives given by the above equations, 3.65, and the first two rows of partials derivatives in the matrix of equation 3.63, the position Jacobian

is assembled as

$$\begin{bmatrix} \partial X \\ \partial Y \\ \partial Z \\ \partial \gamma \\ \partial \beta \end{bmatrix} = \begin{bmatrix} \frac{\partial X}{\partial l_1} & \frac{\partial X}{\partial l_2} & \frac{\partial X}{\partial l_3} \\ \frac{\partial Y}{\partial l_1} & \frac{\partial Y}{\partial l_2} & \frac{\partial Y}{\partial l_3} \\ \frac{\partial Z}{\partial l_1} & \frac{\partial Z}{\partial l_2} & \frac{\partial Z}{\partial l_3} \\ \frac{\partial \gamma}{\partial l_1} & \frac{\partial \gamma}{\partial l_2} & \frac{\partial \gamma}{\partial l_3} \\ \frac{\partial \beta}{\partial l_1} & \frac{\partial \beta}{\partial l_2} & \frac{\partial \beta}{\partial l_3} \end{bmatrix} \begin{bmatrix} \partial l_1 \\ \partial l_2 \\ \partial l_3 \end{bmatrix} \tag{3.66}$$

or equivalently,

$$\partial \vec{P}m = [\mathbf{J_p}]\, \partial \vec{L} \tag{3.67}$$

where $[\mathbf{J_p}]$ is the desired position Jacobian.

The position Jacobian is a transformation of changes between the moving coordinates and the active batten lengths, and the desired relationship is a transformation between the values of the $\vec{P}m$ and $\vec{L}$. But by approximating the partials as increments between the positions and reference positions such that

$$\begin{aligned} \partial \vec{P}m &\approx \vec{P}m - \vec{P}m_{ref} \\ \partial \vec{L} &\approx \vec{L} - \vec{L}_{ref} \end{aligned}$$

and defining the reference positions as $\vec{P}m_{ref} = 0$ and $\vec{L}_{ref} = 0$, the desired linear relationship is established and is given as

$$\vec{P}m = [\mathbf{J_p}]\, \vec{L} \tag{3.68}$$

3.4.2 Velocity Transformation

The velocity transformation approximates the velocities of the coordinates of the moving reference frame as linear combinations of the velocities of the active battens. The velocity transformation, like the position transformation, is developed for a specific position of the truss, requiring the solution to the inverse position problem of Section 3.1 and the solution to the nodal position analysis of Section 3.3.1. Once the position analyses are complete, the nodal velocity analysis of Section 3.3.2 is performed, and the nodal velocities of the three nodes of the top plane are determined and given by equation 3.41 as

$$\begin{bmatrix} \dot{\vec{N}}_7 \\ \dot{\vec{N}}_8 \\ \dot{\vec{N}}_9 \end{bmatrix} = -[\mathbf{P_2}]^{-1}[\mathbf{R_2}][\mathbf{P_1}]^{-1}\dot{\vec{L}}_1$$

or equivalently as

$$\begin{bmatrix} \dot{\vec{N}}_7 \\ \dot{\vec{N}}_8 \\ \dot{\vec{N}}_9 \end{bmatrix} = [\mathbf{Tv}]\dot{\vec{L}}_1 \tag{3.69}$$

where $[\mathbf{Tv}] = -[\mathbf{P_2}]^{-1}[\mathbf{R_2}][\mathbf{P_1}]^{-1}$ and $[\mathbf{P_1}]$ is defined in equation 3.33, and $[\mathbf{P_2}]$ and $[\mathbf{R_2}]$ are defined in equation 3.38. Expanding equation 3.69 results in

$$\begin{bmatrix} \dot{N}_{7x} \\ \dot{N}_{7y} \\ \dot{N}_{7z} \\ \dot{N}_{8x} \\ \dot{N}_{8y} \\ \dot{N}_{8z} \\ \dot{N}_{9x} \\ \dot{N}_{9y} \\ \dot{N}_{9z} \end{bmatrix} = \begin{bmatrix} Tv_{1,1} & Tv_{1,2} & Tv_{1,3} & Tv_{1,4} & Tv_{1,5} & Tv_{1,6} & Tv_{1,7} & Tv_{1,8} & Tv_{1,9} \\ Tv_{2,1} & Tv_{2,2} & Tv_{2,3} & Tv_{2,4} & Tv_{2,5} & Tv_{2,6} & Tv_{2,7} & Tv_{2,8} & Tv_{2,9} \\ Tv_{3,1} & Tv_{3,2} & Tv_{3,3} & Tv_{3,4} & Tv_{3,5} & Tv_{3,6} & Tv_{3,7} & Tv_{3,8} & Tv_{3,9} \\ Tv_{4,1} & Tv_{4,2} & Tv_{4,3} & Tv_{4,4} & Tv_{4,5} & Tv_{4,6} & Tv_{4,7} & Tv_{4,8} & Tv_{4,9} \\ Tv_{5,1} & Tv_{5,2} & Tv_{5,3} & Tv_{5,4} & Tv_{5,5} & Tv_{5,6} & Tv_{5,7} & Tv_{5,8} & Tv_{5,9} \\ Tv_{6,1} & Tv_{6,2} & Tv_{6,3} & Tv_{6,4} & Tv_{6,5} & Tv_{6,6} & Tv_{6,7} & Tv_{6,8} & Tv_{6,9} \\ Tv_{7,1} & Tv_{7,2} & Tv_{7,3} & Tv_{7,4} & Tv_{7,5} & Tv_{7,6} & Tv_{7,7} & Tv_{7,8} & Tv_{7,9} \\ Tv_{8,1} & Tv_{8,2} & Tv_{8,3} & Tv_{8,4} & Tv_{8,5} & Tv_{8,6} & Tv_{8,7} & Tv_{8,8} & Tv_{8,9} \\ Tv_{9,1} & Tv_{9,2} & Tv_{9,3} & Tv_{9,4} & Tv_{9,5} & Tv_{9,6} & Tv_{9,7} & Tv_{9,8} & Tv_{9,9} \end{bmatrix} \begin{bmatrix} 0 \\ 0 \\ \dot{l}_1 \\ 0 \\ \dot{l}_2 \\ 0 \\ \dot{l}_3 \\ 0 \\ 0 \end{bmatrix} \tag{3.70}$$

From equation 3.43, it is noted that the velocities, $\dot{X}$, $\dot{Y}$, and $\dot{Z}$ are linear combinations of the x y and z components of the three nodal velocities of the top plane, $\dot{\vec{N}}_7$, $\dot{\vec{N}}_8$, and $\dot{\vec{N}}_9$, such that $\dot{X}$ is one-third the sum of the x velocity components, and etc. Additionally, since the third, fifth, and seventh elements of $\dot{\vec{L}}_1$ are the only nonzero entries, all but the third, fifth, and seventh columns of [**Tv**] are neglected. In light of these observations, the following relationship can be established

$$\begin{bmatrix} \dot{X} \\ \dot{Y} \\ \dot{Z} \end{bmatrix} = \frac{1}{3} \begin{bmatrix} (Tv_{1,3} + Tv_{4,3} + Tv_{7,3}) & (Tv_{1,5} + Tv_{4,5} + Tv_{7,5}) & (Tv_{1,7} + Tv_{4,7} + Tv_{7,7}) \\ (Tv_{2,3} + Tv_{5,3} + Tv_{8,3}) & (Tv_{2,5} + Tv_{5,5} + Tv_{8,5}) & (Tv_{2,7} + Tv_{5,7} + Tv_{8,7}) \\ (Tv_{3,3} + Tv_{6,3} + Tv_{9,3}) & (Tv_{3,5} + Tv_{6,5} + Tv_{9,5}) & (Tv_{3,7} + Tv_{6,7} + Tv_{9,7}) \end{bmatrix} \begin{bmatrix} \dot{l}_1 \\ \dot{l}_2 \\ \dot{l}_3 \end{bmatrix} \quad (3.71)$$

or

$$\begin{bmatrix} \dot{X} \\ \dot{Y} \\ \dot{Z} \end{bmatrix} = [\mathbf{Tv_1}]\dot{\vec{L}} \quad (3.72)$$

[$\mathbf{Tv_1}$] is a 3×3 matrix that relates the velocities of the active battens to the velocities of the X, Y, and Z coordinates of the moving reference frame.

The angular velocities of the top plane are given by equation 3.47 as a function of the velocities of the nodes of the top plane

$$\begin{bmatrix} \dot{\beta} \\ \dot{\alpha} \\ \dot{\gamma} \end{bmatrix} = \begin{bmatrix} 0 & R_{78z} & -R_{78y} \\ -R_{78z} & 0 & R_{78x} \\ -R_{79z} & 0 & R_{79x} \end{bmatrix}^{-1} \begin{bmatrix} \dot{N}_{7x} - \dot{N}_{8x} \\ \dot{N}_{7y} - \dot{N}_{8y} \\ \dot{N}_{7y} - \dot{N}_{9y} \end{bmatrix}$$

Substituting the corresponding rows of [**Tv**] given in equation 3.70, and again neglecting all but the third, fifth, and seventh columns, the following relationship is established

$$\begin{bmatrix} \dot{\beta} \\ \dot{\alpha} \\ \dot{\gamma} \end{bmatrix} = \begin{bmatrix} 0 & R_{78x} & -R_{78y} \\ -R_{78x} & 0 & R_{78x} \\ -R_{79x} & 0 & R_{79x} \end{bmatrix}^{-1} \begin{bmatrix} (Tv_{1,3} - Tv_{4,3}) & (Tv_{1,5} - Tv_{4,5}) & (Tv_{1,7} - Tv_{4,7}) \\ (Tv_{2,3} - Tv_{5,3}) & (Tv_{2,5} - Tv_{5,5}) & (Tv_{2,7} - Tv_{5,7}) \\ (Tv_{2,3} - Tv_{8,3}) & (Tv_{2,5} - Tv_{8,5}) & (Tv_{2,7} - Tv_{8,7}) \end{bmatrix} \begin{bmatrix} i_1 \\ i_2 \\ i_3 \end{bmatrix} \quad (3.73)$$

or

$$\begin{bmatrix} \dot{\gamma} \\ \dot{\beta} \\ \dot{\alpha} \end{bmatrix} = [\mathbf{Tv_2}] \begin{bmatrix} \dot{l}_1 \\ \dot{l}_2 \\ \dot{l}_3 \end{bmatrix} \quad (3.74)$$

The first and third rows of the above 3×3 matrix $[\mathbf{Tv_2}]$ corresponding to $\dot{\gamma}$ and $\dot{\beta}$ are combined to form a 2×3 matrix $[\mathbf{Tv_3}]$. The velocity transformation relating the velocities of the moving reference frame coordinates as linear combinations of the velocities of the battens is assembled from $[\mathbf{Tv_1}]$ and $[\mathbf{Tv_3}]$ and is given by

$$\begin{bmatrix} \dot{X} \\ \dot{Y} \\ \dot{Z} \\ \dot{\beta} \\ \dot{\gamma} \end{bmatrix} = \begin{bmatrix} \mathbf{Tv_1} \\ \mathbf{Tv_3} \end{bmatrix} \begin{bmatrix} \dot{l}_1 \\ \dot{l}_2 \\ \dot{l}_3 \end{bmatrix} \quad (3.75)$$

or equivalently as

$$\dot{\vec{P}}m = [\mathbf{J_v}]\,\dot{\vec{L}} \quad (3.76)$$

$[\mathbf{J_v}]$ is the desired velocity transformation between the velocities of the moving reference coordinates and the velocities of the active links. Again, the transformation is developed about a specific position of the adaptive truss and is less accurate as the truss is moved further from this position.

3.4.3 Acceleration Transformation

The acceleration transformation approximates the accelerations of the coordinates of the moving reference frame as linear combinations of the accelerations of the active battens. The acceleration transformation is developed for a specific position of the adaptive truss just as the position and velocity transformations are, but in addition, the acceleration relationships of Section 3.3.5 are linearized about a specific set of active link velocities. The choice of link velocities about which to linearize the acceleration relationships is related to the application of the adaptive truss. In this thesis the truss is used as a vibration control actuator and it is expected that the active link velocities will oscillate about zero much like the modal rates that describe the lateral vibrations of the flexible beam. Consequently, the linear acceleration transformation developed in this thesis is linearized about zero link velocities, but could be linearized to nonzero velocities for applications such as a constant velocity slew maneuver.

With the position analyses of Sections 3.1 and 3.3.1 completed, the acceleration relationships of Section 3.3.5 can be developed. Accordingly, the resulting accelerations of the top plane nodes are given by equation 3.57 as

$$\begin{bmatrix} \ddot{\vec{N}}_7 \\ \ddot{\vec{N}}_8 \\ \ddot{\vec{N}}_9 \end{bmatrix} = -[\mathbf{P_2}]^{-1}\left(\vec{Q}_2 + [\mathbf{R_2}][\mathbf{P_1}]^{-1}(\ddot{\vec{L}}_1 - \vec{Q}_1)\right)$$

If the above equation is linearized about zero link velocity the vectors $\vec{Q}_1$ and $\vec{Q}_2$ become zero (note the structure of equation 3.49) and the above equation reduces

to

$$\begin{bmatrix} \ddot{\vec{N}}_7 \\ \ddot{\vec{N}}_8 \\ \ddot{\vec{N}}_9 \end{bmatrix} = -[\mathbf{P_2}]^{-1}[\mathbf{R_2}][\mathbf{P_1}]^{-1}\ddot{\vec{L}}_1 \tag{3.77}$$

which is similar to equation 3.41 used to develop the velocity transformation in Section 3.4.2. The same transformation, $-[\mathbf{P_2}]^{-1}[\mathbf{R_2}][\mathbf{P_1}]^{-1}$, relates the accelerations of the top plane to the link accelerations in the above equation as it relates the velocities of the top plane to the link velocities in equation 3.41. As a result, the transformation between $\ddot{X}$, $\ddot{Y}$, and $\ddot{Z}$ and $\ddot{l}_1$, $\ddot{l}_2$, and $\ddot{l}_3$ is exactly $[\mathbf{Tv_1}]$ given by equation 3.72.

Linearizing the angular acceleration relationship given by equation 3.61 about zero velocities, the angular accelerations are approximated by

$$\begin{bmatrix} \ddot{\gamma} \\ \ddot{\beta} \\ \ddot{\alpha} \end{bmatrix} = \begin{bmatrix} 0 & R_{78z} & -R_{78y} \\ -R_{78z} & 0 & R_{78x} \\ -R_{79z} & 0 & R_{79x} \end{bmatrix}^{-1} \begin{bmatrix} \ddot{N}_{7x} - \ddot{N}_{8x} \\ \ddot{N}_{7y} - \ddot{N}_{8y} \\ \ddot{N}_{7y} - \ddot{N}_{9y} \end{bmatrix} \tag{3.78}$$

Again, the above equation is the same relationship relating the angular velocities to the velocities of the three top plane nodes and is given by equation 3.47. Since, it is the same relationship, the linear transformation between $\ddot{\beta}$ and $\ddot{\gamma}$ and $\ddot{l}_1$, $\ddot{l}_2$, and $\ddot{l}_3$ is developed according to Section 3.4.2 and is exactly $[\mathbf{Tv_3}]$ given in equation 3.75.

As a result of the above discussion, the acceleration transformation linearized about zero velocities is identically the velocity transformation, $[\mathbf{J_v}]$, and the linear acceleration transformation between the accelerations of the moving reference frame and

the accelerations of the active batten links is given by

$$\ddot{\vec{P}}m = [\mathbf{J_v}]\ddot{\vec{L}} \tag{3.79}$$

Chapter 4

Linear Model

The first experiment investigates the control of the transverse vibrations of the flexible beam with the adaptive truss operating with small motions about the zero-angle ($\gamma = 0, \beta = 0$), or equivalently, the equilibrium configuration ($l_1 = l_2 = l_3$). For this case, the beam is vertical and parallel to the gravity field. The dominant system nonlinearities of gravity and large motion kinematics are not prominent, facilitating the development of a linear system model. Additionally, since the first experiment is the only one of the three cases that includes hardware experiments, attempts are made to closely define the hardware parameters such that the differences between the computer and hardware experiments are minimal. As a result, the first experiment accounts for hardware characteristics such as the flexibility of the top triangular plate and the damping in the beam.

The linear modeling approach incorporates the following assumptions. The beam is assumed to behave as an Euler-Bernoulli beam. The plate upon which the beam is attached has stiffness, but the inertia effects are neglected. Additionally, the adaptive truss inertia and flexibility are neglected while the linearized truss kinematics are considered. Finally, effects of friction are not modeled in order to maintain lin-

earity of the system model.

4.1 Linear Beam Dynamics

The linear equations of motion for the rectangular beam are developed using the Lagrangian energy method. Kinetic energy, T, is stored in the beam mass by virtue of its velocity, whereas the potential energy, V, is stored in the form of strain energy in elastic deformation plus the work done in the gravitational field. The equations of motion are developed using the coordinate system shown in Fig. 4.1, where a position vector $\vec{R}$ describes the location of a differential mass along the beam as

$$\begin{aligned}\vec{R} = R_x\hat{n}_1 + R_y\hat{n}_2 + R_z\hat{n}_3 + w_x\hat{b}_1 \\ +w_y\hat{b}_2 + w_z\hat{b}_3\end{aligned} \tag{4.1}$$

where R_x, R_y, and R_z are the Newtonian translations specifying the origin of the $\hat{b}$ coordinate system fixed to the base of the beam, w_z is the vertical distance from the base of the beam, and w_x and w_y are transverse deflections.

Accounting for the rotations, γ_b, β_b, and α_b, of the $\hat{b}$-coordinate system with respect to the Newtonian frame, results in a rotation transformation between the $\hat{b}$ coordinates and the $\hat{n}$ coordinates and is given as

$$\begin{bmatrix}\hat{b}_1\\ \hat{b}_2\\ \hat{b}_3\end{bmatrix} = \begin{bmatrix} c\alpha_b c\beta_b & c\alpha_b s\beta_b s\gamma_b + s\alpha_b c\gamma_b & -c\alpha_b s\beta_b c\gamma_b + s\alpha_b s\gamma_b \\ -s\alpha_b c\beta_b & -s\alpha_b s\beta_b s\gamma_b + c\gamma_b c\alpha_b & s\alpha_b s\beta_b c\gamma_b + c\alpha_b s\gamma_b \\ s\beta_b & -c\beta_b s\gamma_b & c\beta_b c\gamma_b \end{bmatrix} \begin{bmatrix}\hat{n}_1\\ \hat{n}_2\\ \hat{n}_3\end{bmatrix} \tag{4.2}$$

Linearizing the above transformation about $\gamma_b = \beta_b = \alpha_b = 0$ for small rotations

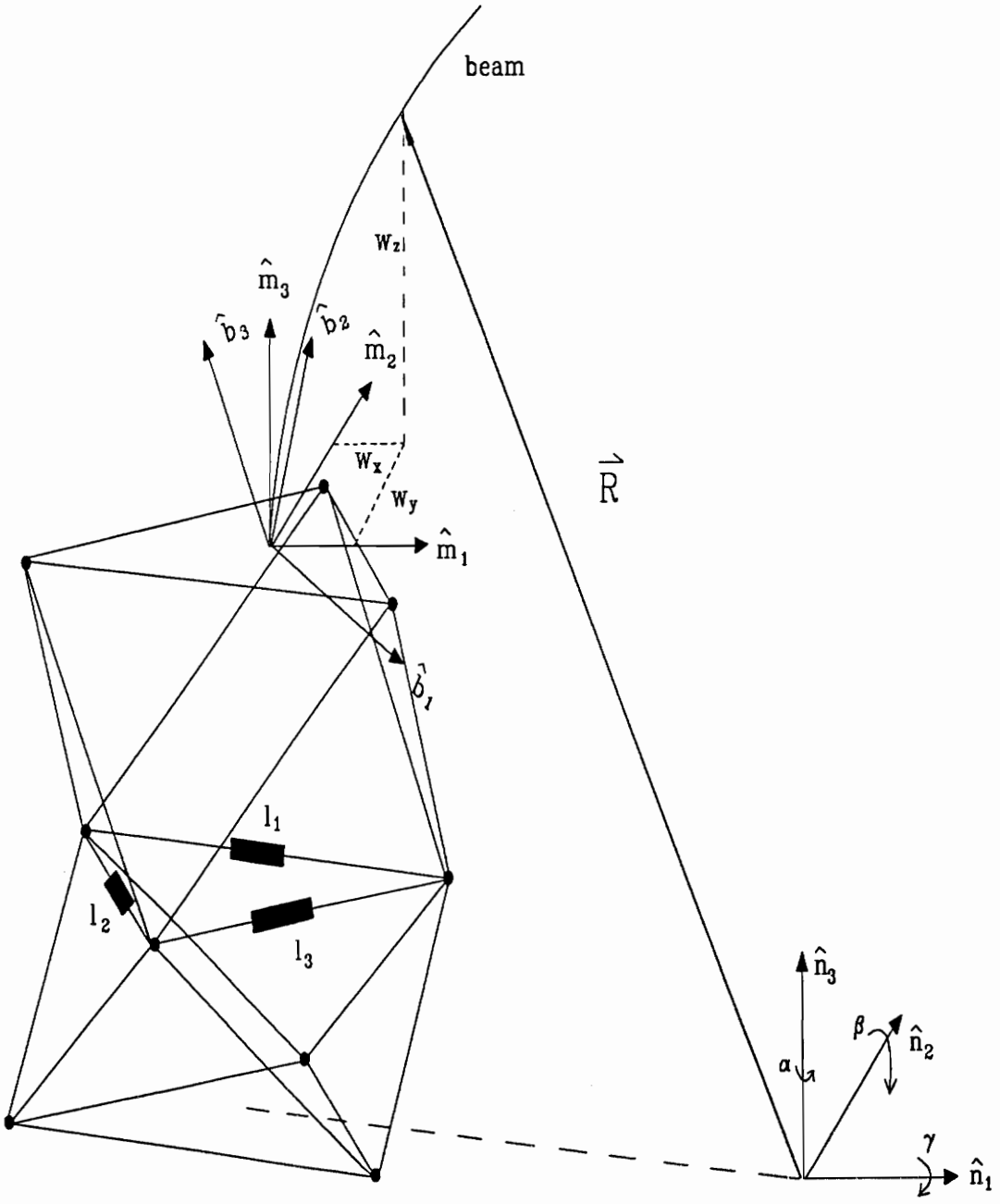

Figure 4.1: Adaptive Truss, Flexible Beam, and Flexible Plate Coordinate Frames

and substituting in equation 4.1 results in the position vector described by

$$\vec{R} = R_x\hat{n}_1 + R_y\hat{n}_2 + R_z\hat{n}_3 + w_x(\hat{n}_1 + \alpha_b\hat{n}_2 - \beta_b\hat{n}_3) \tag{4.3}$$
$$+w_y(-\alpha_b\hat{n}_1 + \hat{n}_2 + \gamma_b\hat{n}_3) + w_z(\beta_b\hat{n}_1 - \gamma_b\hat{n}_2 + \hat{n}_3)$$

The rotations, γ_b, β_b, and α_b, and the translations, R_x, R_y, and R_z, are coordinates describing the $\hat{b}$ reference system fixed to the base of the beam and are defined by $\vec{P}_b = [R_x\ R_y\ R_z\ \gamma_b\ \beta_b\ \alpha_b]^T$

The transverse deflections of the beam, w_x and w_y, are expressed as three-mode Ritz expansions as

$$w_x(s,t) = \sum_{i=1}^{3} \phi_{xi}(s)q_{xi}(t) \tag{4.4}$$
$$w_y(s,t) = \sum_{i=1}^{3} \phi_{yi}(s)q_{yi}(t)$$

where the ϕ_{xi}'s and ϕ_{yi}'s are Euler-shape functions chosen to satisfy clamped-free boundary conditions, and the q_{xi}'s and q_{yi}'s are time-dependent modal coordinates. Substituting equation 4.4 into the position vector, $\vec{R}$, yields

$$\vec{R} = R_x\hat{n}_1 + R_y\hat{n}_2 + R_z\hat{n}_3 + (\phi_{x1}q_{x1} + \phi_{x2}q_{x2} + \phi_{x3}q_{x3})(\hat{n}_1 + \alpha_b\hat{n}_2 - \beta_b\hat{n}_3) \tag{4.5}$$
$$+(\phi_{y1}q_{y1} + \phi_{y2}q_{y2} + \phi_{y3}q_{y3})(-\alpha_b\hat{n}_1 + \hat{n}_2 + \gamma_b\hat{n}_3) + w_z(\beta_b\hat{n}_1 - \gamma_b\hat{n}_2 + \hat{n}_3)$$

At this point R_z and α_b terms are dropped from the position vector $\vec{R}$. They are neglected because R_z and α_b are orthogonal to and, for a linear model, uncoupled from the transverse deflections, w_x and w_y. As a result of this, the position vector $\vec{R}$ reduces to

$$\vec{R} = R_x\hat{n}_1 + R_y\hat{n}_2 + (\phi_{x1}q_{x1} + \phi_{x2}q_{x2} + \phi_{x3}q_{x3})(\hat{n}_1 - \beta_b\hat{n}_3) \\ +(\phi_{y1}q_{y1} + \phi_{y2}q_{y2} + \phi_{y3}q_{y3})(\hat{n}_2 + \gamma_b\hat{n}_3) + w_z(\beta_b\hat{n}_1 - \gamma_b\hat{n}_2 + \hat{n}_3) \tag{4.6}$$

and the remaining coordinates of $\vec{P}_b$ are regrouped as

$$\vec{P}_{b1} = [R_x\ R_y\ \gamma_b\ \beta_b]^T \tag{4.7}$$

The total kinetic energy, T, is the summation of translation and rotation kinetic energy and is given by

$$T = \frac{\xi}{2}\int_0^{L_b} \dot{\vec{R}} \bullet \dot{\vec{R}}\, ds \tag{4.8}$$

$\vec{R}$ is the position vector given by equation 4.6, ξ is the mass per unit length, and L_b is the length of the beam. Performing the dot product, $\dot{\vec{R}} \bullet \dot{\vec{R}}$, and evaluating the above integral results in the total kinetic energy, T.

The total potential energy, V, of the beam is the sum of the elastic strain energy and the gravitation potential energy. The strain energy, V_ϵ, is proportional to the square of the transverse displacements and is given by

$$V_\epsilon = \int_0^{L_b} \frac{EI_x}{2}\left(\frac{d^2w_x}{ds^2}\right)^2 ds + \int_0^{L_b} \frac{EI_y}{2}\left(\frac{d^2w_y}{ds^2}\right)^2 ds \tag{4.9}$$

The potential work, V_g, of the beam acting in the gravity field is the displacement of the position vector, $\vec{R}$, parallel to the gravity field and is found from

$$V_g = g\xi\int_0^{L_b} \vec{R} \bullet \hat{n}_3\, ds \tag{4.10}$$

Evaluating the integrals given by equation 4.9 and equation 4.10 and summing them

together results in the total potential energy, V.

Once the kinetic energy, T, and potential energy, V, terms are evaluated, the Lagrangian is formed as $L = T - V$ and Lagrange's equations are applied. Lagrange's equations are differential equations of motion expressed in terms of generalized coordinates where the six modal coordinates of the beam, $\vec{Q} = [q_{x1}\ q_{x2}\ q_{x3}\ q_{y1}\ q_{y2}\ q_{y3}]^T$ are the generalized coordinates for this problem. The coordinates $\vec{P}_{b1} = [R_x\ R_y\ \gamma_b \beta_b]^T$ aren't generalized coordinates but rather are inputs to the base of the beam and Lagrange's equation is not applied to these coordinates. The six differential equations of the beam are obtained by evaluating Lagrange's equation for each of the generalized coordinates and are given by

$$\frac{d}{dt}\left(\frac{\partial L}{\partial \dot{q}_i}\right) - \frac{\partial L}{\partial q_i} = 0 \tag{4.11}$$

for each $i = 1, \ldots, 6$ modal coordinate. The six differential equations are linearized by neglecting second-order and higher terms and are assembled to form a system of linear dynamic beam equations as

$$[\mathbf{M_{b1}}]\ddot{\vec{Q}} + [\mathbf{K_{b1}}]\vec{Q} = [\mathbf{B_a}]\ddot{\vec{P}}_{b1} + [\mathbf{B_p}]\vec{P}_{b1} \tag{4.12}$$

where

$$[\mathbf{M_{b1}}] = \begin{bmatrix} I_7 & I_8 & I_9 & 0 & 0 & 0 \\ I_8 & I_{10} & I_{11} & 0 & 0 & 0 \\ I_9 & I_{11} & I_{12} & 0 & 0 & 0 \\ 0 & 0 & 0 & I_{22} & I_{23} & I_{24} \\ 0 & 0 & 0 & I_{23} & I_{25} & I_{26} \\ 0 & 0 & 0 & I_{24} & I_{26} & I_{27} \end{bmatrix}$$

$$[\mathbf{K_{b1}}] = \begin{bmatrix} \frac{EI_xI_{34}}{\xi} - gI_{40} & \frac{EI_xI_{52}}{\xi} - gI_{41} & \frac{EI_xI_{53}}{\xi} - gI_{42} & 0 & 0 & 0 \\ \frac{EI_xI_{52}}{\xi} - gI_{41} & \frac{EI_xI_{35}}{\xi} - gI_{43} & \frac{EI_xI_{54}}{\xi} - gI_{44} & 0 & 0 & 0 \\ \frac{EI_xI_{53}}{\xi} - gI_{42} & \frac{EI_xI_{54}}{\xi} - gI_{44} & \frac{EI_xI_{36}}{\xi} - gI_{45} & 0 & 0 & 0 \\ 0 & 0 & 0 & \frac{EI_yI_{37}}{\xi} - gI_{46} & \frac{EI_yI_{55}}{\xi} - gI_{47} & \frac{EI_yI_{56}}{\xi} - gI_{48} \\ 0 & 0 & 0 & \frac{EI_yI_{55}}{\xi} - gI_{47} & \frac{EI_yI_{38}}{\xi} - gI_{49} & \frac{EI_yI_{57}}{\xi} - gI_{50} \\ 0 & 0 & 0 & \frac{EI_yI_{56}}{\xi} - gI_{48} & \frac{EI_yI_{57}}{\xi} - gI_{50} & \frac{EI_yI_{39}}{\xi} - gI_{51} \end{bmatrix}$$

$$[\mathbf{B_a}] = \begin{bmatrix} -I_1 & 0 & 0 & -I_{28} \\ -I_2 & 0 & 0 & -I_{29} \\ -I_3 & 0 & 0 & -I_{30} \\ 0 & -I_4 & I_{31} & 0 \\ 0 & -I_5 & I_{32} & 0 \\ 0 & -I_6 & I_{33} & 0 \end{bmatrix}$$

$$[\mathbf{B_p}] = \begin{bmatrix} 0 & 0 & 0 & -gI_1 \\ 0 & 0 & 0 & -gI_2 \\ 0 & 0 & 0 & -gI_3 \\ 0 & 0 & gI_4 & 0 \\ 0 & 0 & gI_5 & 0 \\ 0 & 0 & gI_6 & 0 \end{bmatrix}$$

The I_j's are integrals of the shape functions, ϕ_{xi}'s and ϕ_{yi}'s, and are defined in Appendix A.

Energy dissipation of the beam vibrations is modeled as viscous damping. A damping matrix is constructed by applying logarithmic decrement to experimental data of the open-loop time response of the beam. A diagonal matrix, $[\mathbf{C_b}]$, is formed and included in the beam model as

$$[\mathbf{M_{b1}}]\ddot{\vec{Q}} + [\mathbf{C_b}]\dot{\vec{Q}} + [\mathbf{K_{b1}}]\vec{Q} = [\mathbf{B_a}]\ddot{\vec{P}}_{b1} + [\mathbf{B_p}]\vec{P}_{b1} \tag{4.13}$$

The modal coordinates, $\vec{Q} = [q_{x1}\ q_{x2}\ q_{x3}\ q_{y1}\ q_{y2}\ q_{y3}]^T$, are now related to the base inputs, $\vec{P}_{b1} = [R_x\ R_y\ \gamma_b\ \beta_b]^T$, by the differential equation 4.13 describing the linear dynamics of the flexible beam.

4.2 Linear Truss Kinematics

In this first experiment, the adaptive truss is positioned in an equilibrium configuration ($\gamma = 0$, $\beta = 0$) such that the three active battens are extended to half of their operating range ($l_1 = l_2 = l_3 = \frac{1}{2} l_{max}$). For this adaptive truss position, the iterative forward solution of Section 3.2 is applied to determine the gimbal axes offset d. With the active batten lengths, $\vec{L} = [l_1\ l_2\ l_3]^T$, and the slew parameters, γ, β, and d, known, the linear position, velocity, and acceleration transformations between the coordinates of the moving reference frame, $\vec{P}_m = [X\ Y\ Z\ \gamma\ \beta]^T$, and the active battens, $\vec{L}$, can be determined from the methods of Section 3.4. Applying these methods, the following linear transformations are established

$$\begin{aligned} \vec{P}_m &= [\mathbf{J_p}]\vec{L} \\ \dot{\vec{P}}_m &= [\mathbf{J_v}]\dot{\vec{L}} \\ \ddot{\vec{P}}_m &= [\mathbf{J_a}]\ddot{\vec{L}} \end{aligned} \tag{4.14}$$

But, the velocity transformation is equal to the acceleration transformation linearized about zero velocity, such that, $[\mathbf{J_a}] = [\mathbf{J_v}]$ as established in Section 3.4.3. Additionally, positioning the adaptive truss in an equilibrium configuration establishes a special property of the linear kinematic transformations. For any equilibrium position ($l_1 = l_2 = l_3$), the position, velocity, and acceleration transformations are

equal such that equation 4.14 becomes

$$\begin{aligned} \vec{P}_m &= [\mathbf{J_p}]\vec{L} \\ \dot{\vec{P}}_m &= [\mathbf{J_p}]\dot{\vec{L}} \\ \ddot{\vec{P}}_m &= [\mathbf{J_p}]\ddot{\vec{L}} \end{aligned} \tag{4.15}$$

Finally, the Z coordinate is dropped from $\vec{P}_m$ since, as explained in Section 4.1, this coordinate is orthogonal to the transverse deflections of the beam. Also, it is noted from Section 3.4 that α has already been dropped, and consequently, the remaining coordinates of the moving reference frame are regrouped as $\vec{P}_{m1} = [X\ Y\ \gamma\ \beta]^T$ and equation 4.15 is redefined as

$$\begin{aligned} \vec{P}_{m1} &= [\mathbf{J_{p1}}]\vec{L} \\ \dot{\vec{P}}_{m1} &= [\mathbf{J_{p1}}]\dot{\vec{L}} \\ \ddot{\vec{P}}_{m1} &= [\mathbf{J_{p1}}]\ddot{\vec{L}} \end{aligned} \tag{4.16}$$

4.3 Plate Flexibility

The transverse deflections of the flexible beam create reaction moments at the clamped interface between the beam and top flexible plate. These moments deflect the flexible plate causing relative rotations between the coordinate system fixed to the base of the beam, $\vec{P}_{b1}$, and the moving reference frame, $\vec{P}_{m1}$, as shown in Fig. 4.2. However, the dynamic effects of the top plate are not significant since a finite-element model of the plate determined that the lowest plate frequency (68 hz) is more than three times greater the highest modeled mode of the flexible beam (21 hz). Thus, the inertia of the top plate is neglected, and only the stiffness is modeled, and in this thesis, only the trunnion stiffness is included.

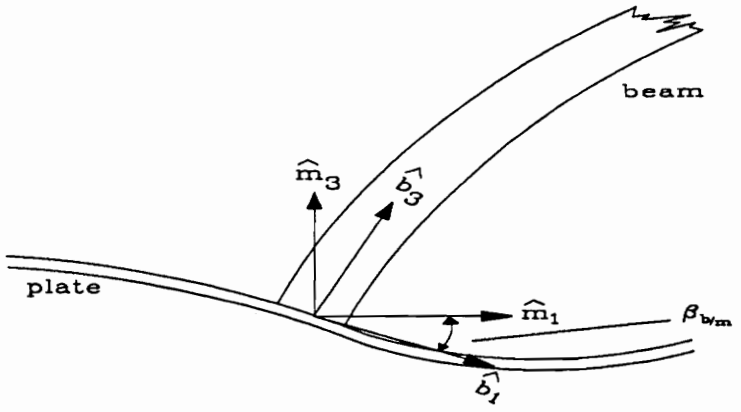

a. Relative rotation about the $\hat{m}_2$ coordinate.

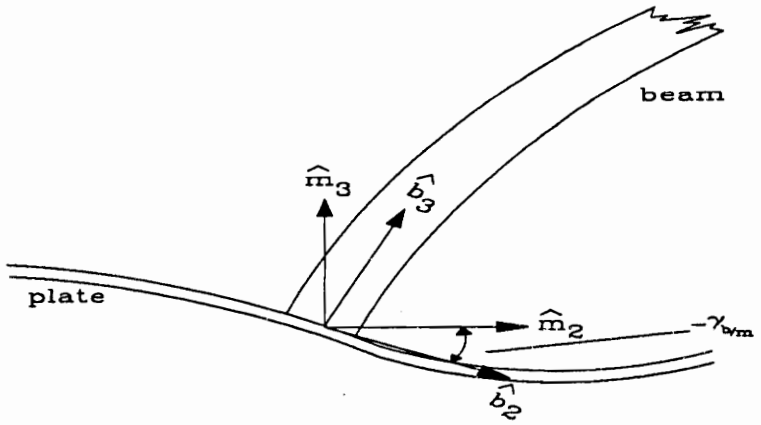

b.Relative rotation about the $\hat{m}_1$ coordinate.

Figure 4.2: Flexible Plate Rotations

The coordinates at the base of the beam are identical to the moving frame coordinates except for the relative rotations so that

$$\vec{P}_{b1} = \vec{P}_{m1} + \vec{P}_{b/m} \tag{4.17}$$

where,

$$\vec{P}_{b/m} = [\ 0 \quad 0 \quad \gamma_{b/m} \quad \beta_{b/m}\ ]^T$$

are the relative rotations of $\vec{P}_{b1}$ with respect to $\vec{P}_{m1}$.

Multiplying the relative rotations by torsional spring rates, the reaction moments at the interface between the base of the beam and the flexible plate are approximated by

$$\vec{F}_{b/m} = \begin{bmatrix} k_\gamma & 0 \\ 0 & k_\beta \end{bmatrix} \begin{bmatrix} \gamma_{b/m} \\ \beta_{b/m} \end{bmatrix} \tag{4.18}$$

where k_γ and k_β are experimentally-determined trunnion stiffness parameters of the plate.

These reactions are equal to the bending moments at the base of the clamped beam. The bending moment is proportional to the second derivative of the transverse displacement and is determined from

$$\begin{aligned} M_\gamma &= EI_x \frac{\partial^2 w_x}{\partial s^2} \\ M_\beta &= EI_y \frac{\partial^2 w_y}{\partial s^2} \end{aligned} \tag{4.19}$$

where s is the length parameter along the beam. Equation 4.4 is substituted for the transverse deflections, w_x and w_y, and evaluated for $s = 0$. The resulting bending moments, M_γ and M_β, are now functions of the modal coordinates $\vec{Q}$ and are related by the transformation $[\mathbf{T_Q}]$ such that

$$\begin{bmatrix} M_\gamma \\ M_\beta \end{bmatrix} = [\mathbf{T_Q}]\vec{Q} \tag{4.20}$$

and

$$[\mathbf{T_Q}] = \begin{bmatrix} 0 & 0 & 0 & -EI_x\frac{\partial^2\phi_{x1}(0)}{\partial s^2} & -EI_x\frac{\partial^2\phi_{x2}(0)}{\partial s^2} & -EI_x\frac{\partial^2\phi_{x3}(0)}{\partial s^2} \\ EI_y\frac{\partial^2\phi_{y1}(0)}{\partial s^2} & EI_y\frac{\partial^2\phi_{y2}(0)}{\partial s^2} & EI_y\frac{\partial^2\phi_{y3}(0)}{\partial s^2} & 0 & 0 & 0 \end{bmatrix}$$

The bending moments, M_γ and M_β, are equated to the reaction moments, $\vec{F}_{b/m}$, such that the relative rotations are solved from

$$\begin{bmatrix} \gamma_{b/m} \\ \beta_{b/m} \end{bmatrix} = \begin{bmatrix} k_\gamma & 0 \\ 0 & k_\beta \end{bmatrix}^{-1} [\mathbf{T_Q}]\vec{Q} \tag{4.21}$$

Substituting the above equation into equation 4.17, the coordinates at the base of the beam assume the form

$$\vec{P}_{b1} = \vec{P}_{m1} + [\mathbf{T_{b/m}}]\vec{Q} \tag{4.22}$$

where

$$[\mathbf{T_{b/m}}] = \begin{bmatrix} 0 & 0 & 0 & 0 & 0 & 0 \\ 0 & 0 & 0 & 0 & 0 & 0 \\ 0 & 0 & 0 & -\frac{EI_x\partial^2\phi_{x1}(0)}{k_\beta\partial s^2} & -\frac{EI_x\partial^2\phi_{x2}(0)}{k_\beta\partial s^2} & -\frac{EI_x\partial^2\phi_{x3}(0)}{k_\beta\partial s^2} \\ \frac{EI_y\partial^2\phi_{y1}(0)}{k_\gamma\partial s^2} & \frac{EI_y\partial^2\phi_{y2}(0)}{k_\gamma\partial s^2} & \frac{EI_y\partial^2\phi_{y3}(0)}{k_\gamma\partial s^2} & 0 & 0 & 0 \end{bmatrix}$$

Finally, equation 4.22 is substituted into the beam equation 4.13 resulting in modified mass and stiffness matrices for the flexible beam such that

$$[\mathbf{M_b}]\ddot{\vec{Q}} + [\mathbf{C_b}]\dot{\vec{Q}} + [\mathbf{K_b}]\vec{Q} = [\mathbf{B_a}]\ddot{\vec{P}}_{m1} + [\mathbf{B_p}]\vec{P}_{m1} \tag{4.23}$$

where

$$[\mathbf{M_b}] = [\mathbf{M_{b1}}] - [\mathbf{B_a}][\mathbf{T_{b/m}}]$$

$$[\mathbf{K_b}] = [\mathbf{K_{b1}}] - [\mathbf{B_p}][\mathbf{T_{b/m}}]$$

4.4 Motor Dynamics

The motor system used is a DC motor driven by a linear, pulse-width modulated amplifier. Attached to the output shaft of the motor is a planetary gear train connected to a lead screw. The amplifier and motor are assumed to perform as a current-driven torque source so that internal motor characteristics such as armature resistance and inductance do not affect the transfer function of input voltage to link accelerations. Incorporating the gain of the amplifier, k_a, the planetary gear

reduction, g_r, and the leadscrew reduction, g_l, the model for this system is

$$\ddot{l} = \frac{k_a k_t g_l}{J_a g_r} V_{in} \tag{4.24}$$

where k_t is the torque constant of the motor and J_a is the motor armature inertia. This equation is written for each active batten to form

$$\begin{bmatrix} \ddot{l}_1 \\ \ddot{l}_2 \\ \ddot{l}_3 \end{bmatrix} = k_m \begin{bmatrix} V_{in1} \\ V_{in2} \\ V_{in3} \end{bmatrix} \tag{4.25}$$

for

$$k_m = \frac{k_a k_t g_l}{J_a g_r}$$

4.5 System Dynamics

The system equations consist of the linear kinematic transformations 4.16, the beam equations 4.23, and the motor equations 4.25. These equations are transformed into state-space representation such that they are assembled in a set of first-order differential equations in terms of two types of variables, state variables and input variables. The state variables are the batten lengths, modal coordinates, and their respective rates. The input variables are motor voltage commands. Arranging these equations into state-space representation results in

$$\dot{\vec{\Psi}} = [\mathbf{F}]\vec{\Psi} + [\mathbf{G}]\vec{U} \tag{4.26}$$

where

$$[\mathbf{F}] = \begin{bmatrix} \begin{bmatrix} 0 & 0 & 0 & 0 & 0 & 0 & 0 & 0 & 0 & 1 & 0 & 0 & 0 & 0 & 0 & 0 & 0 & 0 \\ 0 & 0 & 0 & 0 & 0 & 0 & 0 & 0 & 0 & 0 & 1 & 0 & 0 & 0 & 0 & 0 & 0 & 0 \\ 0 & 0 & 0 & 0 & 0 & 0 & 0 & 0 & 0 & 0 & 0 & 1 & 0 & 0 & 0 & 0 & 0 & 0 \\ 0 & 0 & 0 & 0 & 0 & 0 & 0 & 0 & 0 & 0 & 0 & 0 & 1 & 0 & 0 & 0 & 0 & 0 \\ 0 & 0 & 0 & 0 & 0 & 0 & 0 & 0 & 0 & 0 & 0 & 0 & 0 & 1 & 0 & 0 & 0 & 0 \\ 0 & 0 & 0 & 0 & 0 & 0 & 0 & 0 & 0 & 0 & 0 & 0 & 0 & 0 & 1 & 0 & 0 & 0 \\ 0 & 0 & 0 & 0 & 0 & 0 & 0 & 0 & 0 & 0 & 0 & 0 & 0 & 0 & 0 & 1 & 0 & 0 \\ 0 & 0 & 0 & 0 & 0 & 0 & 0 & 0 & 0 & 0 & 0 & 0 & 0 & 0 & 0 & 0 & 1 & 0 \\ 0 & 0 & 0 & 0 & 0 & 0 & 0 & 0 & 0 & 0 & 0 & 0 & 0 & 0 & 0 & 0 & 0 & 1 \\ 0 & 0 & 0 & 0 & 0 & 0 & 0 & 0 & 0 & 0 & 0 & 0 & 0 & 0 & 0 & 0 & 0 & 0 \\ 0 & 0 & 0 & 0 & 0 & 0 & 0 & 0 & 0 & 0 & 0 & 0 & 0 & 0 & 0 & 0 & 0 & 0 \\ 0 & 0 & 0 & 0 & 0 & 0 & 0 & 0 & 0 & 0 & 0 & 0 & 0 & 0 & 0 & 0 & 0 & 0 \end{bmatrix} \\ \left[[\mathbf{M_b}][\mathbf{B_p}][\mathbf{J_p}] \right]_{6\times3} \quad \left[-[\mathbf{M_b}]^{-1}[\mathbf{K_b}] \right]_{6\times6} \quad [\mathbf{0}]_{6\times3} \quad \left[-[\mathbf{M_b}]^{-1}[\mathbf{C_b}] \right]_{6\times6} \end{bmatrix}$$

$$[\mathbf{G}] = k_m \begin{bmatrix} \begin{bmatrix} 0 & 0 & 0 \\ 0 & 0 & 0 \\ 0 & 0 & 0 \\ 0 & 0 & 0 \\ 0 & 0 & 0 \\ 0 & 0 & 0 \\ 0 & 0 & 0 \\ 0 & 0 & 0 \\ 0 & 0 & 0 \\ 1 & 0 & 0 \\ 0 & 1 & 0 \\ 0 & 0 & 1 \end{bmatrix} \\ \left[[\mathbf{M_b}]^{-1}[\mathbf{B_a}][\mathbf{J_p}] \right]_{6\times3} \end{bmatrix}$$

for

$$\vec{\Psi} = \begin{bmatrix} \vec{L} \\ \vec{Q} \\ \dot{\vec{L}} \\ \dot{\vec{Q}} \end{bmatrix}$$

$$\vec{U} = \begin{bmatrix} V_{in1} \\ V_{in2} \\ V_{in3} \end{bmatrix}$$

Equation 4.26 is discretized since on-line control is implemented with a digital computer. Solving for the homogeneous and particular solutions of the differential equation 4.26 for a zero-order hold on the inputs over sampling interval, T_s, results in the vector difference equation of the form

$$\vec{\Psi}_{k+1} = [\mathbf{\Phi}(T_s)]\vec{\Psi}_k + [\mathbf{\Gamma}(T_s)]\vec{U}_k \tag{4.27}$$

where $[\mathbf{\Phi}(T_s)]$ is the homogeneous solution and defined by the matrix exponential as

$$[\mathbf{\Phi}(T_s)] = e^{[\mathbf{F}]T_s}$$

and $[\mathbf{\Gamma}(T_s)]$ is the particular solution for a constant input over the sampling time, T_s, and is given by

$$[\mathbf{\Gamma}(T_s)] = \int_0^{T_s} e^{[\mathbf{F}]t} dt \; [\mathbf{G}]$$

Chapter 5

Control Law Design and Results: Experiment 1

Physically, the adaptive truss and flexible beam are digitally controlled with a PC-XT computer. The computer provides two fundamental services for the adaptive truss-flexible beam control system. One, the computer serves as host for the analog-to-digital (A/D) and digital-to-analog (D/A) converters, and two, the computer serves as the digital controller where the vector of feedback signals are multiplied by a feedback matrix to form the vector of command signals. The generation of this feedback matrix, and its influence on the vibration control response of the flexible beam are discussed below.

5.1 Control Law Design

The discretized state-space equation 4.27 has 18 state variables, the three active batten lengths $\vec{L}$, the six modal coordinates $\vec{Q}$, the three active batten velocities $\dot{\vec{L}}$, and the six modal rates, $\dot{\vec{Q}}$. Only 12 of the 18 states are fed back to the controller since the modal rates are neither measured nor estimated. The batten displacements are measured directly by "yo-yo" potentiometers, and the batten velocities are de-

termined from tachometer measurements on the motors. The modal coordinates are generated from beam strain measurements by multiplying the beam strains by a transformation matrix, $[\mathbf{T_{q/\epsilon}}]$.

A strain-to-modal-coordinate transformation, $[\mathbf{T_{q/\epsilon}}]$, can be developed from expressing strain at various locations along the beam as functions of beam modal coordinates. Strain due to bending in a beam is proportional to the second derivative of the transverse displacement, and can be expressed as

$$\begin{aligned} \epsilon_x(s) &= c_x \frac{\partial^2 w_x}{\partial s^2} \\ \epsilon_y(s) &= c_y \frac{\partial^2 w_y}{\partial s^2} \end{aligned} \tag{5.1}$$

where $\epsilon_x(s)$ and $\epsilon_y(s)$ are the strains for position, s, along the beam, and c_x and c_y are the distances from the neutral axes. Substituting equation 4.4 for the transverse displacements, w_x and w_y, in the above equation results in

$$\begin{aligned} \epsilon_x(s) &= c_x \left(\frac{\partial^2 \phi_{x1}}{\partial s^2} q_{x1} + \frac{\partial^2 \phi_{x2}}{\partial s^2} q_{x2} + \frac{\partial^2 \phi_{x3}}{\partial s^2} q_{x3} \right) \\ \epsilon_y(s) &= c_y \left(\frac{\partial^2 \phi_{y1}}{\partial s^2} q_{y1} + \frac{\partial^2 \phi_{y2}}{\partial s^2} q_{y2} + \frac{\partial^2 \phi_{y3}}{\partial s^2} q_{y3} \right) \end{aligned} \tag{5.2}$$

The above expression is evaluated for the specific locations, s_1, s_2, s_3, corresponding to the exact placement of the three strain gages in each direction of the beam. Assembling these equations yields the following relationship

$$\vec{\Upsilon} = [\mathbf{T_{\epsilon/q}}]\vec{Q} \tag{5.3}$$

where

$$\vec{\Upsilon} = [\ \epsilon_x(s_1)\quad \epsilon_x(s_2)\quad \epsilon_x(s_3)\quad \epsilon_y(s_1)\quad \epsilon_y(s_2)\quad \epsilon_y(s_3)\ ]^T$$

However, the above transformation, $[\mathbf{T}_{\epsilon/\mathbf{q}}]$, is modal coordinates-to-strains, and the desired transformation is strains-to-modal coordinates, $[\mathbf{T}_{\mathbf{q}/\epsilon}]$. By performing the inversion, the desired relationship is given as

$$\vec{Q} = [\mathbf{T}_{\mathbf{q}/\epsilon}]\vec{\Upsilon} \tag{5.4}$$

where

$$[\mathbf{T}_{\mathbf{q}/\epsilon}] = [\mathbf{T}_{\epsilon/\mathbf{q}}]^{-1}$$

Although the modal coordinates are not measured, they can now be generated by the digital computer by multiplying the measured beam strain signals by the above transformation, $[\mathbf{T}_{\mathbf{Q}/\epsilon}]$.

The motor commands, $\vec{U} = [V_{in1}\ V_{in2}\ V_{in3}]^T$ are generated according to the state feedback law

$$\vec{U} = -[\mathbf{K}]\vec{\Psi} \tag{5.5}$$

where again $\vec{\Psi}$ is the state vector given in equation 4.26. The feedback matrix, $[\mathbf{K}]$, is designed by applying the Linear Quadratic Regulator such that $[\mathbf{K}]$ minimizes the performance index

$$J_{cost} = \int_0^{t_f} \vec{\Psi}^T[\tilde{\mathbf{Q}}]\vec{\Psi} + \vec{U}^T[\tilde{\mathbf{R}}]\vec{U}\ dt \tag{5.6}$$

subject to the constraints of equation 4.26.

$[\tilde{\mathbf{Q}}]$ and $[\tilde{\mathbf{R}}]$ are penalty matrices and the selection of their diagonal entries ($[\tilde{\mathbf{Q}}]$, a positive semi-definite matrix, and $[\tilde{\mathbf{R}}]$, a positive definite matrix, are usually diagonal matrices) depends on the relative importance of the system states and control effort.

First, the diagonal entries of $[\tilde{\mathbf{R}}]$ are selected. $[\tilde{\mathbf{R}}]$ weights the control effort for each of the actuators, but for this method each actuator is treated as equal to any other so each entry is the same. Also, since the ratio of $[\tilde{\mathbf{Q}}]$ and $[\tilde{\mathbf{R}}]$ is important, the actual value of the diagonal entries can be set to one without loss of generality.

Next, the states are ranked in order of importance. For the vibration control problem with the adaptive truss, the modal amplitudes of the flexible beam are ranked as most important since it is the stated fundamental task of the adaptive truss to control these beam vibrations. The diagonal entries for the modal amplitudes are set to 10000. The positions and velocities of the active battens are ranked lower than the modal amplitudes but are ranked equal in importance since position control of the adaptive truss with a current-driven motor system requires feedback of both positions and velocities of the battens. The diagonal entries for the batten positions and velocities are set to 100. Finally, since the modal rates are neither measured nor estimated their respective diagonal entries are set to zero.

Upon selection of the $[\tilde{\mathbf{Q}}]$ and $[\tilde{\mathbf{R}}]$ penalty matrices, the gain matrix is calculated as described previously. Although zero penalties were placed on the modal rates, the LQR procedure will still generate small, nonzero gains for these states. The gain

matrix is slightly modified by setting the gains on the modal rates to zero since the actual control scheme neither measures nor estimates the modal rates. Implementing the control law by substituting equation 5.5 in the discrete equation 4.27 results in the discrete closed-loop equation

$$\vec{\Psi}_{k+1} = [\mathbf{\Phi}(T_s)]\vec{\Psi}_k - [\mathbf{\Gamma}(T_s)][\mathbf{K}]\vec{\Psi}_k \tag{5.7}$$

5.2 Test Procedure and Results

Open-loop and closed-loop initial-condition vibration tests are implemented to demonstrate the effectiveness of the adaptive truss controlling the transverse vibrations of the flexible beam for each direction of the beam principal axes. The initial condition is established by deflecting the tip of the beam and releasing at time zero. The first tests are open-loop tests with the adaptive truss fixed and an initial condition imposed on the beam. Time histories of the strain measurements on the beam are recorded and the open-loop response of the tip of the beam is estimated according to equation 5.4 and plotted in Fig. 5.1 for the two directions of the beam. In the closed-loop tests, the initial condition is again imposed on the beam and released at time zero. After a short period of time, the control is activated and the adaptive truss motors are driven in accordance with equation 5.5. Again the time response of the strains is recorded and the estimated tip response of the beam in the two directions is shown in Fig. 5.2.

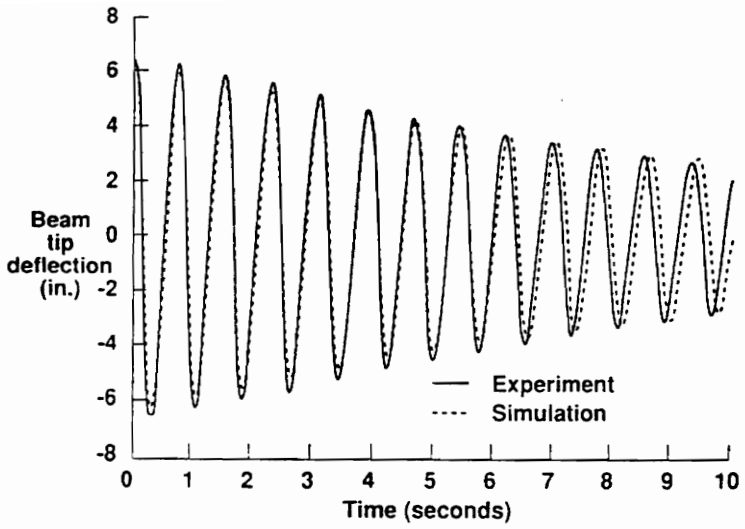

a. Time response of beam tip deflection in $\hat{b}_1$ direction.

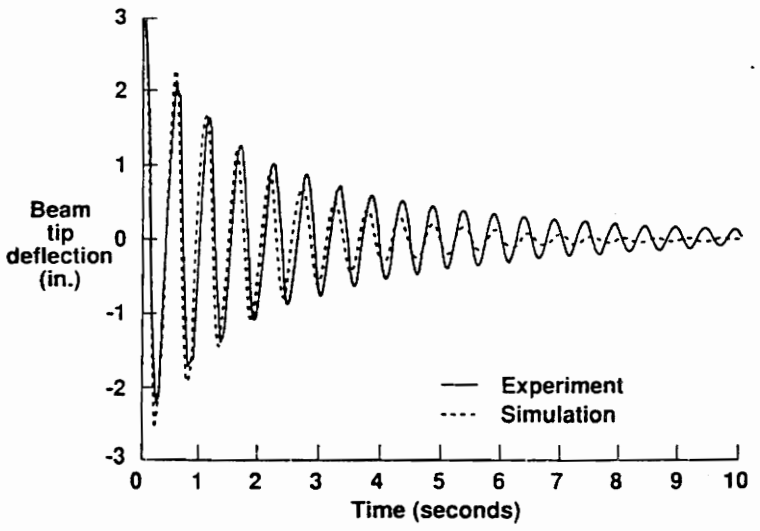

b. Time response of beam tip deflection in $\hat{b}_2$ direction.

Figure 5.1: Simulated and Experimental Uncontrolled Beam Response

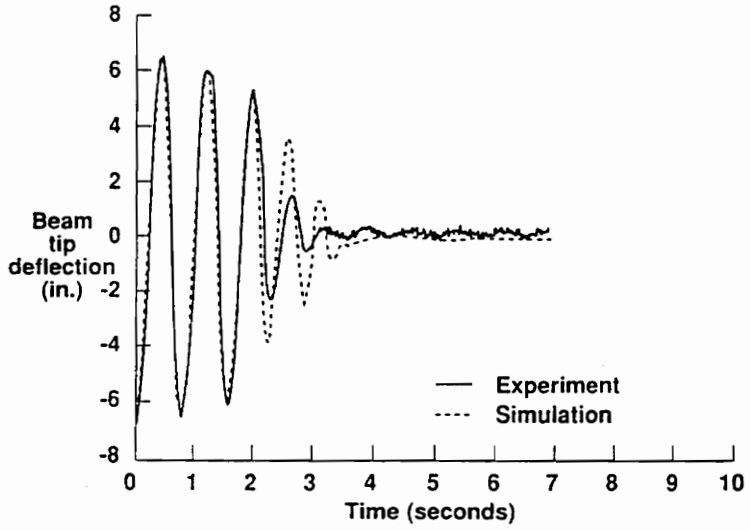

a. Time response of beam tip deflection in $\hat{b}_1$ direction.

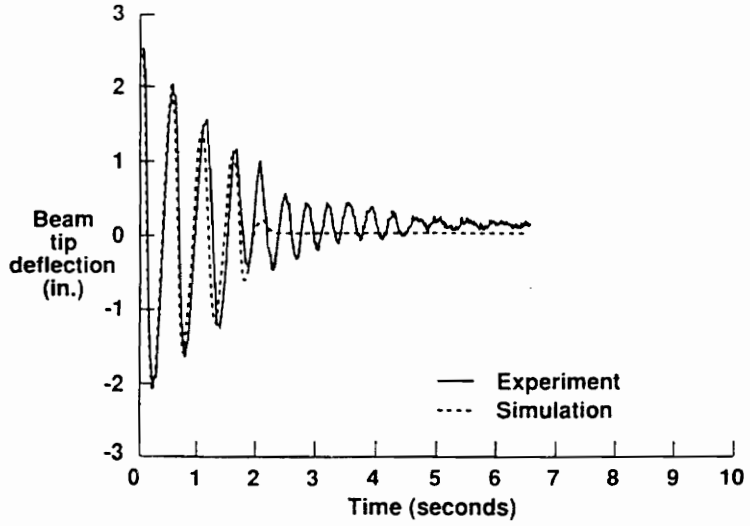

b. Time response of beam tip deflection in $\hat{b}_2$ direction.

Figure 5.2: Simulated and Experimental Controlled Beam Response

By comparison, simulations of the adaptive truss and beam system are performed to analytically predict the controlled and uncontrolled beam response. The closed-loop response is the simulation of equation 5.7 and the open-loop response is the simulation of the same equation with $[\mathbf{K}] = 0$. The uncontrolled beam tip deflection in the $\hat{b}_1$-direction is shown with the experimental results in Fig. 5.1a. Good agreement of frequency and damping is observed between the experimental and simulated responses with a correlation coefficient of 0.92. Uncontrolled beam tip deflection in the $\hat{b}_2$-direction is shown in Fig. 5.1b. It is noted that the simulated response does not accurately predict the experimental response resulting in a correlation coefficient of 0.79. This difference is possibly due to the clamped condition assumed in the beam model. It is not the true boundary condition for the $\hat{b}_2$-direction since the end condition is a stiff-pinned end condition due to $\hat{b}_2$-constraint of the holding device that attaches the beam to the top plate, whereas the $\hat{b}_1$-constraint of the holding device more closely approximates a clamped end-condition.

The closed-loop response in the $\hat{b}_1$-direction is shown in Fig. 5.2a and again the simulation accurately predicts the experimental response with a correlation coefficient of 0.85. This plot also shows good control of the beam tip deflection with experimental damping improved from 0.01 to 0.2. The controlled $\hat{b}_2$-response is shown in Fig. 5.2b with the correlation coefficient between the simulated response and the experimental response of 0.71. Here the controlled response shows some improvement of the damping of the tip deflection, but not as good as the results predicted by the simulation. Again this discrepancy is possibly due to the difference between the assumed and true boundary condition of the holding device as described above.

Chapter 6

Nonlinear Model

Experiment 2 simulates vibration control of the flexible beam while the adaptive truss is positioned at a large-angle configuration, and experiment 3 simulates vibration control of the beam during a large-angle slewing maneuver of the adaptive truss. Both simulations require nonlinear equations of motion to accurately predict the system behavior.

Whether the beam is positioned arbitrarily in the gravity field or slewed through a large angle, it is expected that the nonlinearities of the beam will be severe enough to affect the vibration control. In order to approximate the nonlinear beam behavior, a set of differential equations describing first-mode beam dynamics is developed which retain nonlinear terms up to and including third-order. There are several possibilities for the origins of nonlinear terms in the beam model. The most obvious is in the geometry of slewing the beam through large angles, γ and β. A second possibility is through large deflections of the beam itself, which results in a nonlinear strain energy representation. A long, slender beam such as the one studied in this thesis is a good candidate for such nonlinear effects. The final possible origin of nonlinear terms examined in this thesis is through effects of gravity. When slewing

the beam through large angles, gravitational terms make up a large part of the potential energy of the system. Such nonlinear terms may have a significant effect on the model's performance. Each of these possibilities for nonlinearities will be discussed as the beam equations of motion are presented.

The nonlinear kinematic relationships presented in Section 3.3 are included in the nonlinear equations of motion. The nonlinear kinematic equations are used to predict the motions of the adaptive truss when vibration control is applied in the simulations of experiment 2 and experiment 3. This is in contrast to the linear transformations used to predict the truss motions in the simulations of experiment 1. In addition, the nonlinear kinematic equations are necessary to predict the motions of the adaptive truss for a slewing maneuver as simulated in experiment 3. A brief discussion of how these nonlinear kinematic equations are implemented in experiment 2 and experiment 3 is presented.

Finally, it is noted here that experiments 2 and 3 do not model the top flexible plate nor do they include the damping of the flexible beam. This is because experiments 2 and 3 perform computer simulations and not hardware experiments as in experiment 1. As a result, there is no need to include experimentally measured parameters such as the trunnion stiffness of the plate and the damping ratios of the beam in the analytical models since there is no measured data for these experiments to compare to. Also, experiments 2 and 3 encompass nonlinear modeling techniques and the inclusion of these experimentally determined parameters might cloud the effect of these nonlinearities.

6.1 Nonlinear Beam Model

The beam equations of motion are developed via the Lagrangian energy approach where a general position vector for a differential mass along the beam is found according to Fig. 6.1 and is the starting point in the development for both the linear model of Section 4.1 and the following nonlinear model. This position vector is given as

$$\begin{aligned}\vec{R} = R_x\hat{n}_1 + R_y\hat{n}_2 + R_z\hat{n}_3 + w_x\hat{b}_1 \\ +w_y\hat{b}_2 + z\hat{b}_3\end{aligned} \tag{6.1}$$

The translations R_x, R_y, and R_z, are Newtonian coordinates describing the origin of the $\hat{b}$ reference frame attached to the base of the beam. The $\hat{b}_3$ component of the differential mass is z, and the transverse beam deflections are w_x and w_y. The transformation relating the $\hat{b}$ coordinates to the Newtonian coordinates is given by equation 4.2. Substituting this transformation in equation 6.1 results in the position vector explicitly expressed in terms of the $\hat{n}$ coordinates and is given by

$$\begin{aligned}\vec{R} = R_x\hat{n}_1 + R_y\hat{n}_2 + R_z\hat{n}_3 + w_x[(c\alpha_b c\beta_b)\hat{n}_1 + (c\alpha_b s\beta_b s\gamma_b + s\alpha_b c\gamma_b)\hat{n}_2 \\ +(s\alpha_b s\gamma_b - c\alpha_b s\beta_b c\gamma_b)\hat{n}_3] + w_y[(-s\alpha_b c\beta_b)\hat{n}_1 + (c\gamma_b c\alpha_b - s\alpha_b s\beta_b s\gamma_b)\hat{n}_2 \\ +(s\alpha_b s\beta_b c\gamma_b + c\alpha_b s\gamma_b)\hat{n}_3] + z[(s\beta_b)\hat{n}_1 + (-c\beta_b s\gamma_b)\hat{n}_2 + (c\beta_b c\gamma_b)\hat{n}_3]\end{aligned} \tag{6.2}$$

where the angles γ_b, β_b, and α_b are rotations of the $\hat{b}$ reference frame with respect to the Newtonian frame.

The transverse beam deflections, w_x and w_y, are approximated by a Rayleigh-Ritz discretization which can be written as

$$\begin{aligned}w_x(s,t) = \textstyle\sum_{i=1}^{n} \phi_{xi}(s)q_{xi}(t) \\ w_y(s,t) = \textstyle\sum_{i=1}^{n} \phi_{yi}(s)q_{yi}(t)\end{aligned} \tag{6.3}$$

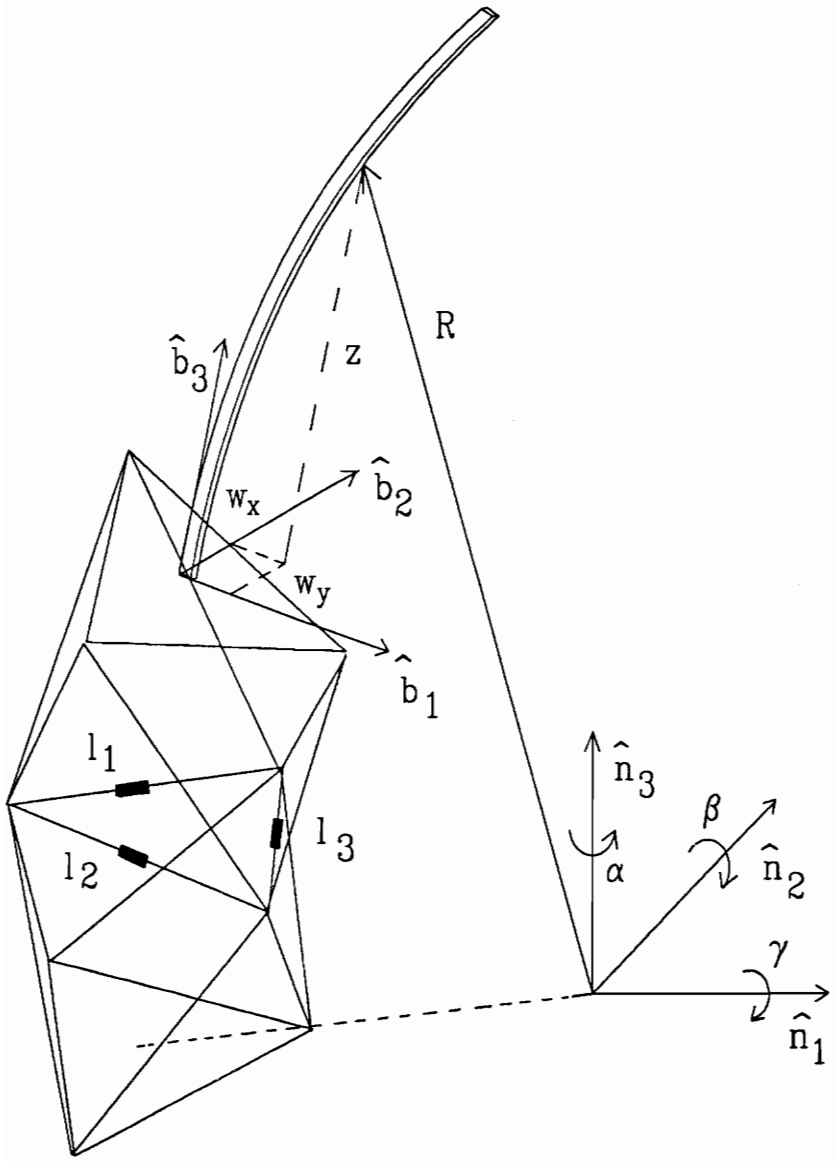

Figure 6.1: Adaptive Truss and Flexible Beam Coordinate Systems

where the $\phi_i(s)$'s are mode shape functions for the ith mode derived from Euler beam theory for a clamped-free beam, and the $q_i(t)$'s are the corresponding modal deflections. In the nonlinear model, the transverse deflections in each bending direction are expanded only to first mode. The nonlinearities in the beam equation become increasingly complicated as more modes are added, so to simplify the problem, only the first mode is retained. This allows the determination of the important nonlinear terms in the model. Upon substituting the single-mode approximations for the transverse deflections in equation 6.2, the position vector becomes

$$\begin{aligned}\vec{R} = {} & R_x\hat{n}_1 + R_y\hat{n}_2 + R_z\hat{n}_3 + \phi_{x1}q_{x1}[(c\alpha_b c\beta_b)\hat{n}_1 + (c\alpha_b s\beta_b s\gamma_b + s\alpha_b c\gamma_b)\hat{n}_2 \\ & +(s\alpha_b s\gamma_b - c\alpha_b s\beta_b c\gamma_b)\hat{n}_3] + \phi_{y1}q_{y1}[(-s\alpha_b c\beta_b)\hat{n}_1 + (c\gamma_b c\alpha_b - s\alpha_b s\beta_b s\gamma_b)\hat{n}_2 \\ & +(s\alpha_b s\beta_b c\gamma_b + c\alpha_b s\gamma_b)\hat{n}_3] + z[(s\beta_b)\hat{n}_1 + (-c\beta_b s\gamma_b)\hat{n}_2 + (c\beta_b c\gamma_b)\hat{n}_3]\end{aligned} \tag{6.4}$$

As previously mentioned, the base of the beam is allowed to move through six general degrees-of-freedom; the three Newtonian displacements, R_x, R_y, and R_z, and three respective rotations about the Newtonian axes, γ_b, β_b, and α_b. But again the α_b rotation about the $\hat{\mathbf{n}}_3$ axis is neglected and is not carried through the remaining equations. However, the rotations γ_b and β_b are not assumed small as in the linear beam model of Chapter 4 where $s\beta_b \approx \beta_b$, $c\beta_b \approx 1$, etc. Instead these expressions are retained and are later expanded as Taylor series in the kinetic and potential energy equations.

The kinetic and potential energy expressions are developed next. Terms up to fourth-order are retained, leading to third-order nonlinearities in the equations of motion. First the kinetic energy, T, is evaluated from

$$T = \frac{1}{2}\int_0^{L_b} \dot{\vec{R}} \bullet \dot{\vec{R}}\, dm \tag{6.5}$$

with the position vector $\vec{R}$ given by equation 6.4. The kinetic energy is expanded in a Taylor series and truncated to keep up to fourth-order terms. As will be shown later, the majority of terms which couple beam deflections in the two directions w_x and w_y arise from the kinetic energy, through geometric nonlinearities. In order for this coupling to show up, there must be motion of the base of the beam through both angles γ_b and β_b.

As mentioned previously, the potential energy is made up of two parts, strain potential and gravity potential. The strain energy is found by the expression

$$V_{strain} = \frac{1}{2} EI \int_0^{L_b} \kappa(s)^2 \, ds \tag{6.6}$$

where $\kappa(s)$ is the curvature of the beam at any location, s, along its length. The curvature in either bending direction, w_x or w_y, is found by the method followed by Aravamudan [1973] where

$$\kappa(s) = \frac{d\phi}{ds} \tag{6.7}$$

but

$$tan(\phi) = \frac{dw}{dz} = \frac{w'}{z'} \tag{6.8}$$

or

$$\phi = \tan^{-1}\left(\frac{w'}{z'}\right) \tag{6.9}$$

where w represents either of the transverse deflections, w_x or w_y, and $'$ denotes differentiation with respect to s. The derivative of the arctangent function can be

expressed as

$$\frac{d\left(\tan^{-1}\left(u(x)\right)\right)}{dx} = \frac{1}{1+u^2}\frac{du}{dx} \tag{6.10}$$

for some $u(x)$. Using equation 6.10 and letting $u = \frac{w'}{z'}$, $\kappa(s)$ can be expressed as

$$\begin{aligned} \kappa(s) &= \frac{d\phi}{ds} = \frac{1}{1+\left(\frac{w'}{z'}\right)}\frac{d\left(\frac{w'}{z'}\right)}{ds} \\ &= \frac{1}{1+\left(\frac{w'}{z'}\right)^2}\frac{z'w'' - z''w'}{z'^2} \\ &= \frac{z'w'' - z''w'}{z'^2 + w'^2} \end{aligned} \tag{6.11}$$

Realizing that in either direction

$$z'^2 + w'^2 = 1 \tag{6.12}$$

The curvature can be written as

$$\kappa(s) = z'w'' - z''w' = \frac{w''}{\sqrt{1-w'^2}} \tag{6.13}$$

Expanding by means of the binomial theorem, this expression can be rewritten as

$$\kappa(s) = w''\left(1 + \frac{1}{2}w'^2 + \cdots\right) \tag{6.14}$$

Substituting the above expression for curvature into equation 6.6, results in the high-order strain potential energy. Note that no coupling between the two bending directions results from this method of representing the strain energy.

The final energy term to be derived is that for potential energy due to gravity, which

is expressed as

$$V_{gravity} = g \int_0^{L_b} \vec{R} \bullet \hat{n}_3 \, dm = g\xi \int_0^{L_b} \vec{R} \bullet \hat{n}_3 \, ds \tag{6.15}$$

where g is acceleration due to gravity, and ξ is the beam's mass per unit length. Using the expression for $\vec{R}$ in equation 6.4, the dot product is found to be

$$\begin{aligned} \vec{R} \bullet \hat{n}_3 = R_z + zc\beta_b c\gamma_b \\ -\phi_{x1} q_{x1} s\beta_b c\gamma_b + \phi_{y1} q_{y1} s\gamma_b \end{aligned} \tag{6.16}$$

In order to perform the integration of equation 6.15, a relationship between z and s is required. Considering a general beam deflection, a differential arc length at any point along the beam can be written as

$$ds^2 = dz^2 + dw_x^2 + dw_y^2 \tag{6.17}$$

which can be rearranged to give z as a function of s

$$z = \int_0^s \left(1 - \left(\frac{dw_x}{ds} \right)^2 - \left(\frac{dw_y}{ds} \right)^2 \right)^{\frac{1}{2}} ds \tag{6.18}$$

Expanding the integrand using the binomial theorem leads to

$$\begin{aligned} z = \int_0^s \left(1 - \tfrac{1}{2}(w_x')^2 - \tfrac{1}{2}(w_y')^2 + \tfrac{1}{8}(w_x')^4 \right. \\ \left. + \tfrac{1}{8}(w_y')^4 + \tfrac{1}{4}(w_x')^2 (w_y')^2 \right) ds \end{aligned} \tag{6.19}$$

By applying equations 6.16, 6.18 and 6.19, the gravitational potential energy is found as a fourth-order truncation of the Taylor series of equation 6.15.

The equations of motion for the beam are found by applying Lagrange's equation to

the kinetic and potential energy expressions derived above. Forming the Lagrangian $L = T - (V_{strain} + V_{gravity})$ and evaluating Lagrangian's equation 4.11 for the first modal coordinate, q_{x1} and q_{y1}, in each bending direction of the beam, results in equations 6.20 and 6.21 shown below. In each equation, the first two lines contain those terms which arise from the kinetic energy, the third line contains the terms which come from the gravity potential, and the fourth line shows the terms arising from the strain energy.

$$\begin{gathered}\ddot{q}_{x1}I_7\xi + \ddot{R}_x\left(I_1\xi - \tfrac{1}{2}I_1\xi\beta_b^2\right) - \ddot{R}_zI_1\xi\beta_b + \ddot{R}_yI_1\xi\gamma_b\beta_b - \ddot{\gamma}_bI_{13}\xi q_{y1}\beta_b \\ +\ddot{\beta}_bI_{28}\xi + \dot{\gamma}_b\left(-2I_{13}\xi\dot{q}_{y1}\beta_b + \dot{\gamma}_b^2I_{28}\xi\beta_b\right) - \dot{\beta}_b^2I_7\xi q_{x1} \\ +g\xi\left(\tfrac{1}{2}\gamma_b^2I_1\beta_b + \tfrac{1}{6}\beta_b^3I_1 - \beta_bI_1 - q_{x1}I_{70} + \tfrac{1}{2}q_{x1}^3I_{71} + \tfrac{1}{2}q_{x1}q_{y1}^2I_{71}\right) \\ +q_{x1}EI_xI_{34} + 2q_{x1}^3EI_xI_{60} = 0\end{gathered} \tag{6.20}$$

$$\begin{gathered}\ddot{q}_{y1}I_{22}\xi + \ddot{R}_y\left(I_4\xi - \tfrac{1}{2}I_4\xi\gamma_b^2\right) + \ddot{R}_zI_4\xi\gamma_b + \ddot{\gamma}_b\left(I_{13}\xi q_{x1}\beta_b + \tfrac{1}{2}I_{31}\xi\beta_b^2 - I_{31}\xi\right) \\ +\dot{\gamma}_b\left(2I_{13}\xi\beta_b\dot{q}_{x1} + 2I_{13}\xi\dot{\beta}_bq_{x1} + 2I_{31}\xi\beta_b\dot{\beta}_b\right) - \dot{\gamma}_b^2I_{22}\xi q_{y1} \\ +g\xi\left(-\tfrac{1}{6}\gamma_b^3I_4 + \gamma_bI_4 - q_{y1}I_{70} + \tfrac{1}{2}q_{y1}^3I_{71} + \tfrac{1}{2}q_{x1}^2q_{y1}I_{71}\right) \\ +q_{y1}EI_yI_{37} + 2q_{y1}^3EI_yI_{60} = 0\end{gathered} \tag{6.21}$$

In the above equations, q_{x1} and q_{y1} are the first-mode deflections in the w_x and w_y directions, respectively, I_x and I_y are the area moments of inertia corresponding to either bending direction, and I_1 - I_{71} are various integrals of mode shape functions given in Appendix A. These equations show the effect of slewing motions on the performance of the system, through geometric nonlinearities of the slew as well as the changing effects of gravity.

Note that we have only shown the equations for the modal coordinates and not for the coordinates at the base of the beam R_x, R_y, R_z, β_b, and γ_b. The nonlinear beam model is developed as a "stiff" model, so that the coordinates representing the base motions of the beam serve only as kinematic inputs to the beam (and act as

forcing terms in the beam equations), and have no structural dynamics associated with them. These coordinates are affected by actuation of the active links in the adaptive truss, and that relationship is discussed next.

6.2 Truss Kinematics

As previously explained, experiments 2 and 3 do not model the flexibility of the top plate and the corresponding rotations. Therefore, for the purposes of the simulations of experiments 2 and 3, the relative rotations between the base of the beam and the adaptive truss are zero. Consequently, the $\hat{b}$ coordinates at the base of the beam shown in Fig. 6.1 are the $\hat{m}$ coordinates of the moving reference frame shown in Fig. 3.1 such that the vector specifying the moving frame coordinates is rewritten as

$$\vec{P}_m = \begin{bmatrix} X \\ Y \\ Z \\ \gamma \\ \beta \end{bmatrix} = \begin{bmatrix} R_x \\ R_y \\ R_z \\ \gamma_b \\ \beta_b \end{bmatrix} \tag{6.22}$$

Now, all of the kinematic relationships of Chapter 3 that describe the moving reference frame equivalently describe the base of the flexible beam.

Experiment 2 simulates linear vibration control about a large-angle operating configuration of the truss. To systematize the required kinematic relations, first, the large-angle orientation of the adaptive truss is chosen in terms of the slew parameters β, γ, and d. With the slew parameters chosen, the various kinematic problems required for experiment 2 are as follows:

1. Use the inverse solution of Section 3.1 to determine the active batten lengths required to orient the truss according to the given slew parameters.

2. Use the methods of Section 3.4 to determine the linear transformations needed for the linear control law development.

3. Use the forward solution of Section 3.2 and the exact kinematic relationships of Section 3.3 to predict the nonlinear kinematic behavior at the base of the flexible beam at each time step in the simulation.

Experiment 3 simulates linear and nonlinear vibration control while the adaptive truss undergoes a large-angle slewing maneuver. For this experiment the initial orientation of the truss is specified by initial slew parameters, γ_i, β_i, and d_i, and the final orientation is specified by final slew parameters, γ_f, β_f, and d_f. With the initial and final slew parameters specified for experiment 3, the required kinematics are:

1. Use the inverse solution of Section 3.1 to determine the active batten lengths for the initial and final truss positions. The final active batten lengths are the reference batten lengths used for position control during the slewing maneuver.

2. Use the methods of Section 3.4 to determine the linear transformations needed for the linear control law development and also for the nonlinear, gain-scheduled control law.

3. Use the forward solution of Section 3.2 and the exact kinematic relationships of Section 3.3 to predict the nonlinear kinematic behavior at the base of the flexible beam at each time step in the simulation.

Chapter 7

Control Law Design and Results: Experiments 2 and 3

Experiments 2 and 3 are computer simulations of control laws applied to the nonlinear equations of motion discussed in Chapter 6. Besides analytically establishing the ability of the adaptive truss to perform vibration control as described in the scenarios of experiments 2 and 3, these experiments attempt to compare the effectiveness of different control strategies. For example, in performing large-angle vibration control with the adaptive truss, it would be advantageous if a linear control law designed about some nominal position of the truss (such as the equilibrium position) could be used for all orientations. To investigate the feasibility of this, two control laws are developed for the large-angle vibration control described by experiment 2, one about the equilibrium position of the truss, and the other about a large-angle position. Both control laws are simulated at the large-angle position of the adaptive truss, with the results of these simulations indicating the effects of the linear kinematic transformations on the performance of these control laws.

The effects of the linear kinematic transformations on the vibration control performance as the adaptive truss undergoes a slewing maneuver are examined in the

simulations of experiment 3. Experiment 3 also compares control strategies that feedback all system states except modal rates to those that feedback all system states except modal positions. There are advantages and disadvantages to both. In a physical system, feeding back modal positions is easily accomplished by multiplying the measured strain signals by a strain-to-mode transformation as was demonstrated in Section 5.1. But as the beam is slewed through large angles in the gravity field, static modal deflections are incurred. These static modal deflections are the reference modal positions, q_{ref}, necessary to achieve vibration control if modal position feedback is used, since driving the difference, $q - q_{ref}$, to zero drives the vibrations to zero. However, updating these reference modal positions during a slewing maneuver is computationally intense since solving a set of coupled nonlinear equations (the static solution of equations 6.20 and 6.21) is required. On the other hand, modal rates are not easily measured (although this may soon change with the advent of new technology such as strain-rate transducers as proposed by Juston [1991]), and estimating them usually results in noisy approximations. But if the modal rates were available, they would be ideally suited for vibration control of the beam during a large-angle slewing maneuver, since driving the modal rates to zero is equivalent to driving the vibrations to zero.

The above effects are investigated in experiment 3 by including them in six different control strategies. Two linear control laws are designed about the equilibrium position of the truss, one feeding back modal rates, and the other feeding back modal positions. Two linear control laws are designed about the final large-angle position of the slewing maneuver, one feeding back modal rates, and the other feeding-back modal positions. Finally, two nonlinear gain-scheduled control laws are designed to

update the linear control law at discrete γ and β locations, with one feeding-back modal rates, and the other feeding-back modal positions.

The development of the above control laws and their respective performance in controlling the beam vibrations in experiments 2 and 3 are presented next.

7.1 Linear Equations of Motion

A linear system of equations is required to derive the linear control laws (as well as the nonlinear gain-scheduled control laws, since it is developed from many linear control laws). The system of equations consists of the beam equations, motor equations, and truss transformations. First, the nonlinear equations of motion for the beam, given by equations 6.21 and 6.20, must be linearized by retaining first-order terms. These linear equations are found to be

$$\begin{bmatrix} I_7 & 0 \\ 0 & I_{22} \end{bmatrix} \begin{bmatrix} \ddot{q}_{x1} \\ \ddot{q}_{y1} \end{bmatrix} + \begin{bmatrix} \frac{EI_xI_{34}}{\xi} - gI_{70} & 0 \\ 0 & \frac{EI_yI_{37}}{\xi} - gI_{70} \end{bmatrix} \begin{bmatrix} q_{x1} \\ q_{y1} \end{bmatrix} =$$

$$\begin{bmatrix} -I_1 & 0 & 0 & 0 & -I_{28} \\ 0 & -I_4 & 0 & I_{31} & 0 \end{bmatrix} \begin{bmatrix} \ddot{R}_x \\ \ddot{R}_y \\ \ddot{R}_z \\ \ddot{\gamma}_b \\ \ddot{\beta}_b \end{bmatrix} + \begin{bmatrix} 0 & 0 & 0 & 0 & gI_1 \\ 0 & 0 & 0 & -gI_4 & 0 \end{bmatrix} \begin{bmatrix} R_x \\ R_y \\ R_z \\ \gamma_b \\ \beta_b \end{bmatrix} \tag{7.1}$$

or equivalently,

$$[\mathbf{M_2}] \begin{bmatrix} \ddot{q}_{x1} \\ \ddot{q}_{y1} \end{bmatrix} + [\mathbf{K_2}] \begin{bmatrix} q_{x1} \\ q_{y1} \end{bmatrix} = [\mathbf{B_{a2}}] \begin{bmatrix} \ddot{R}_x \\ \ddot{R}_y \\ \ddot{R}_z \\ \ddot{\gamma}_b \\ \ddot{\beta}_b \end{bmatrix} + [\mathbf{B_{p_2}}] \begin{bmatrix} R_x \\ R_y \\ R_z \\ \gamma_b \\ \beta_b \end{bmatrix} \tag{7.2}$$

The motor equations are developed in Section 3.4 and are given as

$$\begin{bmatrix} \ddot{l}_1 \\ \ddot{l}_2 \\ \ddot{l}_3 \end{bmatrix} = k_m \begin{bmatrix} V_{in1} \\ V_{in2} \\ V_{in3} \end{bmatrix} \tag{7.3}$$

for

$$k_m = \frac{k_a k_t g_l g_r}{J_a}$$

The beam equations 7.2 and the motor equations 7.3 form five linear first-order differential equations where the dependent variables and their rates are defined as the system states. But, before a state-space model is assembled, the beam and motor equations must be coupled since the beam inputs are written in terms of R_x, R_y, R_z, γ_b, and β_b and not l_1, l_2, and l_3. This discrepancy is handled by noting from Section 6.2 that $\vec{P}_m = [R_x\ R_y\ R_z\ \gamma_b\ \beta_b]$ and by applying the linear kinematic transformations of Section 3.4. These transformations are developed for some orientation, γ and β, of the adaptive truss such that by specifying a different orientation results in a different set of transformations. Upon specifying the truss orientation, the transformations relating the coordinates at the base of the beam, $\vec{P}_m$, to the active batten links, $\vec{L} = [l_1\ l_2\ l_3]^T$, are

$$\begin{aligned} \vec{P}_m &= [\mathbf{J_p}]\vec{L} \\ \ddot{\vec{P}}_m &= [\mathbf{J_v}]\ddot{\vec{L}} \end{aligned} \tag{7.4}$$

Equations 7.2, 7.3, and 7.4 are assembled in state-space representation to form a linear set of differential equations as

$$\dot{\vec{\Psi}}_2 = [\mathbf{F}_2]\vec{\Psi}_2 + [\mathbf{G}_2]\vec{U} \tag{7.5}$$

where

$$[\mathbf{F_2}] = \begin{bmatrix} \begin{bmatrix} 0 & 0 & 0 & 0 & 0 & 1 & 0 & 0 & 0 & 0 \\ 0 & 0 & 0 & 0 & 0 & 0 & 1 & 0 & 0 & 0 \\ 0 & 0 & 0 & 0 & 0 & 0 & 0 & 1 & 0 & 0 \\ 0 & 0 & 0 & 0 & 0 & 0 & 0 & 0 & 1 & 0 \\ 0 & 0 & 0 & 0 & 0 & 0 & 0 & 0 & 0 & 1 \\ 0 & 0 & 0 & 0 & 0 & 0 & 0 & 0 & 0 & 0 \\ 0 & 0 & 0 & 0 & 0 & 0 & 0 & 0 & 0 & 0 \\ 0 & 0 & 0 & 0 & 0 & 0 & 0 & 0 & 0 & 0 \end{bmatrix} \\ \left[[\mathbf{M_2}][\mathbf{B_{p_2}}][\mathbf{J_p}] \right]_{2\times 3} \quad \left[-[\mathbf{M_2}]^{-1}[\mathbf{K_2}] \right]_{2\times 2} \quad [\mathbf{0}]_{2\times 3} \quad [\mathbf{0}]_{2\times 2} \end{bmatrix}$$

$$[\mathbf{G_2}] = k_m \begin{bmatrix} \begin{bmatrix} 0 & 0 & 0 \\ 0 & 0 & 0 \\ 0 & 0 & 0 \\ 0 & 0 & 0 \\ 0 & 0 & 0 \\ 1 & 0 & 0 \\ 0 & 1 & 0 \\ 0 & 0 & 1 \end{bmatrix} \\ \left[[\mathbf{M_2}]^{-1}[\mathbf{B_{a_2}}][\mathbf{J_p}] \right]_{2\times 3} \end{bmatrix}$$

for system states

$$\vec{\Psi}_2 = \begin{bmatrix} l_1 & l_2 & l_3 & q_{x1} & q_{y1} & \dot{l}_1 & \dot{l}_2 & \dot{l}_3 & \dot{q}_{x1} & \dot{q}_{y1} \end{bmatrix}^T$$

and inputs

$$\vec{U} = \begin{bmatrix} V_{in1} \\ V_{in2} \\ V_{in3} \end{bmatrix}$$

7.2 Control Laws

All the control laws used in experiments 2 and 3 are derived from an optimal (Linear Quadratic Regulator) feedback control law, where the control, $\vec{U} = [V_{in1}\ V_{in2}\ V_{in3}]^T$

is a function of the states, $\vec{\Psi}_2$, as

$$\vec{U} = -[\mathbf{K}]\ \vec{\Psi}_2 \tag{7.6}$$

where $[\mathbf{K}]$ is found by minimizing the performance index

$$J_{cost} = \int_0^{t_f} \vec{\Psi}_2^T[\tilde{\mathbf{Q}}]\vec{\Psi}_2 + \vec{U}^T[\tilde{\mathbf{R}}]\vec{U}\ dt \tag{7.7}$$

subject to the constraints of equation 7.5. The matrices, $[\tilde{\mathbf{Q}}]$ and $[\tilde{\mathbf{R}}]$, are penalty matrices and are weighted according to the method described in Section 5.1 with the following modifications. Two types of feedback schemes are considered, feedback of all system states except modal rates and feedback of all system states but modal positions. When either of the two feedback schemes are implemented, the gains on those states which are not fedback are truncated to zero. In order to make fair comparisons between the two feedback strategies, it is necessary to have the gains developed fairly. Consequently, the penalty matrices, $[\tilde{\mathbf{Q}}]$ and $[\tilde{\mathbf{R}}]$, are weighted such that the penalties on the modal rates and the modal positions are identical in anticipation that the resulting gains will have equal control authority.

In addition to designing a control law according to the type of feedback, the control law can be directly tied to the truss orientation. For any slewed orientation (γ and β), the linear transformations can be derived from Section 3.4, and with these transformations, a different set of linearized equations of motion can be formed, and thus a different set of feedback gains. This is how the different linear control laws are developed for different positions of the truss. In light of this, as the truss is slewed to new positions, new control laws can be derived for each orientation (γ

and β). But, by mapping these orientations onto a grid and deriving a control law for each grid space, the control law can be updated, or gain-scheduled, according to the orientation of the truss. So as the adaptive truss moves through each grid space (each discrete γ and β), the control is no longer just a linear function of the states, $\vec{U} = [\mathbf{K}]\ \vec{\Psi}$, but is now a nonlinear function of the states and truss orientation, $\vec{U} = f(\vec{\Psi}, \gamma, \beta)$. This is the nonlinear, gain-scheduled control law applied in experiment 3.

Finally, the reference positions of the batten lengths are filtered for the simulations of experiment 3. This is because at the beginning of the slew, the beam experiences a step input at its base generating large initial condition vibrations. The step input at the base of the beam is caused by the acceleration of the truss when a control law is applied. So as part of the strategy in controlling the beam vibrations during a large-angle slew, a first-order pre-filter is placed on the reference batten positions in an attempt to lessen these step-input vibrations.

7.3 Simulation Results: Experiment 2

Using the nonlinear beam model of Section 6.2, the nonlinear kinematics of Section 3.3, and the motor model of Section 4.4, numerical simulations were performed to show the performance of a linear control law in the face of large-angle nonlinearities. The simulation results shown are based on controlling initial condition beam vibrations when the truss (and therefore, the beam) are oriented with nonzero angles γ and β. The initial condition is a tip deflection in both directions if the beam released at time zero. Two cases are discussed below.

In the first case the angles are $\gamma = 30°$ and $\beta = 30°$ while the second case is a much more severe slew of $\gamma = 50°$ and $\beta = 50°$. Both of these cases are within the range of possible motions of the test article described in Chapter 2, although the second case is near the limits of that range. In each case, two control laws are used, both of which are designed using the linear quadratic regulator method with modal position feedback. The differences between the two control laws are in the linear kinematic transformations used to relate the link motions to the base motions of the beam. In each case, one control law was based on the transformations defined for γ and β rotations equal to zero (if one were to perform general large-angle control using a single linear quadratic regulator control law, this is the most likely candidate), while the other control law was based on the transformations defined for γ and β rotations equal to those of the truss orientation in that particular case. The results of each case are shown in Figures 7.1 and 7.2.

Note that in each case where the control law is developed about the equilibrium position of the truss, the vibration control performance is poor in comparison with the control law developed about the respective large-angle position. The only difference in the control laws is the linear kinematic transformations for which they are developed. Note also that the response plots show that each modal deflection has a static component. This results from slewing the beam into the gravity field.

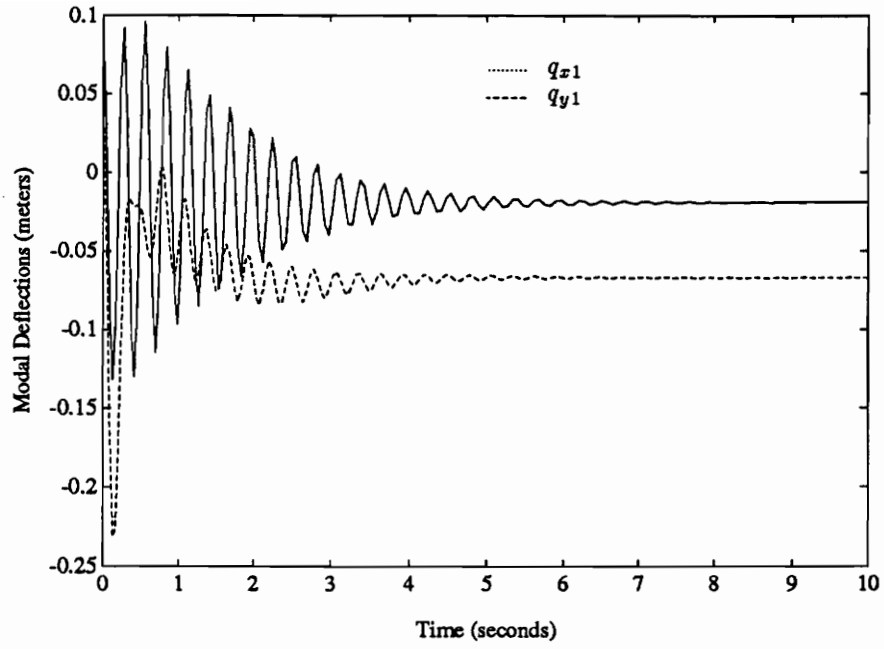

a. Control law developed at $\gamma = 30°$, $\beta = 30°$.

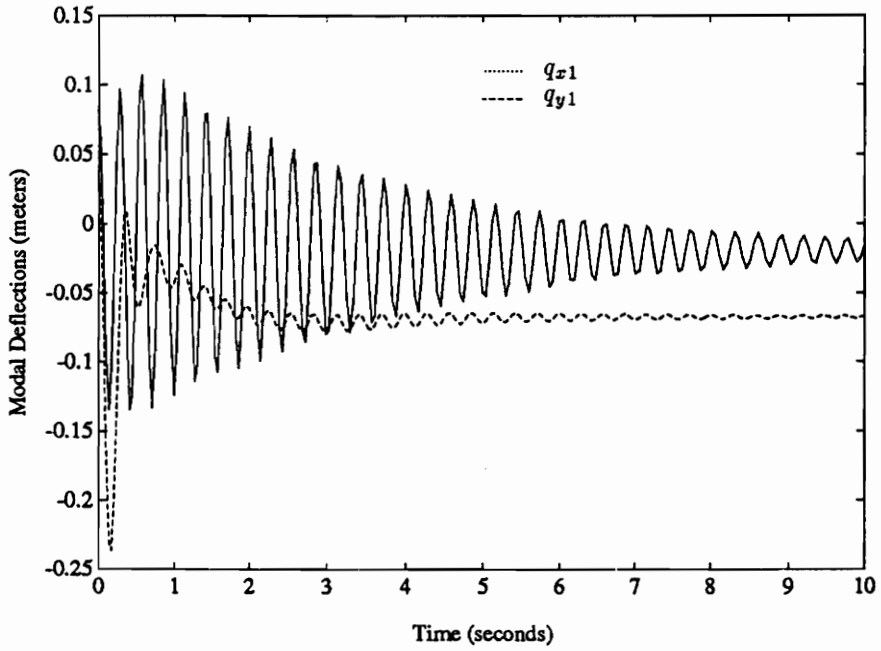

b. Control law developed at $\gamma = 0°$, $\beta = 0°$.

Figure 7.1: Controlled Response at Large-Angle Truss Orientation of $\gamma = 30°$ and $\beta = 30°$

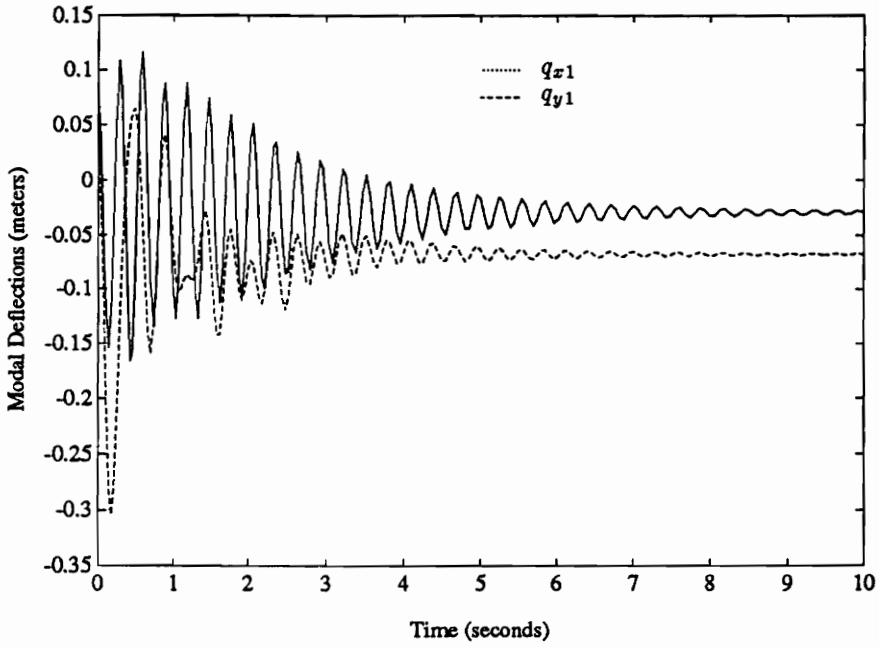

a. Control law developed at $\gamma = 50°$, $\beta = 50°$.

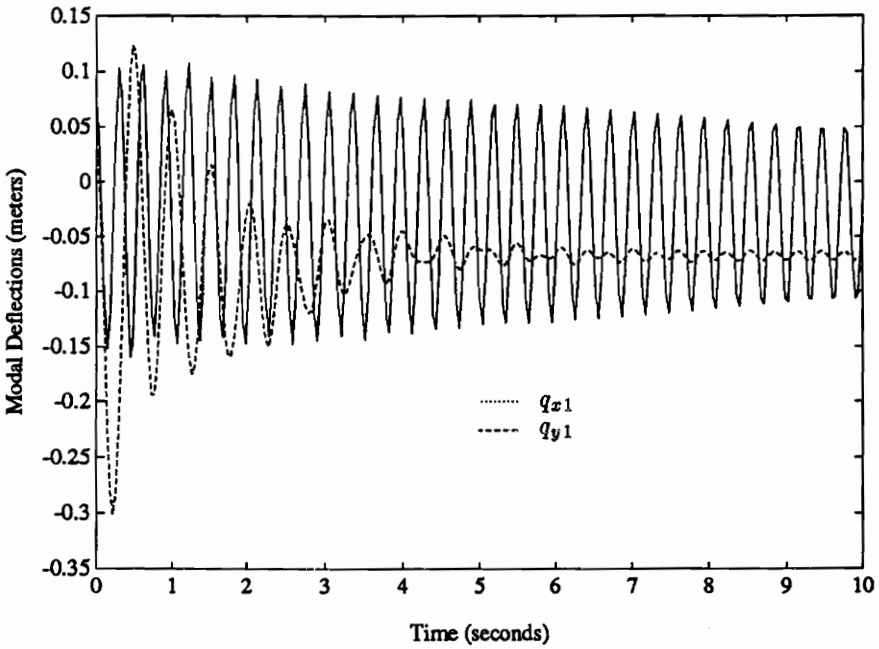

b. Control law developed at $\gamma = 0°$, $\beta = 0°$.

Figure 7.2: Controlled Response at Large-Angle Truss Orientation of $\gamma = 50°$ and $\beta = 50°$

7.4 Simulation Results: Experiment 3

Again using the nonlinear beam model of Section 6.2, the nonlinear kinematics of Section 3.3, and the motor model of Section 4.4, numerical simulations were performed to show the vibration control performance of six different control strategies as the adaptive truss slews the beam from the equilibrium position to a large-angle position of $\gamma = 30°$ and $\beta = 30°$. But, before these six control simulations are presented, the effect of filtering the reference batten positions on the beam vibrations is investigated. To demonstrate the effect of the filter, two simulations were performed of a large-angle slew without vibration control, one using the filter and one not. The difference between the initial conditions generated with and without the filter is shown in Fig 7.3. The filter considerably reduces the initial condition vibrations as shown in Fig. 7.3a with only a slight loss in the time it takes the truss to perform the slew as indicated by the time-trace of link position 1 as shown in Fig. 7.3b. Because of the good performance, this pre-filter is used on the reference batten positions in all of the control simulations. The six simulation cases are discussed below.

The first two cases shown in Fig. 7.4 simulate the linear vibration control of the beam during a large-angle slew of the truss. The linear control law is designed about the equilibrium position of the truss with the first case feeding back all states except modal rates and the second case feeding back all states except modal positions. As Fig. 7.4 shows, both cases control the beam vibrations during the slewing maneuver with the modal rate feedback case performing better than the position feedback case. However, the position feedback case has a faster settling response than the rate

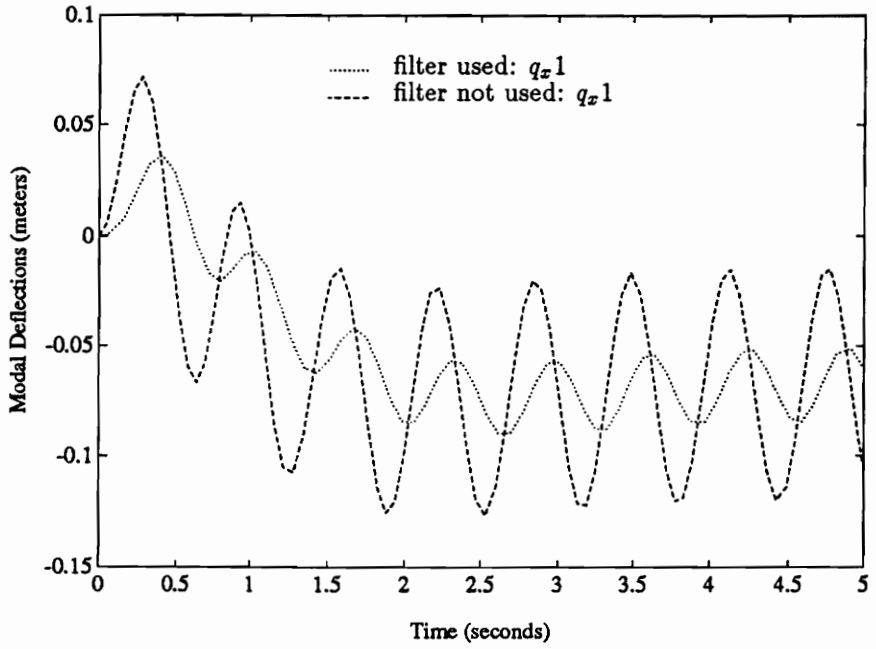

a: Beam response to step input.

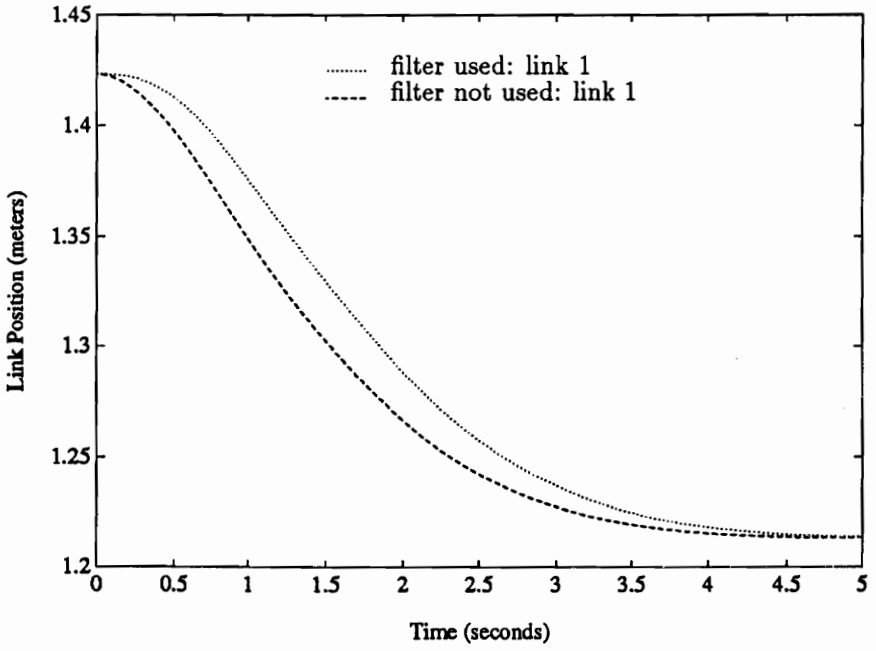

b: Time history of link 1.

Figure 7.3: Filtered and Unfiltered Responses for a Slew of $\gamma = 30°$ and $\beta = 30°$

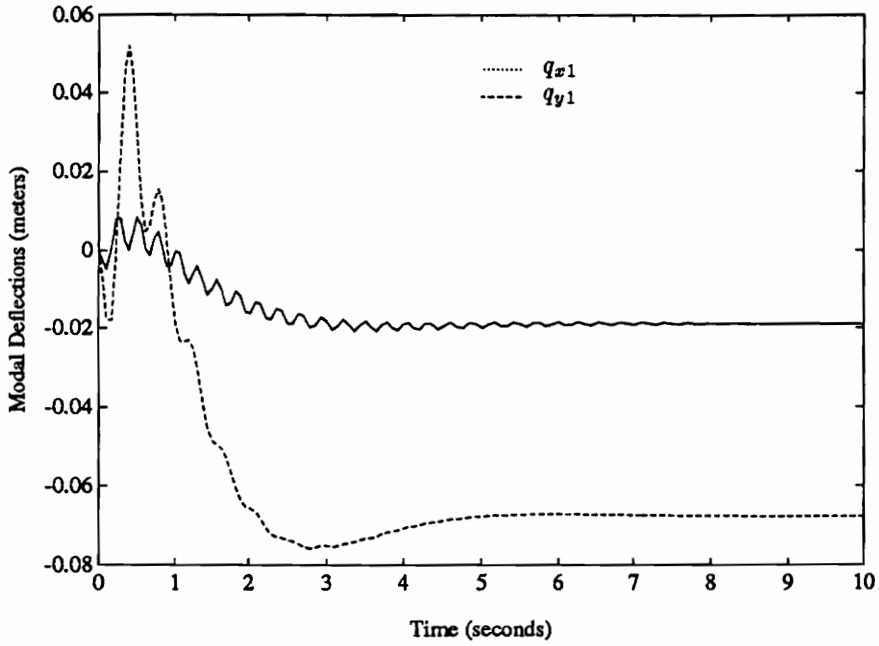

Feed back all states except modal rates.

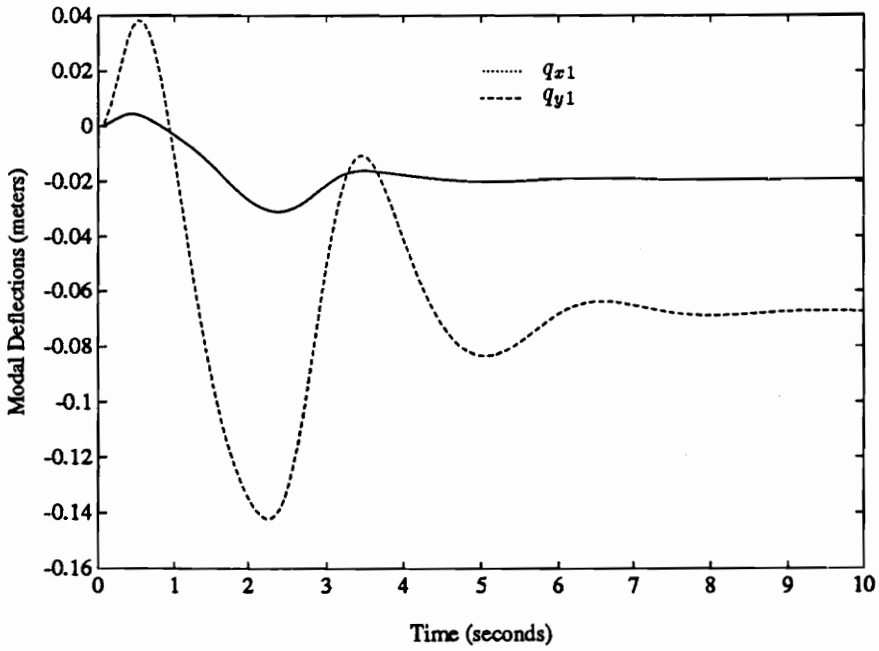

Feed back all states except modal positions.

Figure 7.4: Controlled Response for Slew of $\gamma = 30°$ and $\beta = 30°$, Linear Control Designed at $\gamma = 0°$ and $\beta = 0°$

feedback case. It is also observed from Fig. 7.4 that the higher frequency response of mode q_{y1} in the position feedback case is highly damped in the rate feedback case. This is because damping is generated by feeding back the modal rates, but also since the positions are not fed back in this case, the system is less stiff resulting in a slower frequency. Finally, it is noted from Fig. 7.4b that although the modal positions are not fedback in the modal rate feedback case the modal positions do settle to the same gravity deflections shown in Fig. 7.4a. This is because as the control force recedes there ceases to be any external forces on the system, and the modal coordinates naturally settle in the states of lowest energy which are the static gravity deflections.

The second two cases shown in Fig. 7.5 simulate the linear vibration control of the beam during the same large-angle slew as performed in the first two cases. This time the linear control law is designed about the final orientation of the slew maneuver ($\gamma = 30°$ and $\beta = 30°$) with the first case feeding back all states except modal rates and the second case feeding back all states except modal positions. Figure 7.5 shows that both cases control the beam vibrations during the slewing maneuver with the modal rate feedback case again achieving better vibration control performance than the position feedback. Comparisons between Fig. 7.4 and Fig. 7.5 show that the linear control law designed about the final slewed orientation performs slightly better for both respective feedback schemes than the linear control designed about the equilibrium position.

Finally, the last two cases shown in Fig. 7.6 simulate the nonlinear gainscheduled vibration control of the beam during the same large-angle slew as performed in the

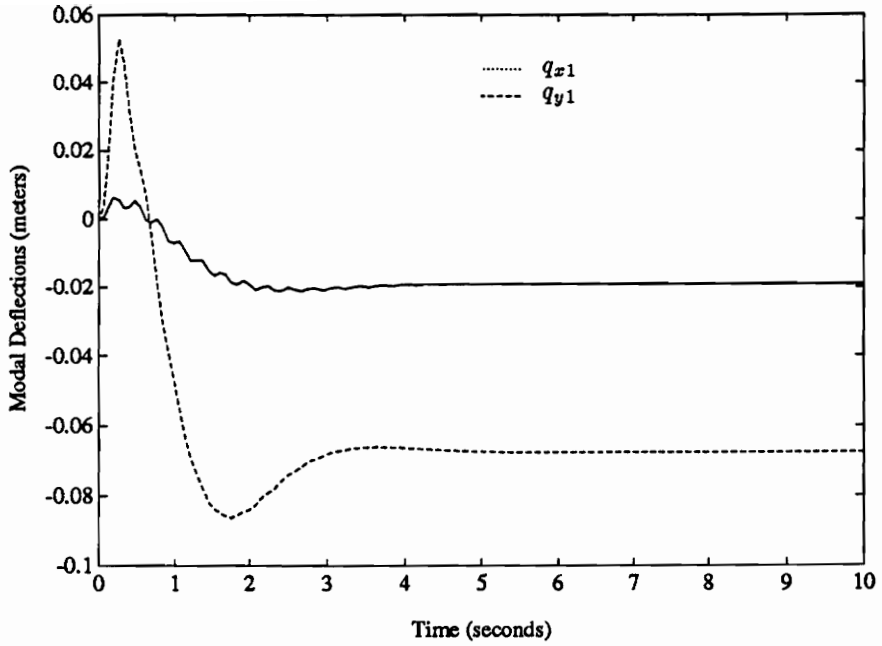

Feed back all states except modal rates.

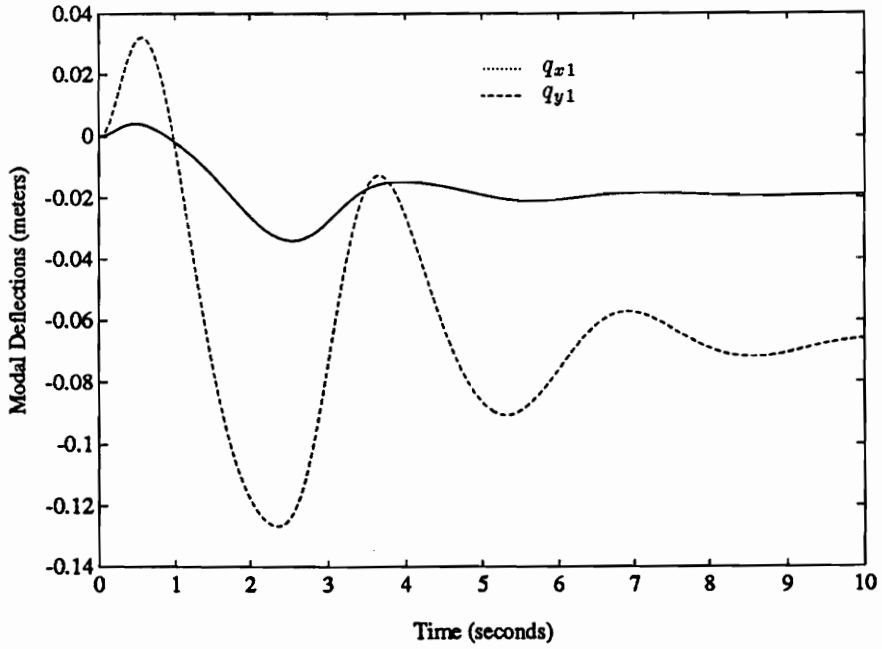

Feed back all states except modal positions.

Figure 7.5: Controlled Response for Slew of $\gamma = 30°$ and $\beta = 30°$, Linear Control Designed at $\gamma = 30°$ and $\beta = 30°$

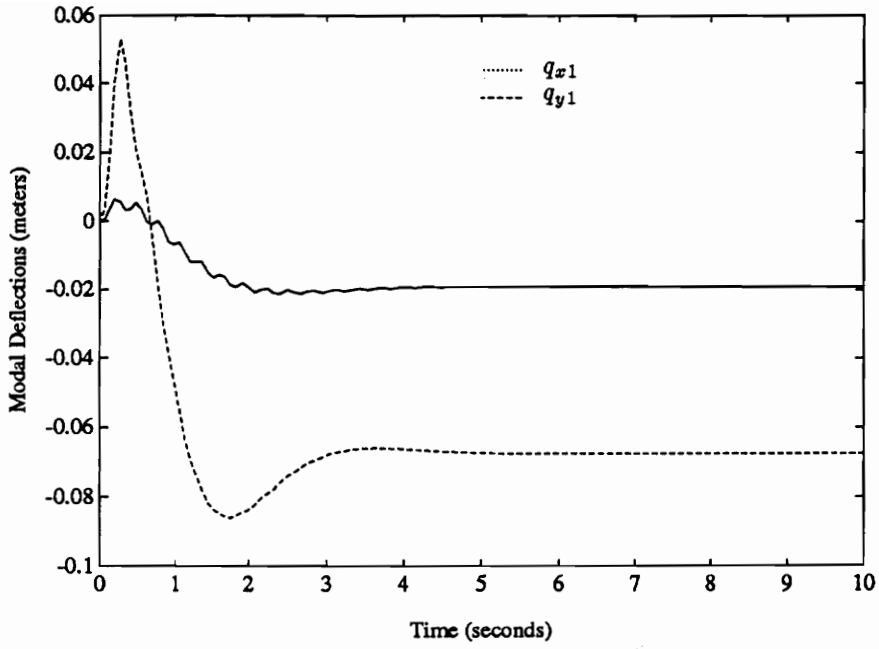

Feed back all states except modal rates.

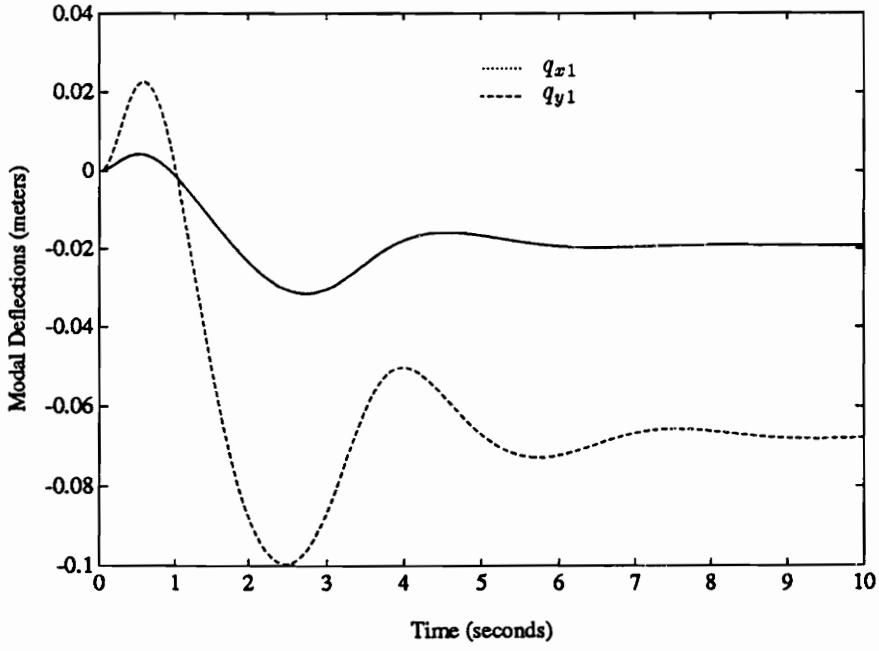

Feed back all states except modal positions.

Figure 7.6: Controlled Response for Slew of $\gamma = 30°$ and $\beta = 30°$, Nonlinear Gain-Scheduled Control Law

previous cases. This time the control law is updated, or gain-scheduled, according to the orientation of the truss. That is, as the adaptive truss moves through each grid space (each discrete γ and β) a new control law is applied where each of these new control laws were previously (off-line) designed about each discrete γ and β. Figure 7.6 shows that again both cases control the beam vibrations during the slewing maneuver with the modal rate feedback case performing better than the position feedback case. Finally, comparisons between Fig. 7.4, Fig. 7.5 and Fig. 7.6 show that the nonlinear gain-scheduled control law using the modal rate feedback scheme achieves a superior response compared to the others.

Chapter 8

Conclusions and Recommendations

Vibration control of a flexible continuum with a double-octahedral adaptive truss has been analytically demonstrated for three different cases: vibration control about a truss equilibrium position, vibration control about a large-angle truss position, and vibration control during a large-angle slewing maneuver. Vibration control has been physically demonstrated about an equilibrium position with a double-octahedral adaptive truss test article different in design, actuation, and plant dynamics from previous studies. In addition to attaining the goals of achieving vibration control for the above mentioned cases, the following conclusions can be made.

- Numerically proved that the linear acceleration and velocity transformations reduce to the position transformation at any equilibrium position.
- The existence of a twisting, α, rotation of the truss was demonstrated first.
- Nonlinear gain-scheduled control laws were shown to be effective for vibration control in a slewing maneuver.
- Showed that linear control laws can be used in large-angle slews, although the performance is degraded in comparison to the gain-scheduled control.

Some of the refinements and improvements to the work presented in this thesis could include,

- Expand nonlinear beam model to include three or more modes.
- Include the α and Z coordinates in the equations of motion.
- For slewing maneuvers, linearize rates around nominal, non-zero values.
- Improve the motor model by incorporating the dynamic truss model developed by Lacy [1991] such that the motor model includes the dynamic loads caused by slewing the truss.
- Perform physical experiments of vibration control during a large-angle slewing maneuver.

These remarks conclude this thesis.

List Of References

1. Aravamudan, K.S., Murthy, P.N., "Nonlinear Vibration of Beams With Time-Dependent Boundary Conditions," *International Journal of Nonlinear Mechanics,* Volume 8, pp.195-212, 1973.

2. Alberts, T.E., Love, L.J., Bayo, E., Moulin, H., "Experiments with End-Point Control of a Flexible Link Using the Inverse Dynamics Approach and Passive Damping," Proceedings of the 1990 American Control Conference, Vol. 1, pp.350-355.

3. Arun, V., Reinholtz, C.F., Watson, L. T., "Enumeration and Analysis of Variable-Geometry Truss Manipulators," Accepted for presentation at the *21st ASME Mechanisms Conference,* Chicago, 1990a.

4. Clark, W.W., Robertshaw, H.H., Warrington, T.J., "A Planar Comparison of Actuators for Vibration Control of Flexible Structures," Accepted for the *Journal of Intelligent Material Systems and Structures,* Technomics Press, October 1990.

5. Fanson, J.L., "An Experimental Investigation of Vibration Suppression in Large Space Structures Using Positive Position Feedback," Ph.D. Thesis, California Institute of Technology, Pasadena, California, 1987.

6. Juang, J.N., Horta, L.G., Robertshaw, H.H., " A Slewing Control of Flexible Structures," *Journal of Guidance, Control, and Dynamics,* Volume 9, Number 5, September-October 1986.

7. Juston, J., and Bauer, D., "Strain Rate Sensing for Vibration Control of Flexible Structures," Proceedings of the 32nd Structures, Structural Dynamics, and Materials Conference, Volume 4, 1991, pp.2888-2899.

8. Lacy, D.T., "An Automated Methodology of Force Analysis in Adaptive Trusses," Masters Thesis, Virginia Polytechnic Institute and State University, 1991.

9. Miura, K., Furuya, H., " An Adaptive Structure Concept for Future Space Applications," International Astronautical Federation, Paper no. IAF-85-211, October 1985.

10. Miura, K., Furuya, H., Suzuki, K.,"Variable Geometry Truss and Its Application to Deployable Truss and Space Crane Arm," *Acta Astronautical*, 1985, Volume 12, Number 7-8.

11. Natori, M., Iwasaki, K., Kuwaco, F., "Adaptive Planar Truss Structures and Their Vibration Characteristics," Proceedings of the 28th Structures, Structural Dynamics and Materials Conference, 1987, AIAA-87-0743, pp. 143-151.

12. Padmanabhan, B., Arun, V., Reinholtz, C.F., "Closed-Form Inverse Kinematic Analysis of Variable Geometry Truss Manipulators," Accepted for the *Transactions of the ASME, Journal of Mechanical Design,* 1990.

13. Reinholtz, C.F., Gokhale, D., "Design and Analysis of Variable Geometry Truss Robots," Proceedings of the 10th Applied Mechanisms Conference, December 1987, New Orleans, La.

14. Rhodes, M. D., Mikulas Jr., M.M.,"Deployable Controllable Geometry Truss Beam," NASA Technical Memorandum 86366, June 1985.

15. Rockwell International, "Development of Deployable Structures for Large Space Platform Systems," Interim Report Volume 1 SDD 82-0121-1 (Contract NAS8-34678), Vought Corp., October 1982.

16. Robertshaw, H.H., "Position Control of Flexible Beams with Root Actuation," Final Report of NASA Grant NAG-1-5-70, December 17, 1985.

17. Robertshaw, H.H., Wynn Jr., R.H., Kung, H.F., Hendricks, S.L., Clark, W.W., "Dynamics and Control of a Spatial Active Truss Actuator," Proceedings of the 30th Structures, Structural Dynamics, and Materials Conference, 1989, Volume 3, pp.1473-1479.

18. Sincarsin, W.G., Hughes, P.C., "Truss Arm Candidate Geometries," Dynacon Report 28-611/0401, Dynacon Enterprises Limited, Ontario, Canada, 1987.

19. Tidwell, P.H., Reinholtz, C.F., Robertshaw, H.H., Horner, C.G., "Kinematic Analysis of Generalized Adaptive Trusses," Presented at the First Joint US/Japan Conference on Adaptive Structures, November 1990.

20. Wynn, Jr., R.H.,"The Control of Flexible Structure Vibrations Using a Cantilevered Adaptive Truss," Ph.D. Thesis, Virginia Polytechnic Institute and State University, Blacksburg, Virginia, 1990.

Appendix A

Integrals of Shape Functions

$$I_1 = \int_0^L \phi_{x1} ds$$
$$I_2 = \int_0^L \phi_{x2} ds$$
$$I_3 = \int_0^L \phi_{x3} ds$$
$$I_4 = \int_0^L \phi_{y1} ds$$
$$I_5 = \int_0^L \phi_{y2} ds$$
$$I_6 = \int_0^L \phi_{y3} ds$$
$$I_7 = \int_0^L \phi_{x1}^2 ds$$
$$I_8 = \int_0^L \phi_{x1}\phi_{x2} ds$$
$$I_9 = \int_0^L \phi_{x1}\phi_{x3} ds$$
$$I_{10} = \int_0^L \phi_{x2}^2 ds$$
$$I_{11} = \int_0^L \phi_{x2}\phi_{x3} ds$$
$$I_{12} = \int_0^L \phi_{x3}^2 ds$$
$$I_{13} = \int_0^L \phi_{x1}\phi_{y1} ds$$
$$I_{14} = \int_0^L \phi_{x1}\phi_{y2} ds$$
$$I_{15} = \int_0^L \phi_{x1}\phi_{y3} ds$$
$$I_{16} = \int_0^L \phi_{x2}\phi_{y1} ds$$
$$I_{17} = \int_0^L \phi_{x2}\phi_{y2} ds$$
$$I_{18} = \int_0^L \phi_{x2}\phi_{y3} ds$$
$$I_{19} = \int_0^L \phi_{x3}\phi_{y1} ds$$
$$I_{20} = \int_0^L \phi_{x3}\phi_{y2} ds$$
$$I_{21} = \int_0^L \phi_{x3}\phi_{y3} ds$$
$$I_{22} = \int_0^L \phi_{y1}^2 ds$$
$$I_{23} = \int_0^L \phi_{y1}\phi_{y2} ds$$
$$I_{24} = \int_0^L \phi_{y1}\phi_{y3} ds$$
$$I_{25} = \int_0^L \phi_{y2}^2 ds$$
$$I_{26} = \int_0^L \phi_{y2}\phi_{y3} ds$$
$$I_{27} = \int_0^L \phi_{y3}^2 ds$$
$$I_{28} = \int_0^L s\phi_{x1} ds$$
$$I_{29} = \int_0^L s\phi_{x2} ds$$
$$I_{30} = \int_0^L s\phi_{x3} ds$$
$$I_{31} = \int_0^L s\phi_{y1} ds$$
$$I_{32} = \int_0^L s\phi_{y2} ds$$
$$I_{33} = \int_0^L s\phi_{y3} ds$$
$$I_{34} = \int_0^L (\frac{\partial^2\phi_{x1}}{\partial s^2})^2 ds$$
$$I_{35} = \int_0^L (\frac{\partial^2\phi_{x2}}{\partial s^2})^2 ds$$
$$I_{36} = \int_0^L (\frac{\partial^2\phi_{x3}}{\partial s^2})^2 ds$$
$$I_{37} = \int_0^L (\frac{\partial^2\phi_{y1}}{\partial s^2})^2 ds$$
$$I_{38} = \int_0^L (\frac{\partial^2\phi_{y2}}{\partial s^2})^2 ds$$
$$I_{39} = \int_0^L (\frac{\partial^2\phi_{y3}}{\partial s^2})^2 ds$$
$$I_{40} = \int_0^L (\frac{\partial\phi_{x1}}{\partial s})^2 ds$$
$$I_{41} = \int_0^L \frac{\partial\phi_{x1}}{\partial s}\frac{\partial\phi_{x2}}{\partial s} ds$$
$$I_{42} = \int_0^L \frac{\partial\phi_{x1}}{\partial s}\frac{\partial\phi_{x3}}{\partial s} ds$$
$$I_{43} = \int_0^L (\frac{\partial\phi_{x2}}{\partial s})^2 ds$$
$$I_{44} = \int_0^L (\frac{\partial\phi_{x2}}{\partial s})(\frac{\partial\phi_{x3}}{\partial s}) ds$$
$$I_{45} = \int_0^L (\frac{\partial\phi_{x3}}{\partial s})^2 ds$$
$$I_{46} = \int_0^L (\frac{\partial\phi_{y1}}{\partial s})^2 ds$$
$$I_{47} = \int_0^L (\frac{\partial\phi_{y1}}{\partial s})(\frac{\partial\phi_{y2}}{\partial s}) ds$$
$$I_{48} = \int_0^L (\frac{\partial\phi_{y1}}{\partial s})(\frac{\partial\phi_{y3}}{\partial s}) ds$$
$$I_{49} = \int_0^L (\frac{\partial\phi_{y2}}{\partial s})^2 ds$$
$$I_{50} = \int_0^L (\frac{\partial\phi_{y2}}{\partial s})(\frac{\partial\phi_{y3}}{\partial s}) ds$$
$$I_{51} = \int_0^L (\frac{\partial\phi_{y3}}{\partial s})^2 ds$$
$$I_{52} = \int_0^L (\frac{\partial^2\phi_{x1}}{\partial s^2})(\frac{\partial^2\phi_{x2}}{\partial s^2}) ds$$
$$I_{53} = \int_0^L (\frac{\partial^2\phi_{x1}}{\partial s^2})(\frac{\partial^2\phi_{x3}}{\partial s^2}) ds$$
$$I_{54} = \int_0^L (\frac{\partial^2\phi_{x2}}{\partial s^2})(\frac{\partial^2\phi_{x3}}{\partial s^2}) ds$$
$$I_{55} = \int_0^L (\frac{\partial^2\phi_{y1}}{\partial s^2})(\frac{\partial^2\phi_{y2}}{\partial s^2}) ds$$
$$I_{56} = \int_0^L (\frac{\partial^2\phi_{y1}}{\partial s^2})(\frac{\partial^2\phi_{y3}}{\partial s^2}) ds$$
$$I_{57} = \int_0^L (\frac{\partial^2\phi_{y2}}{\partial s^2})(\frac{\partial^2\phi_{y3}}{\partial s^2}) ds$$

Vita

The author was born on March 1st, 1965 in Pasadena, California. The author went to Virginia Tech to fulfill his quest for knowledge in mechanical systems and subsequently completed his undergraduate and, with this thesis, Master of Science degrees. The author is now unemployed.

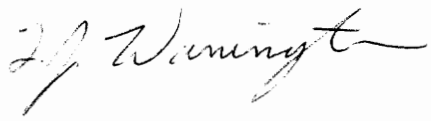

T.J. Warrington